(12) INTERNATIONAL APPLICATION PUBLISHED UNDER THE PATENT COOPERATION TREATY (PCT)

(19) World Intellectual Property Organization
International Bureau

(43) International Publication Date
09 February 2023 (09.02.2023)

WIPO | PCT

(10) International Publication Number
WO 2023/015162 A1

(51) International Patent Classification:
A61P 35/00 (2006.01) *G16B 25/10* (2019.01)
C07K 16/28 (2006.01)

(21) International Application Number:
PCT/US2022/074383

(22) International Filing Date:
01 August 2022 (01.08.2022)

(25) Filing Language: English

(26) Publication Language: English

(30) Priority Data:
63/203,862 02 August 2021 (02.08.2021) US

(71) Applicant: **THE REGENTS OF THE UNIVERSITY OF CALIFORNIA** [US/US]; 1111 FRANKLIN STREET, TWELFTH FLOOR, OAKLAND, California 94607-5200 (US).

(72) Inventor: **LO, Roger S.**; C/O UCLA TECHNOLOGY DEVELOPMENT GROUP, 10889 WILSHIRE BLVD, SUITE 920, LOS ANGELES, California 90024 (US).

(74) Agent: **CANADY, Karen S.** et al.; CANADY + LORTZ LLP, 3435 Wilshire Blvd., Suite 1400, Los Angeles, CA 90010 (US).

(81) Designated States *(unless otherwise indicated, for every kind of national protection available)*: AE, AG, AL, AM, AO, AT, AU, AZ, BA, BB, BG, BH, BN, BR, BW, BY, BZ, CA, CH, CL, CN, CO, CR, CU, CV, CZ, DE, DJ, DK, DM, DO, DZ, EC, EE, EG, ES, FI, GB, GD, GE, GH, GM, GT, HN, HR, HU, ID, IL, IN, IQ, IR, IS, IT, JM, JO, JP, KE, KG, KH, KN, KP, KR, KW, KZ, LA, LC, LK, LR, LS, LU, LY, MA, MD, ME, MG, MK, MN, MW, MX, MY, MZ, NA, NG, NI, NO, NZ, OM, PA, PE, PG, PH, PL, PT, QA, RO, RS, RU, RW, SA, SC, SD, SE, SG, SK, SL, ST, SV, SY, TH, TJ, TM, TN, TR, TT, TZ, UA, UG, US, UZ, VC, VN, WS, ZA, ZM, ZW.

WO 2023/015162 A1

(54) **Title:** METHODS TO ENHANCE EFFICACY OF COMBINED TARGETING OF IMMUNE CHECKPOINT AND MAPK PATHWAYS

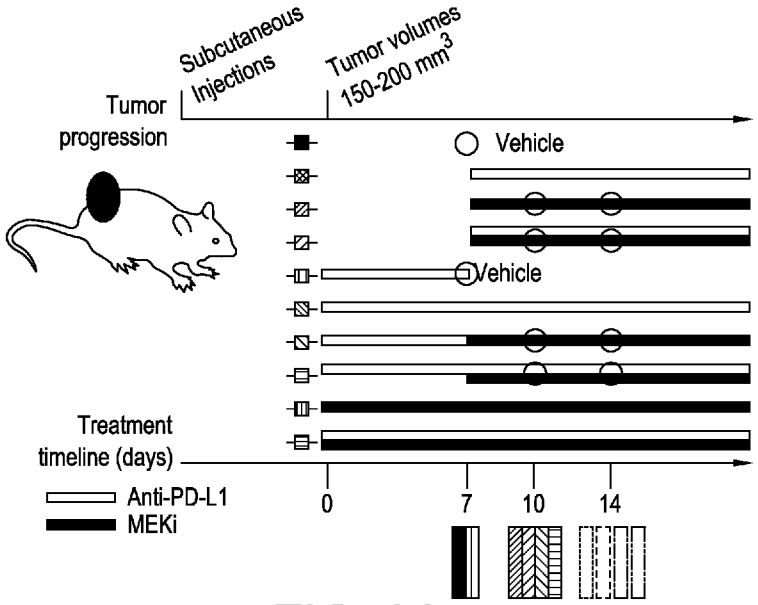

FIG. 2A

(57) **Abstract:** A method of enhancing efficacy of mitogen-activated protein kinase inhibitor (MAPKi) therapy or immune checkpoint therapy (ICT), as well as a method of suppressing melanoma brain metastasis in a subject, and a method of inhibiting intratumoral M2-like tumor associated macrophages (TAMs) or regulatory T cells (T_{REG}) in a subject comprises (a) pretreating a subject appropriate for and in need of MAPKi therapy by administering one or more doses of ICT to the subject; and (b) subsequent to the pretreating of (a), administering to the subject a combination of MAPKi and ICT. The ICT typically comprises an anti-PD-1 or anti-PD-L1 agent. Optionally, the ICT further comprises additional agents (such as anti-CTLA4 and/or anti-LAG3) to enhance the efficacy of MAPKi therapy.

[Continued on next page]

(84) Designated States *(unless otherwise indicated, for every kind of regional protection available)*: ARIPO (BW, GH, GM, KE, LR, LS, MW, MZ, NA, RW, SD, SL, ST, SZ, TZ, UG, ZM, ZW), Eurasian (AM, AZ, BY, KG, KZ, RU, TJ, TM), European (AL, AT, BE, BG, CH, CY, CZ, DE, DK, EE, ES, FI, FR, GB, GR, HR, HU, IE, IS, IT, LT, LU, LV, MC, MK, MT, NL, NO, PL, PT, RO, RS, SE, SI, SK, SM, TR), OAPI (BF, BJ, CF, CG, CI, CM, GA, GN, GQ, GW, KM, ML, MR, NE, SN, TD, TG).

Published:

— *with international search report (Art. 21(3))*

— *before the expiration of the time limit for amending the claims and to be republished in the event of receipt of amendments (Rule 48.2(h))*

METHODS TO ENHANCE EFFICACY OF COMBINED TARGETING OF IMMUNE CHECKPOINT AND MAPK PATHWAYS

[0001] This application claims benefit of United States provisional patent application number 63/203,862, filed August 2, 2021, the entire contents of which are incorporated by reference into this application.

STATEMENT REGARDING FEDERALLY SPONSORED RESEARCH

[0002] This invention was made with government support under Grant Numbers CA176111, CA215910, CA255837 and CA168585, awarded by the National Institutes of Health. The government has certain rights in the invention.

BACKGROUND

[0003] Programmed cell death protein-1/programmed death-ligand 1 (PD-1/PD-L1 or PD-1/L1)- and mitogen-activated protein kinase (MAPK)-targeted therapies have revolutionized the treatment of *BRAF*^{V600MUT} melanoma and beyond. For MAPK inhibitors (MAPKi) consisting of BRAF inhibitor (BRAFi) + MEK inhibitor (MEKi), 5-year survival is under 30%, and acquired resistance occurs within one year in the majority of patients with *BRAF*^{V600MUT} melanoma. In contrast, for patients with *BRAF*^{V600WT} melanoma, BRAFi is contraindicated, and MEKi monotherapy provides limited benefits due to innate or rapid development of resistance. Immune checkpoint therapy (ICT) with anti-PD-1 agents results in 30-40% response rates in patients with either *BRAF*^{V600MUT} or *BRAF*^{V600WT} melanoma. Combination ICT with anti-PD-1 + anti-CTLA-4 agents reduces the rate of innate resistance from 60-70% to 40-50%. Simultaneous initiation of treatments with anti-PD-1/L1 and BRAFi + MEKi (aka triplet therapy) in *BRAF*^{V600MUT} has been tested in clinical trials (Ascierto et al., 2019; Gutzmer et al., 2020; Ribas et al., 2019) and has been hypothesized to reduce both innate anti-PD-1/L1 resistance and acquired MAPKi resistance.

[0004] Retrospective analyses of clinical data suggest that progression on MAPKi is associated with inferior responses to subsequent anti-PD-1 therapy and that any second-line therapy results in inferior outcomes versus the same therapy in the first-line setting (Ackerman et al., 2014; Johnson et al., 2017; Mason et al., 2020; Reijers et al., 2020; Simeone et al., 2017; Tetu et al., 2018). Whether treatment first with ICT until progression alters subsequent MAPKi responsiveness is still unclear. Prospectively, the optimal sequencing of MAPKi *vs.* ICT is being tested in multiple clinical trials. These trials test one therapy modality until disease progression before switching to the alternative. However, treatment until progression may induce cross-resistance.

[0005] Thus, although methods to target the mitogen-activated protein kinase (MAPK) pathway and immune checkpoints (PD-1, PD-L1, CTLA-4) are clinically approved, therapeutic resistance is commonplace. Moreover, resistance of brain metastasis to these therapeutic agents limits patient survival.

[0006] There remains a need for methods to improve the efficacy of combined targeting of immune checkpoint and MAPK pathways.

SUMMARY

[0007] The methods described herein meet these needs and others by providing a method of enhancing efficacy of mitogen-activated protein kinase inhibitor (MAPKi) therapy or immune checkpoint therapy (ICT), as well as a method of suppressing melanoma metastasis in a subject, and a method of inhibiting intratumoral M2-like tumor associated macrophages (TAMs) and regulatory or suppressor T (T_{REG}) cells in a subject.

[0008] In some embodiments, the method comprises (a) pretreating a subject appropriate for and in need of MAPKi therapy by administering one to two doses of ICT to the subject; and (b) subsequent to the pretreating of (a), administering to the subject a combination of MAPKi and ICT. In some embodiments, the ICT comprises an anti-PD-1 or anti-PD-L1 agent. Optionally, the pretreating with ICT further comprises administering an anti-CTLA-4 and/or anti-LAG3 agent. In some embodiments, the pretreating further comprises administering a modulator of T_{REG} cells, such as an anti-CD20 antibody, or a modulator of M2-like TAMS, such as an agonist of CD206 (e.g., RP832c).

[0009] In some embodiments, the subject has a *BRAF* V600 mutant cancer, and the MAPKi comprises a BRAF inhibitor (BRAFi) plus a MEK inhibitor (MEKi). In some embodiments, the subject has a *NRAS*, *KRAS*, and/or *NF1* mutant cancer and the MAPKi is a MEKi, ERKi, and/or a type II RAFi (aka pan-RAFi, omni-RAFi).

[0010] In some embodiments, the pretreating of (a) consists of administering one to two doses of a single-agent or double-agent ICT over one to eight weeks. In some embodiments, the pretreating of (a) consists of administering one to two doses of a single-agent or double-agent ICT over one to five weeks. The dose to be administered is tailored to the individual ICT and individual patient, taking into account disease progression, patient history, and other indicators of sensitivity or toxicities, as is understood by those skilled in the art. While pretreating typically comprises administering one to two doses of ICT (and, optionally, an anti-CTLA-4 or anti-LAG3 agent, anti-M2 TAM agent, and/or a modulator of T_{REG} cells), it is understood that additional doses during the pretreatment stage are contemplated. For example, a pretreatment dose can be administered every one to four weeks, over the course

of one to two months. In some embodiments, a total of four pretreatment doses are administered prior to initiation of MAPKi co-treatment.

[0011] In some embodiments, the administering of (b) begins two to five, or up to eight weeks after the initiation of the pretreating of (a). In some embodiments, the administering of (b) begins at least two weeks after the initiation of the pretreating of (a). In some embodiments, the administering of (b) begins at no later than four weeks after the pretreating of (a). In some embodiments, the administering of (b) begins at no later than five weeks after the pretreating of (a). In some embodiments, the administering of (b) begins at no later than eight weeks after the pretreating of (a).

[0012] For the method of suppressing melanoma metastasis in a subject, the pretreating of a subject in need of treatment for melanoma comprises administering one to one to two doses of ICT to the subject. In some embodiments, the melanoma metastasis is a brain metastasis. In some embodiments, the melanoma metastasis is an extracranial metastasis. The method can be further enhanced by combining the ICT pretreatment with administration of an anti-CTLA-4 agent and/or a modulator of T_{REG} or M2-like TAMs cells, as mentioned above. The method is of benefit to subjects at risk for brain metastases as well as those at risk of extracranial metastases. Thus, a subject in need of treatment for melanoma brain metastases includes subjects at risk of brain or brain plus extracranial metastases. Subsequent to the pretreating step, the method further comprises administering to the subject a combination of MAPKi and ICT. Since therapeutic resistance of melanoma brain metastasis (MBM) limits patient survival, the sequencing of anti-PD-1/L1 (± anti-CTLA-4 and/or modulator of M2-like TAM or T_{REG} cells) pretreatment before MAPKi combination suppresses MBM and improves survival with robust T-cell clonal expansion in both intracranial and extracranial metastatic sites.

[0013] In some embodiments, the method is a method of enhancing the inhibition of M2-like TAMs. In some embodiments, the pretreating further comprises administering a pharmacologic M2-like TAM inhibitor to the subject, in addition to the ICT. The inhibition of M2-like TAMs effects a selective upregulation of pro-inflammatory TAMs in the subject. The inhibition of M2-like TAMs effects a selective upregulation M1-like TAMs.

[0014] In some embodiments, the pretreatment comprises administering a CD25-T_{REG}-depleting antibody.

BRIEF DESCRIPTION OF THE DRAWINGS

[0015] **FIG. 1** shows progression-free survival of patients with *BRAF*^{V600MUT} melanoma treated with dabrafenib plus trametinib and stratified by prior exposure to ICT. Results from

the S1320 SWOG trial and analyzed by the univariate Cox regression model. ICT, immune checkpoint therapy.

[0016] **FIGS. 2A-2K** demonstrate that two doses of anti-PD-1/L1 before MAPKi combination forestall therapy resistance and induce pro-inflammatory TAM polarization. (2A) Schematic of timelines for subcutaneous tumor progression and for dosing anti-PD-L1 and/or MEKi therapies in (2B to 2I) and for tumor sampling in (J and K). Anti-PD-L1 (200 mg/mouse) twice per week IP; MEKi (dosage variable depending on the tumor model) daily PO via chow. Circles indicate regimen and time points for CyTOF analysis in Figure 2J and scRNA-seq + scTCR-seq analysis in Figure 3. (2B to 2H) Tumor volumes of YUMM1.7ER (2B), NIL (2C), NILER1-4 (2D), mSK-Mel254 (2E, 2H), CT26 (2F), and KPC (2G) treated with indicated regimens in (2A). Trametinib at 1 (2B, 2C, 2D), 2 (2G), 3 (2E) or 5 (2F) mg/kg/d PO via chow. Anti-PD-L1 (200 mg/mouse) and anti-PD-1 (300 mg/mouse first week only and then 200 mg/mouse) twice per week IP. N = 8 tumors/group. Data are means ± SEMs (P-values, Student's *t* test) and representative of two independent experiments. (2I) Overall survival (cutoff tumor volume ≥ 1000 mm^3) of mice bearing YUMM1.7ER tumors treated as indicated. PLX4032, 50 mg/kg/d PO; trametinib, 0.3 mg/kg/d PO. CTRL, historical control. All p-values (logrank test) are for pairwise comparisons relative to mice treated with anti-PD-L1 (d0 to d7) followed by the triplet (anti-PD-L1 + PLX4032 + trametinib) combination. (2J) t-SNE maps (left) of tumor-infiltrating $CD45^+$ cells analyzed by CyTOF in three indicated syngeneic subcutaneous tumor models at time points and in treatment regimens indicated in (2A). Heatmaps (right) showing the expression values of immune phenotypic protein markers normalized to the maximum mean value across subsets. (2K) Frequencies of $iNOS^+$ TAMs in the $CD45^+$ population of three syngeneic tumor models at time points and treatment regimens indicated in (2A). Mean ± SEMs. Pairwise comparisons were performed in (i) vehicle *vs.* two doses of anti-PD-L1, (ii) MEKi d7 *vs.* MEKi d7, anti-PD-L1 d0 to d7, (iii) MEKi d7, anti-PD-L1 d7 *vs.* MEKi d7, anti-PD-L1 d0. P-value, Student's *t* test. *$p < 0.05$, **$p < 0.01$ and ***$p < 0.001$. See (2A). A color-coded version of FIGS. 2A-2K is available (Wang Y, et al. Cancer Cell. 2021 Oct 11;39(10):1375-1387).

[0017] **FIGS. 3A-3N** show TAM and T-cell phenotypes associated with response to optimized therapy regimen. (3A) Uniform manifold approximation and projection (UMAP) of tumor-infiltrating $CD45^+$ cells (n = 53,841) analyzed by scRNA-seq. Dissociated live, $CD45^+$ cells were pooled from 4 tumors (mSK-Mel254) per regimen and per time point. Inferred cell types are indicated by clusters as denoted by labels based on distinct colors. (3B) UMAP of tumor-infiltrating Mo/MΦ population (n = 28,857) analyzed by scRNA-seq. Clusters with differentially expressed genes are denoted by labels based on distinct colors. (3C) Heatmap showing differentially expressed genes (rows) among different Mo/MΦ subpopulations

(columns). Representative genes of each cluster are highlighted (right). (3D) Ratios between the proportions of pro- and anti-inflammatory MΦ clusters across distinct regimens and time points. See Figure 2A. (3E) UMAP of tumor-infiltrating T cells (n = 13,803) analyzed by scRNA-seq. Clusters with differentially expressed genes are denoted by labels based on distinct colors. (3F) Heatmap showing differentially expressed genes (rows) among different T-cell clusters (columns) and highlighted genes of each cluster (right). (3G) UMAP in (3E) colored by clonality based on scTCR-seq. (3H) Clonal expansion indices of T-cell subpopulations. P-value, Kruskal–Wallis test. (3I) Developmental transition indices of $CD8^+$ T_C cells with other $CD8^+$ subpopulations. Pairwise comparisons were performed between Ki-67^{hi} $CD8^+$ T cells and each of the other $CD8^+$ subpopulations with the Wilcoxon test. P-values, ***$p < 0.001$. (3J) Relative expansion ratios between T_C *vs.* T_{REG} (left) and Ki-67^{hi} $CD8^+$ *vs.* T_{REG} (right) across different treatment regimens and time points. See Figure 2A. (3K) Developmental transition indices between $CD8^+$ T_C and Ki-67^{hi} $CD8^+$ T cells across distinct regimens and time points. See Figure 2A. (3L) Fold changes of top 5 (top) or 10 (bottom) clone sizes for $CD8^+$ T_C or Ki-67^{hi} $CD8^+$ T cells *vs.* $CD4^+$ T_{REG} cells. See Figure 2A. (3M) Violin plots of *Ifng* expression in distinct T-cell subpopulations. (3N) Heatmap displaying the scaled mean expression levels of highlighted functional genes (rows) in T_C cells across treatment regimens and time points (see Figure 2A). Gene expression levels were row-scaled for only T_C cells. See also Figure 9 and Table 3. A color-coded version of FIGS. 3A-3N is available (Wang Y, et al. Cancer Cell. 2021 Oct 11;39(10):1375-1387).

[0018] **FIGS. 4A-4C** illustrates functional roles of TAMs and CD8+ T cells in the development of acquired resistance. Tumor volumes of mSK-Mel254 without active treatment or treated with the indicated regimens. Trametinib at 3 mg/kg/d PO; RP-832c (CD206 peptide) at 10 mg/kg/d subcutaneously; anti-PD-L1 (200 mg/mouse IP twice per week); and anti-CD8 antibody at 200 mg/mouse IP initiated one day before any treatment regimen and then twice a week. N = 8 tumors/group. Data are means ± SEMs (P-values, Student's t test).

[0019] **FIGS. 5A-5N** demonstrate that immune checkpoint blockade before MAPKi co-treatment prolongs MBM suppression and survival. (5A) Schematic of timelines for metastatic tumor progression of *Braf*^{V600MUT} murine melanoma (YUMM1.7ER) and for dosing anti-PD-L1 and/or MEKi therapies in (B to F). Anti-PD-L1 (200 mg/mouse) IP on d-4 and d-2, when applicable, and, thereafter, twice per week; MEKi, 1 mg/kg/d PO. Circles indicate regimens and time points for TCR-seq analysis in Figure 6. (5B) Representative *ex vivo* BLI of organs from necropsies at experimental endpoints (total ventral or dorsal BLI signal in the range of 1e9-1e10, moribund state of health, or death). Scale for radiance, photons/sec. (5C, 5D) Temporal BLI quantification (radiance, photons/sec) based on the dosing timeline in (5A)

of dorsal extracranial (5C) or intracranial (5D) tumor burden. Data are mean ± SD based on the indicated numbers of mice in the untreated and treatment regimen groups. Pairwise comparisons (mixed model framework with Bonferronic correction for multiple testing) of the group MEKi d0, anti-PD-L1 d-4 *vs.* the group denoted by the specific corresponding symbol #. # p = 0.05-0.001 , ## p < 0.001. *Indicates death of mouse or mice, resulting in drops in mean BLI values. True or confirmed complete responses or CRs defined in Methods. (5E) *In vivo* BLI of representative mice from the untreated group *vs.* all mice treated with MEKi d0 monotherapy at indicated timepoints. All images were adjusted to the same radiance scale. (5F) Survival of untreated mice and mice on each treatment regimen. *p < 0.05, **p < 0.01, ***p < 0.001, ****p < 0.0001; ns, not significant (logrank test). Survival criteria indicated in (5B). (5G, 5H) Survival of untreated mice and mice on indicated treatment regimens. P values, logrank test. Day on which BRAFi + MEKi in (5G) were started, defined as day 0, was the same as in (5A) but pushed back by 2 days (day 10 after intracardiac injection) in (5H). Low tumor burden model, MAPKi started on day 8 after IC injection; high tumor burden model, MAPKi started on day 10 after IC injection. (5I, 5J) As in (5C, 5D). (5K) As in (5F). (5L, 5M) As in (5C, 5D), except anti-CTLA-4 at 200 mg/mouse twice a week IP and # p < 0.05, ## p < 0.01, ### p < 0.001, #### p < 0.0001. Pairwise comparisons (mixed model framework with Bonferronic correction for multiple testing) of the group BRAFi+MEKi d0, anti-PD-L1 d-4 *vs.* the group denoted by the specific color of symbol #. (5N) As in (5F) except anti-CTLA-4 at 200 mg/mouse twice a week IP. (5G to 5N) BRAFi, PLX4032, 50 mg/kg/d PO; MEKi, trametinib, 0.3 mg/kg/d PO. See also FIG. 10.

[0020] **FIGS. 6A-6C** show that anti-PD-L1 lead-in before MAPKi co-treatment augments clonal T-cell expansion. (6A) Tumor cell-involved brain and ovarian tissues were collected from mice at time points and in groups as indicated in Figure 5A (brain, n = 2 mice per group, except the no treatment group; ovary, n = 1 mouse per group; two geographically distinct regions of each organ site were sampled for TCR-seq analysis). The total sizes of large TCR clones (≥ 5%) for the α or β chain in tumor-involved brain or ovarian tissues (red dots, average values). Pairwise comparisons were performed between the group of MEKi d0, anti-PD-L1 d-4 vs. each of the other groups with Student's t-test. P-values, *p < 0.05, **p < 0.01, ***p < 0.001. (6B) The fractions of overlapping TCR clones (α or β chain) between two distinct geographic regions of tumor-involved brain tissues from individual mice. (6C) Total sizes of large clones (≥ 5%) shared by two distinct geographic regions of tumor-involved brain or ovarian tissues in each mouse. Pairwise comparisons were performed as in (6A).

[0021] **FIG. 7** provides Kaplan-Meier plots of overall survival from the S1320 trial stratified by prior exposure to ICT, Related to Figure 1. Results from univariate Cox regression model.

[0022] **FIGS. 8A-8G** show the impacts of treatment regimens containing anti-PD-L1 and/or MEKi on tumor cells, CD45+ cells, CD45+ sub-populations, and CD8+ T-cell sub-populations, Related to Figure 2. (7A) Immunofluorescence of p-ERK levels in tumors of indicated tumor models, with or without trametinib treatment (3 days). DAPI, nuclear stain. Scale bar, 50 μm. Representative images shown for two of five tumors analyzed per group. (8B) Tumor volumes of mSK-Mel254 treated with indicated regimens and on the timelines in Figure 2A. Trametinib at 3 mg/kg/d. Anti-PD-L1 (200 μg/mouse) and anti-CTLA-4 (200 μg/mouse), both twice per week IP. N = 8 tumors/group. Data are means ± SEMs (P-values, Student t-test). (8C, 8D, 8E, 8G) Frequencies of CD45+ population in the total live cells (8C), immune cell types in the CD45+ population (8D), CD4+ Th1-like T-cells in the CD45+ population (8E), and CD8+ subsets in the CD8+ population (8G) of three syngeneic tumor models. Mean± SEMs. Pairwise comparisons were performed in (i) vehicle vs. two doses of anti-PD-L1, (ii) MEKi starting d7 vs. anti-PD-L1 d0-d7, MEKi starting d7, (iii) MEKi+anti-PD-L1 starting d7 vs. anti-PD-L1 d0-d7, anti-PD-L1+MEKi starting d7. P-value, Student's t test. *$p < 0.05$, **$p < 0.01$ and ***$p < 0.001$. See Figure 2A. (8F) Heatmaps showing the expression values of immune phenotypic protein markers across multiple subsets in tumor-infiltrating CD8+ cells analyzed by CyTOF in three indicated syngeneic SC tumor models. The expression values of each marker were normalized to the maximum mean value across subsets. TCM (central memory): CD62L+CD44+GZMB-; TEM (effector memory): CD62L-CD44+GZMB-; TC (cytotoxic): GZMB+; TTD (terminally differentiated): CD62L-CD44-GZMB-.

[0023] **FIGS. 9A-9G** show coupled scRNA-seq/scTCR-seq analysis of mSK-Mel254 tumors from mice undergoing anti-PD-L1 and/or MEKi treatment regimens, Related to Figure 3. (9A, 9B) UMAP in Figure 3A was colored by single-cell expression patterns of indicated cell lineage markers (9A) and TCR (9B). (9C to 9E) Frequencies of immune subpopulations in the CD45+ population (9C), Mo/MΦ subpopulations among CD45+ cells (9D), subpopulations among CD4+ T-cells (9E, top) and CD8+ T-cells (9E, bottom). See Figure 2A. (9F) Boxplots of Tcf1+ stem-like gene signature scores in CD8+ T-cell subsets. Pairwise comparisons were performed in (i) vehicle vs. anti-PD-L1 d0-d7, (ii) MEKi d7 vs. anti-PD-L1 d0-d7, MEKi d7, (iii) anti-PD-L1+MEKi d7 vs. anti-PD-L1 d0-d7, anti-PD-L1+MEKi d7. P-value, Wilcoxon test. *$p < 0.05$, ***$p < 0.001$. See Figure 2A. (9G) Heatmap displaying the scaled mean expression levels of highlighted genes (rows) in each treatment regimen group and time point (column) for TC, TREG, TH1/TH2, NKT and Tγδ subpopulations. See Figure 2A. Gene expression levels were row-scaled across CD8+ TC, TREG, TH1/TH2, NKT, Tγδ, and Ki-67hiCD8+ subpopulations.

[0024] **FIGS. 10A-10J** demonstrate that anti-PD-L1 lead-in before MAPKi co-treatment optimizes suppression of extracranial and intracranial metastatic progression and augments T-cell clonal expansion, Related to Figures 5 and 6. (10A) In vivo BLI of representative mice bearing metastatic YUMM1.7ER cells from the untreated group on indicated timepoints. All images were adjusted to the same radiance scale. (10B) Ex vivo photo (left) and BLI (right) at necropsy of a mouse from the untreated group on day 23 post-IC injection. All images were adjusted to the same radiance scale. (10C, 10D) Temporal BLI quantification (radiance, photons/sec) based on the dosing timeline in Figure 5A of ventral extracranial (10C) or intracranial (10D) tumor burden. Data are mean ± SD based on the indicated numbers of mice in the untreated and treatment regimen groups. Pairwise comparisons (mixed model framework with Bonferronic correction for multiple testing) of the group MEKi d0, anti-PD-L1 d-4 vs. the group denoted by the specific corresponding symbol #. # $p = 0.05$-0.001 , ## $p < 0.001$. *Indicates death of mouse or mice, resulting in drops in mean BLI values. True complete responses or CRs defined in Methods. (10E) Flowchart showing the status of surviving mice from experiment in Figure 5G as they were monitored and grouped beyond 10 weeks (post MAPKi treatment initiation). Specific mice (number designations in 10F) and their final status at the end of long-term follow-ups are shown. (10F) Schematic of the individual natural histories of long-term surviving mice from experiment in Figure 5G and their disease, treatment, and vital status. (10G) Tumor cell-involved brain and ovarian tissues were collected from mice at time points and in groups as indicated in Figure 5A (brain, n = 2 mice per group, except the no treatment group; ovary, n = 1 mouse per group; two geographically distinct regions of each organ site were sampled for TCR-seq analysis). Dot plot showing the diversity and gini clonality indices for α or β chain in brain or ovarian tissues (red dots, average values). Pairwise comparison was performed between MEKi d0, anti-PD-L1 d-4 and each of the other treatment groups with Student's t test. P-values, *$p < 0.05$, **$p < 0.01$, ***$p < 0.001$. (10H) The total sizes of large TCR clones (≥ 8%) for the α or β chain in tumor-involved brain or ovarian tissues (hatched dots, average values). Pairwise comparisons were performed as in 10E. (10I) The total sizes of largest, top 5, and top 10 TCR clones (≥ 8%) for the α or β chain in tumor-involved brain or ovarian tissues (hatched dots, average values). Pairwise comparisons were performed as in 10E. (10J) Venn plots showing the overlapping fractions of TCR clones (α or β chain) between brain and ovarian tissues in each individual.

DETAILED DESCRIPTION

[0025] The invention described herein is based on the surprising discovery that sequencing of just two doses of anti-PD-1/L1 prior to combining with MAPKi maximizes antitumor efficacy. Data presented here support the conclusions that anti-PD-1/L1 therapy primes a

more durable MAPKi response and that MAPKi combination therapy overcomes innate anti-PD-1/L1 resistance. These findings provide a basis for methods to enhance the efficacy of MAPKi therapy as well as of ICT, and to suppress melanoma brain metastases. In addition, the efficacy of treatment can be further enhanced by inhibition of M2-like TAMs, and of regulatory T cells. The data described herein demonstrate that the superior antitumor activity of the regimen consisting of anti-PD-1/L1 lead-in followed by MAPKi combination was positively linked to multiple cell types, including M1 TAMs, Th1 CD4+ T-cells, as well as CD8+ cytotoxic and proliferative T cells and their persistence.

Definitions

[0026] All scientific and technical terms used in this application have meanings commonly used in the art unless otherwise specified. As used in this application, the following words or phrases have the meanings specified.

[0027] As used herein, "anti-PD-1 therapy" means treatment with an anti-PD-1 antibody (nivolumab/BMS-936558/MDX-1106, pembrolizumab/MK-3475, Pidilizumab), and/or an anti-PD-L1 antibody (BMS-986559, MPDL3280A, and MEDI4736).

[0028] As used herein, "combinatorial therapy" means MAPK targeted therapy, anti-CTLA-4 immunotherapy in any combination, with or without anti-PD-1 antibody and/or anti-PD-L1 antibody treatment.

[0029] As used herein, "MAPK/ERK kinase (MEK)" refers to a mitogen-activated protein kinase also known as mitogen-activated protein kinase (MAPK) or extracellular signal-regulated kinase (ERK).

[0030] MEK, also known as mitogen-activated protein kinase kinase and MAP2K, is a kinase enzyme that phosphorylates mitogen activated protein kinases (MAPKs), ERK, p38 and JNK. Seven MEK subtypes have been identified, all mediate cellular responses to different growth signals.

[0031] BRAF (v-raf murine sarcoma viral oncogene homolog B1) is a serine/threonine protein kinase that plays a critical role in the RAS-RAF-MEK-ERK mitogen activated protein kinase (MAPK) cell signalling pathway.

[0032] As used herein, "therapy", "treatment" or "treating" means any administration of a therapeutic agent according to the present disclosure to a subject (e.g. human) having or susceptible to a condition or disease, such as cancer, for the purpose of: preventing or protecting against the disease or condition, that is, causing the clinical symptoms not to develop; inhibiting the disease or condition, that is, arresting or suppressing the development of clinical symptoms; or relieving the disease or condition that is causing the regression of

clinical symptoms. In some embodiments, the term “therapy”, "treatment" or "treating" refers to relieving the disease or condition, i.e. which is causing the regression of clinical symptoms.

[0033] As used herein, the term "preventing" refers to the prophylactic treatment of a patient in need thereof. The prophylactic treatment can be accomplished by providing an appropriate dose of a therapeutic agent to a subject at risk of suffering from an ailment, thereby substantially averting onset of the ailment. The presence of a genetic mutation or the predisposition to having a mutation may not be alterable. However, prophylactic treatment (prevention) as used herein has the potential to avoid/ameliorate the symptoms or clinical consequences of having the disease engendered by such genetic mutation or predisposition. It will be understood by those skilled in the art that in human medicine, it is not always possible to distinguish between "preventing" and "suppressing" since the ultimate inductive event or events may be unknown, latent, or the patient is not ascertained until well after the occurrence of the event or events. Therefore, as used herein the term "prophylaxis" is intended as an element of "treatment" to encompass both "preventing" and "suppressing" as defined herein. The term "protection," as used herein, is meant to include "prophylaxis."The term "effective amount" refers to that amount of a therapeutic agent that is sufficient to effect treatment when administered to a subject in need of such treatment. The effective amount will vary depending upon the specific activity of the therapeutic agent being used, the severity of the patient's disease state, and the age, physical condition, existence of other disease states, and nutritional status of the patient. Additionally, other medication the patient may be receiving will affect the determination of the effective amount of the therapeutic agent to administer.

[0034] As used herein, "pharmaceutically acceptable carrier" or “excipient” includes any material which, when combined with an active ingredient, allows the ingredient to retain biological activity and is non-reactive with the subject's immune system. Examples include, but are not limited to, any of the standard pharmaceutical carriers such as a phosphate buffered saline solution, water, emulsions such as oil/water emulsion, and various types of wetting agents. Preferred diluents for aerosol or parenteral administration are phosphate buffered saline or normal (0.9%) saline.

[0035] Compositions comprising such carriers are formulated by well-known conventional methods (see, for example, *Remington's Pharmaceutical Sciences*, 18th edition, A. Gennaro, ed., Mack Publishing Co., Easton, PA, 1990).

[0036] As used herein, the term "subject" includes any human or non-human animal. The term "non-human animal" includes all vertebrates, e.g., mammals and non-mammals, such

as non-human primates, horses, sheep, dogs, cows, pigs, chickens, and other veterinary subjects. In a typical embodiment, the subject is a human.

[0037] As used herein, "a" or "an" means at least one, unless clearly indicated otherwise.

Methods

[0038] The methods described herein meet these needs and others by providing a method of enhancing efficacy of mitogen-activated protein kinase inhibitor (MAPKi) therapy or immune checkpoint therapy (ICT), as well as a method of suppressing melanoma metastasis in a subject, and a method of inhibiting M2-like tumor associated macrophages (TAMs) in a subject.

[0039] In some embodiments, the method comprises (a) pretreating a subject appropriate for and in need of MAPKi therapy by administering one to two doses of ICT to the subject; and (b) subsequent to the pretreating of (a), administering to the subject a combination of MAPKi and ICT. In some embodiments, the ICT comprises an anti-PD-1 or anti-PD-L1 agent. Optionally, the pretreating with ICT further comprises administering an anti-CTLA-4 agent or an anti-LAG3 agent. In some embodiments, the pretreating further comprises administering a modulator of T_{REG} cells, such as a CD25-T_{REG}-depleting antibody or a modulator of M2-like TAMs, such as an agonist of CD206 (e.g., RP832c).

[0040] In some embodiments, the subject has a *BRAF* V600 mutant cancer, and the MAPKi comprises a BRAF inhibitor (BRAFi) plus a MEK inhibitor (MEKi). In some embodiments, the subject has a *NRAS*, *KRAS*, and/or *NF1* mutant cancer and the MAPKi is a MEKi, ERKi, and/or a type II RAFi (aka pan-RAFi, omni-RAFi).

[0041] In some embodiments, the pretreating of (a) consists of administering one to two doses of a single-agent, double-agent,or triple-agent ICT over one to eight weeks. In some embodiments, the pretreating of (a) consists of administering one to two doses of a single-agent, double-agent,or triple-agent ICT over one to five weeks. The dose to be administered is tailored to the individual ICT and individual patient, taking into account disease progression, patient history, and other indicators of sensitivity or toxicities, as is understood by those skilled in the art. While pretreating typically comprises administering one to two doses of ICT (and, optionally, an anti-CTLA-4/LAG3 agent and/or a modulator of T_{REG} or M2-like TAM cells), it is understood that additional doses during the pretreatment stage are contemplated. For example, a pretreatment dose can be administered every one to four weeks, over the course of one to two months. In some embodiments, a total of four pretreatment doses are administered prior to MAPKi treatment begins.

[0042] In some embodiments, the administering of (b) begins two to eight weeks after the initiation of the pretreating of (a). In some embodiments, the administering of (b) begins two to five weeks after the initiation of the pretreating of (a). In some embodiments, the administering of (b) begins at least two weeks after the initiation of the pretreating of (a). In some embodiments, the administering of (b) begins at no later than eight weeks after the pretreating of (a). In some embodiments, the administering of (b) begins at no later than four weeks after the pretreating of (a).

[0043] For the method of suppressing melanoma metastasis in a subject, the pretreating of a subject in need of treatment for melanoma comprises administering one to one to two doses of ICT to the subject. In some embodiments, the melanoma metastasis is a brain metastasis. In some embodiments, the melanoma metastasis is an extracranial metastasis. The method can be further enhanced by combining the ICT pretreatment with administration of an anti-CTLA-4/LAG3 agent and/or a modulator of T_{REG} or M2-like TAM cells, as mentioned above. The method is of benefit to subjects at risk for brain metastases as well as those at risk of extracranial metastases. Subsequent to the pretreating step, the method further comprises administering to the subject a combination of MAPKi and ICT. Since therapeutic resistance of melanoma brain metastasis (MBM) limits patient survival, the sequencing of anti-PD-1/L1 (± anti-CTLA-4/LAG3 and/or modulator of T_{REG} or M2-like TAM cells) pretreatment before MAPKi combination suppresses MBM and improves survival with robust T-cell clonal expansion in both intracranial and extracranial metastatic sites.

[0044] In some embodiments, the method is a method of enhancing the inhibition of M2-like TAMs. In some embodiments, the pretreating further comprises administering a pharmacologic M2-like TAM inhibitor to the subject, in addition to the ICT. The inhibition of M2-like TAMs effects a selective upregulation of pro-inflammatory TAMs in the subject. The inhibition of M2-like TAMs effects a selective upregulation M1-like TAMs.

[0045] In some embodiments, the pretreatment comprises administering a CD25-T_{REG}-depleting antibody.

Kits & Compositions

[0046] The invention provides kits and/or compositions comprising one or more reagents and/or therapeutic agents suitable for use in the methods described herein, and optionally, one or more suitable containers containing reagents and/or agents of the invention. Such kits can comprise a carrier, package or container that is compartmentalized to receive one or more containers such as vials, tubes, and the like, each of the container(s) comprising one of the separate elements to be used in the method. The reagents and/or agents of the kit

may be provided in any suitable form, including frozen, lyophilized, or in a pharmaceutically acceptable buffer such as TBS or PBS.

[0047] Agents include an inhibitor of MAPKi, an anti-CTLA4 agent, an agonist of CD206, such as RP832c, and/or a modulator of regulatory T cells, such as CD25-T_{REG}-depleting antibody. Examples of CD25-T_{REG}-depleting antibodies include, but are not limited to, daclizumab. Agents can be provided in the form of a composition suitable for administration to a subject in accordance with the methods described here.

[0048] The kit of the invention will typically comprise the container(s) described above and one or more other containers comprising materials desirable from a commercial and user standpoint, including buffers, diluents, filters, needles, syringes, and package inserts with instructions for use. In addition, a label can be provided on the container to indicate that the composition is used for a specific application, and can also indicate directions for use, such as those described herein. Directions and or other information can also be included on an insert, which is included with the kit.

EXAMPLES

[0049] The following examples are presented to illustrate the present invention and to assist one of ordinary skill in making and using the same. The examples are not intended in any way to otherwise limit the scope of the invention.

Example 1: Anti-PD-1/L1 lead-In before MAPK inhibitor combination maximizes antitumor immunity and efficacy

[0050] This Example demonstrates that rationally sequencing and combining PD-1/L1- and MAPK-targeted therapies can overcome innate and acquired resistance. Since increased clinical benefit of MAPK inhibitors (MAPKi) is associated with prior immune checkpoint therapy, this Example compares the efficacies of sequential and/or combinatorial regimens in subcutaneous murine models of melanoma driven by $Braf^{V600}$, *Nras*, or *Nf1* mutations as well as colorectal and pancreatic carcinoma driven by $Kras^{G12C}$. Anti-PD-1/L1 lead-in preceding MAPKi combination optimizes response durability by promoting pro-inflammatory polarization of macrophages and clonal expansion of $IFNg^{hi}$, $CD8^+$ cytotoxic and proliferative (versus $CD4^+$ regulatory) T cells that highly express activation genes. Since therapeutic resistance of melanoma brain metastasis (MBM) limits patient survival, this Example demonstrates that sequencing anti-PD-1/L1 therapy before MAPKi combination suppresses MBM and improves mouse survival with robust T-cell clonal expansion in both intracranial

and extracranial metastatic sites. These results support brief anti-PD-1/L1 (± anti-CTLA-4) dosing prior to MAPKi co-treatment to suppress therapeutic resistance.

[0051] To date, the impact of shorter exposures to one therapy (to generate a priming effect) before switching to or combining with another therapy has not yet been evaluated. This sequential-combinatorial fusion may avoid the development of cross-resistance, raise the threshold for resistance evolution by stacking multiple therapeutic mechanisms of action, and permit one mode of therapy to prime responsiveness to the other, thereby creating synergy. Importantly, prior studies have implicated a role of antitumor immunity in prolonging, clinically and preclinically, the durability of MAPKi responses (Hong et al., 2021; Hugo et al., 2015).

[0052] Since prior ICT exposure seems to prime subsequent MEKi responsiveness in patients with *NRAS*^{MUT} melanoma (Dummer et al., 2017), we test the hypothesis that the same association exists in patients with *BRAF*^{V600MUT} melanoma. We also test the hypothesis that brief anti-PD-1/L1 dosing or lead-in before MAPKi combination maximizes antitumor efficacy and identify intratumoral immune cell phenotypes that associate with superior efficacy. Since MAPKi or ICT appears to be less durably active against intracranial (*vs.* extracranial) melanoma metastases (Flaherty et al., 2012; Ribas et al., 2016), we evaluate whether the optimal sequential-combinatorial regimen suppresses resistance in an organ-specific context. In particular, BRAFi + MEKi elicit lower response rates against clinical melanoma brain metastasis (MBM) (Davies et al., 2017), and clinically acquired MAPKi resistance emerges preferentially in the brain (Seifert et al., 2016). Thus, we develop a murine model of experimental melanoma metastases where MBM limits survival and compare the relative efficacies of anti-PD-1/L1 (± anti-CTLA-4) and MAPKi sequential-combinatorial regimens and their impacts on T-cell clonality.

[0053] **EXPERIMENTAL MODELS AND SUBJECT DETAILS**

[0054] Human subjects

[0055] Patient characteristics and sample sizes are presented in Table 1. Patients were enrolled in the S1320 clinical trial with informed consent obtained from all patients and participation of sites approved by local institutional review boards.

[0056] Mice

[0057] C57BL/6 and Balb/c (for subcutaneous models) were obtained from the Radiation Oncology breeding colony at UCLA (Los Angeles, CA). C57BL/6 (for experimental metastasis model) were purchased from Jackson Laboratory. Female mice were used at 6-8

weeks of age. All animal experiments were conducted according to the guidelines approved by the UCLA Animal Research Committee.

[0058] Subcutaneous syngeneic tumor models

[0059] For syngeneic subcutaneous tumor models, C57BL/6 (YUMM1.7ER, NIL, NILER1-4, mSK-Mel254 and KP4662) or Balb/c (CT26) mice were injected on both flanks with one million cells. Tumors were measured with a calliper every 2 days, and tumor volumes were calculated using the formula (length x width^2)/2. Once tumors reached a size of 120-140 mm^3, mice were assigned randomly into experimental groups. Special mouse diets (for C57BL/6 and Balb/c) were generated by incorporating trametinib at 1, 2, 3 or 5 mg/kg to facilitate daily drug dosing and to reduce animal stress (TestDiet). The combination of BRAFi+MEKi (PLX4032 50 mg/kg/day and trametinib 0.3 mg/kg/day; both resuspended in 10% DMSO with 0.1% methylcellulose) was administered to mice *via* oral gavage (subcutaneous model) or incorporated in chow (TestDiet). Anti-PD-L1 (200 μg/mouse, BioXcell), anti-PD-1 (300 μg/mouse for the first 2 doses, then 200 μg/mouse, Leinco Technologies) and anti-CTLA-4 (200 μg/mouse, BioXcell) were intraperitoneally administered twice per week. Anti-CD8 antibody was intraperitoneally administrated (200 μg/mouse, BioXcell) on day −1, day 0 or on day 6, day 7, and then twice a week. RP-832c was subcutaneously administrated (10 mg/kg, Riptide Bioscience) from day 0 to day 14, daily. On indicated days, tumors were excised from mice, minced, and digested to single-cell suspensions using a tumor dissociation kit and gentleMACS™ Octo Dissociator (Miltenyi Biotech) and prepared for CyTOF staining or/and 10X Genomics single cell RNA sequencing followed by sorting for live CD45$^+$ cells.

[0060] Experimental metastasis of syngeneic melanoma

[0061] YUMM1.7ER melanoma cells were engineered to express firefly luciferase (YUMM1.7ER-luc). Before every IC injection, cells were selected for stable luciferase expression by blasticidin treatment, yielding cells (1 million) that emitted luciferase light units of 5e8 to 5e9 *in vitro*. C57BL/6 (6-8 weeks old, female), after anesthesia with vaporized isoflurane (2.0-2.5%), were injected with 1×10^6 cells/mouse into the left ventricle for intracardiac inoculation. Progression of metastatic tumor burden and treatment effects in mice were monitored *in vivo* and *ex vivo* by bioluminescent imaging (BLI). We acquired BLI on both ventral and dorsal sides twice weekly until study endpoints (total ventral or dorsal BLI signal in the range of 1e9-1e10, moribund, or death). Mice were anesthetized with vaporized isoflurane; D-luciferin (150 mg luciferin/kg, Caliper Life Sciences) dosed by intraperitoneal injections; and, 10 minutes after injections, luciferase activities were measured with IVIS Lumina II Imaging System (PerkinElmer). Image analysis was performed

with Living Image 4.7.2 Version (PerkinElmer). For *ex vivo* BLI, mice were euthanized 10 minutes after intraperitoneal injection of D-luciferin by cervical dislocation and organs were excised and imaged *ex vivo* by the IVIS system. Special mouse diets (for C57BL/6 mice) were generated by incorporating trametinib at 1 mg/kg/day or PLX4032 at 50 mg/kg/day plus trametinib at 0.3 mg/kg/day to facilitate daily drug dosing and to reduce animal stress (TestDiet). Anti-PD-L1 (200 μg/mouse, BioXcell) or anti-PD-1 (200 μg/mouse, Leinco Technologies) was intraperitoneally administered twice per week. Anti-CTLA-4 (200 μg/mouse, BioXcell) was intraperitoneally administered every four days starting at d-4 and ending d+4. We visualized BLI data on a logarithmic scale (means and corresponding standard deviations). Down error bars were not presented when they extended to zero or negative values. For mice in the experimental metastasis model treated with MEKi + anti-PD-L1 regimens, mice with no BLI signal beyond background for > ~60 days after starting treatment were deemed to have unconfirmed complete responses (CRs). For mice in the experimental metastasis model treated with BRAFi + MEKi + anti-PD-1/L1 regimens, mice with no BLI signal beyond background for ~75-100 days after starting treatment were deemed to have unconfirmed complete responses (CRs). To confirm CRs in these mice, treatment was stopped. Mice were confirmed to display complete CRs if only background radiance was detected twice weekly for two consecutive months after treatment cessation or until the experimental endpoint (death by euthanasia in situations of deteriorating health), whichever comes first. If tumor burden becomes detectable after treatment cessation, the protocol in the flowchart (Figure 10E) was followed.

[0062] Cell lines

[0063] All mouse cancer cell lines were routinely tested for mycoplasma and profiled and identified by RNA-seq and the GenePrint 10 system (Promega) at periodic intervals during the course of this study for banking and experimental studies. All cell lines were maintained in either DMEM (YUMM1.7ER, YUMMER1.7-luc, NIL, NILER1-4, mSK-Mel254 and KP4662) or RPMI (CT26) supplemented with high glucose with 10% heat-inactivated FBS (Omega Scientific) and 2 mM glutamine in humidified, 5% CO2 incubator. To establish YUMM1.7ER-luc, the pHIV-Luc-Zsgreen vector (Addgene) was subcloned into the lentiviral vector pLV-EF1a-IRES-Blast (Addgene). YUMM1.7ER cells transduced by luciferase-expressing lentiviruses were selected using blasticidin (Sigma-Aldrich).

[0064] **METHOD DETAILS**

[0065] Mass cytometry of murine tumors

[0066] $2x10^6$ or fewer cells were incubated with 2% of FBS in PBS with 25 μg/mL of 2.4G2 antibody at 4°C for 10 min prior to surface staining with an antibody cocktail at 4°C for

30 min in a 50 μL volume. Cells were incubated with 2.5 μM 194Pt monoisotopic cisplatin (Fluidigm) at 4°C for 1 min. Cells were then washed twice with FACS buffer and barcoded using palladium metal barcoding reagents according to manufacturer's protocol (Fluidigm). Subsequently, fixation and permeabilization were performed using the Foxp3 fix and permeabilization kit according to the manufacturer's protocol (Fluidigm). Cells were then stained with an intracellular stain antibody cocktail (Foxp3, Ki67, granzyme B, T-bet, iNos, Eomes) for 30 min at room temperature. Cells were then washed twice with Foxp3 permeabilization buffer, twice with FACS buffer, and incubated overnight in 1.6% PFA PBS with 100 nM iridium nucleic acid intercalator (Fluidigm). Cells were then washed twice with PBS with 0.5% BSA, filtered, and washed twice with water with 0.1% BSA prior to analysis. Samples were analyzed using a Helios mass cytometer based on the Helios 6.5.358 acquisition software (Fluidigm).

[0067] Single cell 5' gene expression and V(D)J sequencing

[0068] Four different tumors per regimen and per time point were dissociated to single-cell suspensions using a tumor dissociation kit (Miltenyi Biotech) and gentleMACS™ Octo Dissociator (Miltenyi Biotech). $5X10^5$ cells per tumor were pooled together ($2X10^6$ in total) as one sample for each regimen and each time point. Cells were incubated with 20% FBS in PBS with 25 mg/mL of anti-mouse CD16/CD32 antibody (eBioscience) at 4°C for 10 min to minimize background antibody binding. Then cells were stained with BV510-anti-CD45 (1 mg/mL, Biolegend) and PerCP-anti-TER119 (2 mg/mL, Biolegend) at room temperature for 20 minutes, followed by 7AAD (10 mL in 500 mL PBS per sample, BD Pharmigen) staining for 5 minutes on ice. Cells after staining were sorted by BD FACSAria II sorting system to harvest the BV510 (CD45) positive and PerCP (TER119, 7AAD) negative population as live $CD45^+$ cells. Cells recovered were subjected to 10X Genomics standard protocol for coupled scRNA-seq and scTCR-seq library preparation using Chromium Next GEM Single Cell 5' Library and Gel Bead Kit v1.1 (10X Genomics) and V(D)J Enrichment Kit for Mouse T Cells (10X Genomics). Libraries were sequenced by Novaseq 6000 S2 flow cell with 2X50 reads targeting a minimum of 20,000 read pairs per cell for scRNA-seq library and 5,000 read pairs per cell for scTCR-seq library.

[0069] Generation of bulk tumor TCR-seq data

[0070] Total RNA was extracted from frozen tissue stored in RNALater using the QIAGEN All Prep DNA/RNA Mini Kit. RNA quality was measured using Bioanalyzer (Agilent). 710 ng-1,000 ng of RNA from ovary and brain tissues (RNA Integrity Number (RIN) score > 7) was used as input to construct libraries with the QIAGEN QIAseq Immune Repertoire RNA Library Kit – T cell Receptor Panel (Qiagen). Briefly, RNA was reverse transcribed using a

pool of TCR gene-specific primers against the constant region for the T cell receptor alpha, beta, gamma, and delta genes. The resulting cDNA was then ligated to an oligo containing one side of sample index and unique molecular index (UMI). After reaction cleanup, a single primer extension was used to capture the T cell receptor using a pool of gene-specific primers. The resulting captured sequences were amplified and purified using QIAseq beads. Libraries were then sample-indexed on the other side by using a unique sample index primer and an universal primer to amplify the library and introduce platform-specific adapter sequences. The dual-indexed sample PCR fragment was purified and then quantified for absolute quantification of amplifiable libraries (DNA with adaptors at both ends) in triplicate by real-time qPCR using QIAGEN QIAseq Library Quant Array Kit. For sequencing, each library was diluted to 4 nM, pooled, and denatured. 12 pM of denatured library pool was run with QIAseq A Read1 Primer on Illumina NextSeq 500 Mid Output Kit using v2.5 chemistry for 300 cycles with an asymmetrical paired end 261/41 bp read for CDR3 region.

[0071] Tissue staining

[0072] For immunofluorescence (IF), tissues were fixed in formalin followed by embedding in paraffin. After deparaffinization and rehydration, tissue sections were subjected to heat for antigen retrieval. After tissue sections were permeabilized and blocked, primary antibodies (phospho-ERK1/2 (Cell Signaling Technology, #4370)) were added overnight. IF was performed with Alexa Fluor–conjugated secondary antibodies (Life Technologies, #A21429). Nuclei were counterstained by DAPI (ThermoFisher Scientific). Signals were captured with a Zeiss microscope (AXIO Imager A1) mounted with a charge-coupled device camera (Retiga EXi QImaging), and the images captured by Image-pro plus 6.0.

[0073] A detailed listing of all reagents and resources used in these methods is available at Wang et al., 2021, Cancer Cell 39, 1375–1387. Raw sequencing files of scRNA-seq, scTCR-seq, and bulk TCR-seq data have been deposited at GEO (GSE177902) and are publicly available.

[0074] **QUANTIFICATION AND STATISTICAL ANALYSIS**

[0075] Clinical trial data analysis

[0076] Details of S1320 (ClinicalTrials.gov Identifier: NCT02196181; SWOG Identifier: S1320) have been published with the primary outcome manuscript (Algazi et al., 2020). Association between prior ICT and categorical and quantitative variables were compared using Fisher's exact and Wilcoxon tests, respectively. PFS and OS were estimated using the Kaplan-Meier method, and Cox regression models were used to evaluate associations.

[0077] CyTOF data analysis

[0078] Mass cytometry flow cytometry standard (FCS) data files were concatenated, bead-normalized and debarcoded using Helios software (Fluidigm), and then exported into individual files for each sample. Total $CD45^+$ and $CD8^+$ and $CD4^+$ T-cell populations were manually identified and exported using negative and positive gating strategies of lineage markers in Cytobank (Kotecha et al., 2010). We applied Cytofkit (Chen et al., 2016) to perform the t-Distribution Stochastic Neighbor Embedding (t-SNE) analysis separately on the manually gated $CD45^+$, $CD4^+$ and $CD8^+$ populations. We selected 5,000 (in sub-clustering $CD45^+$) or 2,000 events (in sub-clustering $CD4^+/CD8^+$ T-cells) in each sample to ensure equal representation of cells across samples. All the cell lineage markers in the immune panel were used in $CD45^+$ analysis. For T-cell analysis, all markers excluding the following were used: CD90, CD14, F480, Ly6G, CXCR2, CD19, and CD335. We chose the 3,000 iterations, perplexity of 30 and theta of 0.5, as the standard t-SNE parameters. Mean intensity values of markers in each cluster were calculated and visualized *via* heatmaps. Cells were assigned to different functional populations on the basis of the local gradient expression of known cell lineage markers. The percentages of different immune cell subsets were calculated for each sample.

[0079] Analysis of scRNA-seq data

[0080] Alignment to GRCm38 reference genome, barcode and unique molecular identifier (UMI) counting were performed using Cell Ranger (10x Genomics, v2.1.0). Seurat package (Butler et al., 2018) was used for downstream analysis. Cells with fewer than 500 genes detected or greater than 10% mitochondrial RNA content were excluded from further analysis. Raw UMI counts were normalized to UMI count per million total counts and log-transformed. Variable genes were detected based on average expression and dispersion for each dataset independently. We then use CellCycleScoring function to calculate scores of S and G2/M cell cycle phases for each cell. Single cells from different conditions were integrated into a single assay based on variable genes identified from each sample. We then use the ScaleData function to calculate scaled z-scores of each variable gene in the integrated assay and regress out the effect of number of genes per cell, mitochondrial RNA content, and cell cycle scores (S phase score and G2/M phase score). This scaled data set was then used for principal component analysis (PCA) for cells. Clusters and UMAP projections were generated based on the top 30 PCA dimensions. Clusters were annotated based on expression of known marker genes, including *Cd14* (myeloid), *Igtam*, *Csf1r* (monocyte/macrophage), *Flt3* (dendritic cell), *S100a8*, *S100a9* (neutrophil), *Ncr1* (NK cell), *Cd19*, *Cd79a* (B-cell), *Cd3d*, *Cd3e*, *Cd3g* (T-cell). Cell clusters co-expressing markers of multiple cell types were defined as doublets and excluded from further analysis. We next isolated the monocyte/macrophage and T-cell populations identified from the broad

clustering analysis and performed re-clustering analysis on them separately. Cells were re-clustered as described above and functional subpopulations were inferred and annotated by identifying differentially expressed marker genes with log-fold change higher than 0.4 using MAST in FindAllMarkers function. The pro/anti-inflammation ratio in the macrophage population was calculated as the fold changes of proportions between the inferred pro- *vs.* anti-inflammatory clusters. For the identified $CD8^+$ T-cell subpopulations, we calculated the score of *Tcf1+* stem-like signature for each cell by using Seurat's AddModuleScore function based on the gene sets previously reported (Siddiqui et al., 2019).

[0081] Analysis of scTCR-seq data

[0082] Alignment to the GRCm38 reference genome and TCR contig annotation were performed by Cell Ranger vdj pipeline (10x Genomics, v2.1.0). For the TCR clonotype analysis, only cells assigned with both productive TRA and TRB sequences were kept for further analysis. If one cell had two or more TRA-TRB pairs identified, the pair with higher UMIs was considered as the dominant TRA-TRB pair in the corresponding cell and used in the analysis. We defined each unique TRA-TRB pair as a clonotype. The clonal status of TCR clones were characterized as non-clonal ($n = 1$) and clonal ($n \geq 2$) based on their cell numbers. The TCR clonotype of each cell was further linked to inferred functional subsets based on the barcode information. We used STARTRAC package to calculate the expansion and transition indices of distinct T-cell subsets.

[0083] Bulk tumor TCR-seq data analysis

[0084] As reported previously (10), raw reads were submitted to the QIAGEN GeneGlobe Data Analysis Center (qiagen.com/us/shop/genes-and-pathways/data-analysis-center-overview-page/) to estimate the abundance of reads of unique CDR3 sequence and generate TCR clonotype calls. R package tcR (Nazarov et al., 2015) was used to perform all the statistical analysis for TCR repertoires, including: i) size of large clones with frequency not less than 5%; ii) diversity estimates using ecological diversity and Gini-Simpson indices, and iii) common TCR repertories (identified based on unique alpha or beta chains' CDR3 sequences) shared by distinct tumor-involved regions within an organ tissue or by different organ tissues.

[0085] Statistical analysis of non-clinical data

[0086] No statistical methods were used to predetermine sample size. We used the paired t-test to determine the statistical significance of differences between two variables. Survival curves were compared *via* the logrank test. We applied the linear mixed effects model on the log_{10}-transformed BLI intensity data. In this model, treatment group, days, and treatment*day interactions were treated as fixed effects, while a random intercept and time slope were

assumed for individual mouse. Pairwise comparisons between treatment regimen groups were conducted within the mixed model framework with Bonferroni correction for multiple testing. All other statistical analyses were carried out using R and GraphPad Prism 7.

[0087] **RESULTS**

[0088] Prior ICT enhances MAPKi responses in melanoma patients

[0089] In a trial of the MEKi binimetinib *vs.* dacarbazine for patients with *NRAS*^{MUT} melanoma, greater clinical benefit (median progression-free survival or PFS, confirmed overall response, and median duration of objective response) of binimetinib was associated with prior ICT (Dummer et al., 2017). S1320 was a phase 2 randomized clinical trial comparing intermittent (n = 101) versus continuous (n = 105) dosing of the BRAFi dabrafenib and MEKi trametinib for *BRAF*$^{V600E/K}$ metastatic melanoma. The trial randomized patients between 2013 and 2019. After an eight-week lead-in period of continuous treatment, patients who did not progress were randomized to either continuous or intermittent dosing of both drugs on a 3-week-off, 5-week-on schedule. As reported (Algazi et al., 2020), PFS was longer with continuous *vs.* intermittent dosing. Prior exposure to ICT was a randomization stratification factor in the trial, with 61 patients (30%) with prior exposure (anti-CTLA-4 alone, n = 21; anti-PD-1 alone, n = 22; anti-CTLA-4 and anti-PD-1 separately, n = 6; anti-PD-1 alone and anti-PD-1 + anti-CTLA-4 separately, n = 1; anti-PD-1, anti-CTLA-4, anti-PD-1 + anti-CTLA-4 separately, n = 1; unknown, n = 4). Patient characteristics were similar between patients who did and did not have prior ICT (Table 1). PFS was longer among patients with prior ICT on univariate (hazard ratio (HR) = 0.64, 95% confidence interval (CI) 0.44-0.92, p = 0.017) and multivariable analysis (HR = 0.60, 95% CI 0.47-0.77, p = 0.009; Figure 1; Table 2A). There were no significant differences in overall survival (**OS**) by prior ICT on univariate (HR = 0.86, 95% CI 0.54-1.35, p = 0.51) or multivariable analysis (HR = 0.85, 95% CI 0.63-1.17, p = 0.52; Figure 7, Table 2B). There was no evidence of heterogeneity in these results by treatment arm (interaction p-value = 0.55 for PFS, p = 0.67 for OS).

[0090] Anti-PD-1/L1 lead-in preceding MAPKi combination optimizes antitumor efficacy

[0091] Using syngeneic subcutaneous tumor models, we tested whether brief anti-PD-L1 (or anti-PD-1) pretreatments (two doses over one week) can improve subsequent responses to MEKi, with or without continuing anti-PD-L1 dosing with MEKi. We defined time at which the average tumor volumes reach 120-140 mm^3 as day 0 (d0) and d0 to d7 as the anti-PD-1/L1 lead-in period (Figure 2A). We treated tumor-bearing mice in the following control (no active treatment, single-agent treatment, or simultaneous combination treatment) groups: (i) vehicle (starting on d7), (ii) anti-PD-L1 (starting on d0, d7 or from d0 to d7 only), (iii) MEKi (starting on d0 or d7), and (iv) MEKi + anti-PD-L1 (simultaneously starting on d0 or d7). We expected

superior antitumor activity with anti-PD-L1 lead-in before MEKi dosing in two experimental groups: (i) MEKi d7, anti-PD-L1 d0 to d7 (anti-PD-L1 started on d0 and stopped on d7 followed by MEKi started on d7), and (ii) MEKi d7, anti-PD-L1 d0 (anti-PD-L1 started on d0 followed by MEKi started on d7, while continuing anti-PD-L1) (Figure 2A). Trametinib dose level for each tumor model was chosen based on the minimal dose required to elicit tumor stabilization or regression early on-treatment and near complete p-ERK suppression on day 3 (Figure 8A). We used six murine syngeneic tumor models: (i) $Braf^{V600E}$ melanoma with high mutational burden (YUMM1.7ER; Figure 2B) (Wang et al., 2017), (ii) $Nras^{Q61R}$ melanoma (NIL; Figure 2C) (Hong et al., 2018), (iii) $Nras^{Q61R}$ melanoma with high mutational burden (NILER1-4; Figure 2D) (Hong et al., 2021), (iv) $Nf1^{-/-}$ melanoma (mSK-Mel254; Figure 2E), (v) $Kras^{G12C}$ colorectal carcinoma (CT26; Figure 2F), and (vi) $Kras^{G12C}$ pancreatic adenocarcinoma (KPC; Figure 2G).

[0092] In all models, anti-PD-L1 treatment alone (d0, d0 to d7, or d7) had minimal (YUMM1.7ER, NILER1-4, mSK-Mel254) to no (NIL, CT26, KPC) tumor growth-inhibitory effect (Figures 2B to 2G). In all models (Figures 2B to 2G), at the trametinib doses chosen, treatment with MEKi d7 vs. MEKi d7, anti-PD-L1 d7 elicited only transient tumor regression and small differences, if any, in the average tumor volumes over time. In general (Figures 2B and Figures 2D to 2G), MEKi d0 or MEKi d0, anti-PD-L1 d0 (i.e., treatments started on smaller tumors) still did not improve the durability of antitumor activities, except in CT26 (MEKi d0, anti-PD-L1 d0 vs. MEKi d7, anti-PD-L1 d7; $p < 0.008$). In one tumor model (mSK-Mel254) (Figure 8B), using MEKi started on d0 against smaller tumors, we observed that the efficacies of regimens MEKi d0, anti-CTLA-4 d0 and MEKi d0, anti-PD-L1 d7 were lower than that of the regimen MEKi d0, anti-PD-L1 d0. Thus, anti-CTLA-4 and delayed dosing of anti-PD-L1 (vs. MEKi) were not studied further in subcutaneous tumor models. Importantly, between the two regimens we hypothesized to elicit the most robust antitumor activity, anti-PD-L1 lead-in followed by MEKi combination consistently led to the most extensive and durable tumor regression (Figures 2B to 2G). This regimen was either not associated with body weight loss or associated with a weight loss that was < 10% compared to any other concurrent regimen. In contrast, the efficacy of the regimen of MEKi d7, anti-PD-L1 d0 to d7 was not superior to the efficacies of the regimens MEKi d7 or MEKi d7, anti-PD-L1 d7. Thus, brief dosing with anti-PD-L1 prior to its combination with MEKi in MAPK-addicted tumor models overcame anti-PD-L1 innate resistance and delayed acquired MEKi resistance.

[0093] Using mSK-Mel254, we tested whether anti-PD-1 would produce a similar priming effect (Figure 2H). As with anti-PD-L1 d0 (Figure 2E), anti-PD-1 d0 yielded little to no tumor growth inhibition. Clearly, the regimen of MEKi d7, anti-PD-1 d0 was superior to the regimen of MEKi d7, anti-PD-1 d7 (Figure 2H). Using YUMM1.7ER, we also tested regimens

containing the combination of BRAFi + MEKi. We started BRAFi + MEKi ± anti-PD-L1 treatments either on d0 or d7. For the latter group (starting on d7), we tested the impact of anti-PD-L1 lead-in (2 doses). Consistent with previous data using MEKi alone (Figure 2B), anti-PD-L1 lead-in followed by BRAFi + MEKi combination consistently led to the most durable antitumor activity (Figure 2I), which was associated with mice weight loss that was < 10% compared to any other concurrent regimen.

[0094] Pro-inflammatory TAM polarization distinguishes the tumor microenvironment after sequential-combinatorial therapy

[0095] To identify immune cell alterations specifically elicited by the regimen of anti-PD-L1 lead-in prior to MEKi combination, we sampled tumors (n = 3-4/group) with vehicle or anti-PD-L1 (priming) treatments on d7 and tumors (n = 3-4/group) on d10 and d14 in four regimens: (i) MEKi d7, (ii) MEKi d7, anti-PD-L1 d7, (iii) MEKi d7, anti-PD-L1 d0 to d7, and (iv) MEKi d7, anti-PD-L1 d0 (Figure 2A). Dissociated cells from three tumor models (YUMM1.7ER, mSK-Mel254, CT26) were subjected to analysis by an immune cytometry by time-of-flight (CyTOF) panel published previously (Hong et al., 2021). We found that the three tumor models were highly distinct in the levels of infiltration by $CD45^+$ cells, which ranged from 20-80% without treatment or after two doses of anti-PD-L1 treatments (Figure 8C). These percentages increased (YUMM1.7ER), decreased (mSK-Mel254), or decreased and then increased (CT26) over time after MEKi-containing treatments (Figure 8C). Among $CD45^+$ cells, two doses of anti-PD-L1 increased the abundance of $CD8^+$ T cell (*vs.* vehicle) only in YUMM1.7ER tumors (Figure 8D). After MEKi-containing treatments (*vs.* vehicle treatment), the percentages of $CD8^+$ T cells among $CD45^+$ cells increased only in YUMM1.7ER and CT26, but these increases did not associate with treatment efficacy (Figure 8D).

[0096] Among $CD45^+$ cells in all treatment groups, tumor-associated macrophages (TAMs) were the most abundant subpopulation across the three tumor models (Figures 2J and 8D). We identified 6-9 TAM subpopulations across the three tumor models (Figure 2J). iNOS-high or $iNOS^+$ M1-like TAMs were identified in 6 of 9 and 6 of 8 TAM subpopulations in YUMM1.7ER and mSK-Mel254 but only in 1 of 6 TAM subpopulations in CT26 (Figure 2J). Despite these differences, we observed specific induction of $iNOS^+$ M1-like TAMs only in the regimen of MEKi d7, anti-PD-L1 d0 (Figure 2K). Moreover, after sub-clustering $CD4^+$ T-cells, we found that Th1-like (T-bet high) $CD4^+$ T cells were also specifically induced only in the regimen of MEKi d7, anti-PD-L1 d0 (Figure 8E). After sub-clustering $CD8^+$ T-cells, we found that two doses of anti-PD-L1 elevated the levels of granzyme B-high $CD8^+$ cytotoxic T-cells (T_C) (Figures 8F and 8G). However, this elevation was not maintained after initiating any

MEKi-containing regimen (YUMM1.7ER) or not specifically maintained in the most efficacious regimen (mSK-Mel254, CT26) (Figure 8G).

[0097] We sought to corroborate TAM findings above (Figure 2K) at the transcriptomic level. Sorted CD45$^+$ cells from four mSK-Mel254 tumors per regimen, per time point (Figure 2A) were admixed and then subjected to coupled 5' single-cell RNA-sequencing (scRNA-seq) and T-cell receptor-sequencing (scTCR-seq). In total, data from 53,841 CD45$^+$ cells passed quality control. Based on expression profiles of known lineage marker genes, we annotated seven major immune cell types, including monocyte/macrophages (Mo/MΦ), T cells, B cells, natural killer (NK) cells, tumor-associated neutrophils (TANs), and two dendritic cell (DC) subsets (monocyte-derived DC and classical DC) (Figures 3A, 9A and 9B). Consistent with CyTOF analysis (Figures 2J and 8D), TAMs constituted the most abundant CD45$^+$ subpopulation, followed by T cells (Figure 9C). Re-clustering the monocyte/macrophage population identified seven sub-populations (Figures 3B, 3C and 9D). Cells in MΦ1 and MΦ3 displayed significant upregulation of pro-inflammatory genes (e.g., *Neat1*, *Malat1*, *Cxcl9*, and *Cxcl10*). MΦ2, MΦ4, and MΦ5 subpopulations upregulated anti-inflammatory genes (e.g., *Apoe*, *C1qa*, *Chil3*, and *Arg1*). One subpopulation (Mo->MΦ) highly-expressed *Ccrl2*, *Il1b*, and *Rgs1*, suggesting monocytes transitioning into to macrophages. We then calculated the pro- *vs.* anti-inflammatory ratios and found that two lead-in doses of anti-PD-L1 (*vs.* vehicle treatment) enhanced this ratio from < 1 to > 1 (Figure 3D). However, this enhanced ratio was reversed subsequently with any MEKi-containing regimen, except the most efficacious regimen (MEKi d7, anti-PD-L1 d0), which further enhanced this ratio on day 10 (Figure 3D).

[0098] Activated, proliferative, and cytolytic CD8+ T-cell gene expression tracks with optimized regimen

[0099] We next analyzed the T-cell population (n = 13,803 cells) using coupled scRNA- and scTCR-seq. By sub-clustering, we identified nine T-cells subpopulations (Figures 3E and 3F). These included three CD8$^+$ subpopulations (naïve, T_C and Ki-67^{hi}); three CD4$^+$ subpopulations (naïve, regulatory or T_{REG}, T helper 1/2 or Th1/h2 that co-expressed Th1 and Th2 genes such as *Cxcr3* and *Gata3*), NK T cells or NKTs, interferon (Ifn)-stimulated T cells, and gamma-delta T cells ($T_{\gamma\delta}$). As predicted, two lead-in doses of anti-PD-L1 elevated CD8$^+$ T_C levels (Figure 9E). Importantly, these elevated CD8$^+$ T_C levels were either maintained or surpassed with subsequently switching to or combining with MEKi (Figure 9E). By d14 in tumors treated with MEKi d7 or MEKi d7, anti-PD-L1 d7, CD8$^+$ T_C levels dropped clearly below that in the vehicle-treated tumors.

[0100] Among 7,017 TCR clonotypes identified with unique a and b chain pairs, 350 were represented by two or more cells, which resulted in 1,384 clonal T cells (Figure 3G). We

calculated the expansion indices across all nine T-cell subpopulations and observed that CD8$^+$ T_C cells harbor the highest degree of clonal expansion, followed by the Ki-67^{hi} CD8$^+$ T cells (Figure 3H and Table 3). Consistently, clonal T cells were concentrated in the T_C subpopulation (Figures 3E and 3G). Interestingly, transition index analysis associated Ki-67^{hi} CD8$^+$ T cells with T_C subpopulations (Figure 3I), suggesting a differentiation trajectory from proliferative CD8$^+$ T cells to the clonally expanded T_C subpopulation. We then calculated the ratios of expansion indices of CD8$^+$ T_C or Ki-67^{hi} CD8$^+$ T cells to T_{REG} to estimate the net antitumor status in each regimen and time point. Two lead-in doses of anti-PD-L1 increased both ratios, the elevation of which was either maintained or surpassed after MEKi combination (Figure 3J). In tumors treated with MEKi d7 or MEKi d7, anti-PD-L1 d7 (i.e., no prior priming doses of anti-PD-L1), these ratios persisted at low levels near that observed in the vehicle-treated group. When we examined the transition indices of CD8$^+$ T_C from Ki-67^{hi} CD8$^+$ T cells over time, we observed increased transition after anti-PD-L1 lead-in doses, and this transition was maintained and highest at both subsequent time points in and only in tumors on the regimen of MEKi d7, anti-PD-L1 d0 (Figure 3K).

[0101] To corroborate the specific association of CD8$^+$ T_C and Ki-67^{hi} T cells with the most efficacious regimen, we analyzed the largest (i.e., most expanded) TCR clonotypes (Table 3), stemness, or expression of specific functional genes. The fold changes in the total clone size of top 5 or top 10 TCR clonotypes of either CD8$^+$ T_C or Ki-67^{hi} T cells were calculated compared to that of CD4$^+$ T_{REG} cells. This revealed that the most efficacious regimen yielded the highest expansion of top T_C clonotypes (vs. T_{REG}) at both time points and of top Ki-67^{hi} CD8$^+$ T cell clonotypes (vs. T_{REG}) at the last time point (Figure 3L). Tcf1$^+$ stem-like CD8$^+$ T cells are thought to be critical for tumor control in response to ICT (Siddiqui et al., 2019). Hence, we scored CD8$^+$ T cell subpopulations for enrichment of this signature across regimens and time points (Figure 9F). For the Ki67^{hi} CD8$^+$ T cell subpopulation, this score trended higher (*vs.* vehicle treatment) after two anti-PD-L1 lead-in doses and stayed high on d10 only in the most efficacious regimen. By d14, this score dropped across all MEKi-containing regimens but remained highest in the tumors from the most efficacious regimen. Moreover, we visualized the expression levels of functional genes across T-cell subpopulations (Figure 9G). We noted that the critical gene, *Ifng*, was expressed (Figures 3M and 9G) by most CD8$^+$ T_C and Ki-67^{hi} T cells, supportive of their antitumor functional importance. Critically, within the T_C subpopulation, two anti-PD-L1 lead-in doses upregulated the expression of activation genes (*Cd44*), inhibitory genes (*Lag3*, *Ctla4*, *Havcr2*), cytolytic genes (*Prf1*, *Gzmb*), and effector genes (*Ifng*) (Figure 3N). On d10, treatment on the most efficacious regimen led to the highest levels of activation/exhaustion gene (*Pdcd1*) and *Ifng*. By d14, treatment on the most efficacious regimen led to the highest expression of both *Pfr1*

and *Gzmb* and the highest ratio of *Pdcd1* to *Tox*, the master regulator of T-cell exhaustion. Interestingly, MEKi monotherapy induced the highest levels of *Ctla-4* at both time points (Figure 3N), suggesting anti-CTLA-4 antibody as a combinatory agent. *Foxp3* expression was down-regulated in T_{REG} specifically in the most efficacious regimen (Figure 9G).

[0102] Functional contributions of TAM polarization and CD8+ T cells

[0103] We assessed whether targeting of M2-like TAMs by a peptide agonist of CD206 (Ghebremedhin et al., 2020; Jaynes et al., 2020) would augment the priming effects of anti-PD-L1 (Figure 4A). Using the mSK-Mel254 model, we observed that the CD206 agonist, RP832c, on its own (dosed from d0 to d14) elicited a small degree of growth inhibition, but, on top of MEKi d7, CD206 peptide d0 to d14, elicited no priming effect (Figure 4A). However, combining the CD206 agonist with anti-PD-L1 improved priming, as the regimen of MEKi d7, anti-PD-L1 d0, CD206 peptide d0 to d14 elicited deeper and more durable tumor regression when compared to the regimen of MEKi d7, anti-PD-L1 d0 (Figure 4A). We also tested using mSK-Mel254 whether neutralizing $CD8^+$ T cells systemically would diminish or abolish the priming effect of two doses of anti-PD-L1. In the context of two regimens (MEKi d7; MEKi d7, anti-PD-L1 d7) without anti-PD-L1 lead-in (Figure 4B), $CD8^+$ T-cell neutralization had no impact on tumor regression or resistance development. This lack of effect is consistent with the lack of additivity when MEKi is initiated with anti-PD-L1 on established (700-900 mm^3) tumors (Figures 2B to 2G). Moreover, when we neutralized $CD8^+$ T cells, we reversed the growth deceleration effect elicited by the two priming anti-PD-L1 doses from d0 to d7 (Figure 4C). Importantly, while $CD8^+$ T-cell neutralization did not change the onset of acquired resistance in the regimen MEKi d7, anti-PD-L1 d0 to d7, it abolished the benefit (i.e., durability of tumor regression) of the regimen MEKi d7, anti-PD-L1 d0 (Figure 4C).

[0104] PD-1/L1 plus CTLA-4 blockade before MAPKi combination prolongs MBM suppression and survival of mice

[0105] Since responses of MBM to therapies may be inferior, we tested sequencing-combinatorial regimens for their antitumor impacts across multiple organ sites. We engineered $Braf^{V600E}$ (YUMM1.7ER) melanoma cells to express luciferase and injected YUMM1.7ER-Luc cells into the left ventricle. By *in vivo* bioluminescence imaging (BLI), dissemination of $Braf^{V600E}$ melanoma cells resulted in tumor growth in 100% of mice in both intracranial and extracranial sites 8d after intracardiac (IC) injection (Figure 5A). *In vivo* BLI signals (ventral or dorsal extracranial and intracranial) grew from a nadir on d3 to d4 after IC injection and surpassed an average of 1e9 by ~d21 after IC injection (Figures 5B to 5E and 10A). Median survival of untreated mice (defined in Figure 5B) was 3.5 weeks after IC injection (n = 19) (Figure 5F). When the dorsal intracranial BLI signals averaged 1e6-1e7 on

day 8 (when 100% of mice harbored MBM) after IC injection, we designated this time point of initiating MEKi-containing regimens as d0 (Figure 5A). At necropsy when untreated mice were moribund, *ex vivo* BLI revealed tumor burden in the lung, adrenal glands, ovaries, pancreas, and brain in 100% of mice (Figure 5B) as well as in the kidney (6/13 or 46%), heart (9/13 or 69%), and liver (6/13 or 46%) (Figure 10B).

[0106] To evaluate impacts on multi-organ metastatic growth, we compared the following regimens: (i) anti-PD-L1 d-4 or d0; (ii) MEKi d0; (iii) MEKi d0 plus anti-PD-L1 d-4, d0, or d4 (Figure 5A). Although anti-PD-L1 d0 elicited no discernable impact on extracranial or intracranial metastatic growth (Figures 5C, 5D, 10C and 10D), anti-PD-L1 d-4 suppressed MBM (Figures 5D and 10D) and extended survival (Figure 5F). MEKi d0 clearly reduced extracranial metastatic tumor burden in surviving mice past 4 weeks (Figures 5B, 5C, 5E, and 10C) but only delayed MBM by ~1.5 weeks (Figures 5B, 5D, 5E, S4C and S4D), which limited the survival benefit of MEKi monotherapy (Figure 5F) (Davies et al., 2017; Seifert et al., 2016). Comparing among the group (iii) regimens, we observed that the regimen of MEKi d0, anti-PD-L1 d-4 was superior in controlling both extracranial and intracranial tumor burdens (Figures 5C, 5D, S4C and 10D). Survival of mice on the regimen of MEKi d0, anti-PD-L1 d-4 was superior to that in every other group, except the regimen of MEKi d0, anti-PD-L1 d0 (Figure 5E). In contrast, survival of mice on the regimen of MEKi d0, anti-PD-L1 d0 was not significantly superior to that on any other group except for the no treatment group and the anti-PD-L1 monotherapy groups (Figure 5F). Thus, in mice with metastatic *Braf*^{V600E} melanoma, two doses of anti-PD-L1 prior to its combination with MEKi overcame innate anti-PD-L1 resistance and delayed acquired MEKi resistance in MBM.

[0107] We further evaluated the two most efficacious group iii regimens, namely MEKi d0, anti-PD-L1 d-4 and MEKi d0, anti-PD-L1 d0, by substituting MEKi monotherapy with BRAFi + MEKi combo therapy. As expected, both of these regimens were superior in efficacy to BRAFi + MEKi (Figure 5G). Importantly, the regimen of BRAFi + MEKi d0, anti-PD-L1 d-4 (median survival, not reached at 10 weeks) trended ($p = 0.0543$) toward greater survival benefit compared to the regimen of BRAFi + MEKi d0, anti-PD-L1 d0 (median survival of 4 weeks) (Figure 5G). We devised a protocol to follow surviving mice longer-term, up to about ~34 weeks (Figure 10E). For mice treated on the regimen of BRAFi + MEKi d0, anti-PD-L1 d-4, the median survival was reached at ~13.5 weeks (Figure 10F), which tripled mice survival on the regimen of BRAFi + MEKi d0, anti-PD-L1 d0. Moreover, two long-term survivors displayed confirmed or true CRs. We then challenged the two most efficacious regimens with greater metastatic tumor burden (i.e., high tumor burden) by delaying the start of BRAFi + MEKi treatment by two days post-IC injection (Figure 5H). Although the survival benefits of both regimens were decreased, run-in with anti-PD-L1 prior to combination with

BRAFi + MEKi yielded superior survival benefit compared with simultaneously initiating all three therapeutic agents (p = 0.0006) (Figure 5H). In the context of high tumor burden, we also evaluated the most efficacious group (BRAFi + MEKi d0, anti-PD-L1 d-4) by substituting anti-PD-L1 with anti-PD-1. Similar to the observations from a subcutaneous tumor model (Figure 2H), the antitumor (Figures 5I and 5J) and pro-survival (Figure 5K) activity of the regimen BRAFi + MEKi d0, anti-PD-1 d-4 was greater than that of anti-PD-1 d-4. Furthermore, since anti-PD-1 plus anti-CTLA-4 improve anti-melanoma and anti-MBM efficacy clinically (Tawbi et al., 2018; Wolchok et al., 2017), we tested whether anti-CTLA-4 (2 doses from d-4 to d0) in the high tumor burden model would further the priming action of anti-PD-L1 (Figures 5L to 5N). Indeed, priming with combined ICT improved the antitumor activity (Figures 5L and 5M) and survival benefit (Figure 5N) of the sequential-combinatorial regimen.

[0108] Anti-PD-1/L1 priming of MAPKi responses via T-cell clonal expansion

[0109] We tracked the intratumoral (ovarian and brain tumors) T-cell clonotypes by TCR-seq of five regimens at d0 and d3 (Figure 5A). We excluded from this analysis two regimens (anti-PD-L1 d0; MEKi d0, anti-PD-L1 d4), which respectively lacked superiority over the no treatment group and over the regimens of MEKi d0 or MEKi d0, anti-PD-L1 d0. We calculated the Gini or clonality and diversity indices and observed that T-cell clonality (based on a and b chains) was higher on d3 after treatment with MEKi d0, anti-PD-L1 d-4 than that in any other regimen in both tumor-involved brain and ovarian tissues (Figure 10G). Consistently, TCR diversity was lower on d3 after treatment with MEKi d0, anti-PD-L1 d-4 especially compared to the d3 tissues on-treatment with MEKi d0 or MEKi d0, anti-PD-L1 d0. We also analyzed the sizes of large (≥ 5%) TCR clones and found that the regimen of MEKi d0, anti-PD-L1 d-4 on d3 led to the highest accumulation of large TCR clones (on average 10-20% in tumor-involved brain or 15-35% in tumor-involved ovaries) (Figure 6A). The pattern was consistent when we analyzed the sizes of large clones defined as ≥ 8% or of the largest, top 5 or top 10 clones (Figures 10H and 10I). Moreover, we calculated the fractions of overlapping TCR clones between two distinct regions of tumor-involved brain tissues in each animal (Figure 6B). Increasing overlap may reflect greater tumor-specific T-cell expansion. In this regard, the fraction ranged from 4.56-5.71% on d0 in untreated mice; 1.89-8.58% on d0 in mice treated with anti-PD-L1 d-4; 6.17-9.77% on d3 in mice treated with MEKi d0; 7.09-11.90% on d3 in mice treated with MEKi d0, anti-PD-L1 d0; and, importantly, 13.50-19.50% on d3 in mice treated with MEKi d0, anti-PD-L1 d-4. The differences in this overlap between the most efficacious regimen (MEKi d0, anti-PD-L1 d-4) and MEKi d0 monotherapy were significant (p = 0.045 and 0.017 for a and b chain, respectively; Student's t-test). Thus, the regimen of anti-PD-L1 lead-in followed by MEKi combination led to greater

geographic convergence of TCR clones across distinct brain tumor lesions. Furthermore, within the overlapping TCR clones between two distinct tumor-involved lesions from brain or ovary tissues in each mouse, we calculated the sizes of common large (≥ 5%) TCR clones (Figure 6C). For both a or b TCR chains and for both brain and ovary tissues, the average size was greatest from tumor-bearing mice treated with anti-PD-L1 lead-in followed by MEKi combination. In further analysis, we calculated the fractions of overlapping TCR clones between all tumor-involved brain and ovary tissues (Figure 10J). The average of fractions for the a and b TCR chains from the regimen of MEKi d0, anti-PD-L1 d-4 trended higher versus any other group. Hence, the regimen consisting of two doses of anti-PD-L1 followed by MEKi combination elicited the most robust T-cell clonal expansion and clonotypic convergence between distinct tumor-involved regions of each organ and across intracranial and extracranial organs.

[0110] **DISCUSSION**

[0111] Combination therapies are typically initiated together. Whether sequencing therapies instead of or in addition to combining therapies would augment antitumor efficacy remains under explored. Here, we found that sequencing of just two doses of anti-PD-1/L1 (± two doses of anti-CTLA-4, without further dosing) prior to MAPKi combination maximizes antitumor immunity and efficacy.

[0112] Post hoc analyses of clinical data performed here and published previously (Dummer et al., 2017) in patients (with *BRAF*^{V600MUT} or *NRAS*^{MUT} melanoma) treated with MAPKi found increased benefit from MAPKi in those who have been treated with ICT immediately prior to MAPKi. That antitumor immunity may be a critical element elicited by and modulating the efficacy of MAPK-targeted therapy was suggested by our prior studies of patients with *BRAF*^{V600MUT} melanoma whose acquired MAPKi-resistant melanoma display signs of immune evasion (Hugo et al., 2015; Hugo et al., 2016; Song et al., 2017). Based on the current study, superior antitumor activity of the regimen consisting of anti-PD-1/L1 lead-in followed by MAPKi combination was positively linked to multiple cell types, including M1-like TAMs, CD4$^+$ Th1, and CD8$^+$ T cells. Thus, strategies to target M2-like TAMs and to improve clonal expansion and persistence of tumor-specific CD8$^+$ cytotoxic T cells may further improve the proposed sequential-combinatorial strategy.

[0113] The finding here that anti-PD-1/L1 lead-in followed by MAPKi combination can improve anti-MBM activity (and thereby survival) in mice has immediate clinical implications. This sequential-combinatorial strategy may present an alternative strategy to combination ICT with anti-PD-1 + anti-CTLA-4, which improves anti-MBM responses elicited by anti-PD-1 monotherapy (Tawbi et al., 2018). Melanoma has a high propensity for CNS metastasis (40-

80%), which is associated with poor overall survival (median 4-5 months) (Davies et al., 2011). CNS is often the initial site of acquired resistance (which often persists in isolation without extracranial disease progression) in patients on MAPKi (Frenard et al., 2016; Long et al., 2016). The experimental metastatic model established here recapitulated the propensity of MBM to escape from MAPKi therapy. Importantly, sequencing of anti-PD-1/L1 therapy prior to MAPKi addition resulted in the most durable anti-MBM activity. This benefit may be extended by priming with anti-PD-1/L1 plus anti-CTLA-4 (with a limited duration of anti-CTLA-4 dosing to avoid added toxicities).

[0114] Data presented here support the conclusions that anti-PD-1/L1 therapy primes a more durable MAPKi response and that MAPKi combination helps to overcome innate anti-PD-1/L1 resistance. These findings prompted the design and initiation of a single-site clinical trial (NCT04375527) testing the activity of binimetinib plus nivolumab in patients with *BRAF*^{V600WT} melanoma that display innate resistance to ICT. Findings here should concentrate a larger effort to evaluate prospectively the activity of anti-PD-1/L1 agents combined with BRAFi + MEKi or MEKi (in *BRAF*^{V600MUT} or *BRAF*^{V600WT} melanoma, respectively) after distinct predefined periods of prior ICT exposure, with or without objective evidence of innate resistance to ICT. Moreover, the benefit of triplet therapy with anti-PD-1/L1 + BRAFi + MEKi may be clinically meaningful for anti-PD-1/L1-experienced (*vs.* naïve) patients despite objective evidence of innate ICT resistance and for patients with symptomatic or non-symptomatic MBM.

[0115] While the animal model studies do not address the impacts of prolonging anti-PD-1/L1 lead-in before MAPKi combination, these *in vivo* models collectively serve as an important platform to compare and mechanistically dissect alternative sequential-combinatorial regimens, including those inclusive of additional targeted agents.

[0116] **References**

[0117] Ackerman, A., *et al.* (2014). Cancer *120*, 1695-1701.

[0118] Algazi, A. P., *et al.* (2020). Nat Med *26*, 1564-1568.

[0119] Ascierto, P. A., *et al.* (2019). Nat Med *25*, 941-946.

[0120] Butler, A., *et al.* (2018). Nat Biotechnol *36*, 411-420.

[0121] Chen, H., *et al.* (2016). PLoS Comput Biol *12*, e1005112.

[0122] Davies, M. A., *et al.* (2011). Cancer *117*, 1687-1696.

[0123] Davies, M. A., *et al.* (2017). Lancet Oncol *18*, 863-873.

[0124] Dummer, R., *et al.* (2017). Lancet Oncol *18*, 435-445.

[0125] Flaherty, K. T., *et al.* (2012). N Engl J Med.

[0126] Frenard, C., *et al.* (2016). J Neurooncol *126*, 355-360.

[0127] Ghebremedhin, A., *et al.* (2020). bioRxiv.

[0128] Gutzmer, R., *et al.* (2020). Lancet *395*, 1835-1844.

[0129] Hong, A., *et al.* (2018). Cancer Discov *8*, 74-93.

[0130] Hong, A., *et al.* (2021). Cancer Discov *11*, 714-735.

[0131] Hugo, W., *et al.* (2015). Cell *162*, 1271-1285.

[0132] Hugo, W., *et al.* (2016). Cell *165*, 35-44.

[0133] Jaynes, J. M., *et al.* (2020). Sci Transl Med *12*.

[0134] Johnson, D. B., *et al.* (2017). J Immunother *40*, 31-35.

[0135] Kotecha, N., *et al.* (2010). Curr Protoc Cytom *Chapter 10*, Unit10 17.

[0136] Long, G. V., *et al.* (2016). Lancet Oncol *17*, 1743-1754.

[0137] Mason, R., *et al.* (2020). Pigment Cell Melanoma Res *33*, 358-365.

[0138] Nazarov, V. I., *et al.* (2015). BMC Bioinformatics *16*, 175.

[0139] Reijers, I. L. M., *et al.* (2020). Pigment Cell Melanoma Res *33*, 498-506.

[0140] Ribas, A., *et al.* (2016). JAMA *315*, 1600-1609.

[0141] Ribas, A., *et al.* (2019). Nat Med *25*, 936-940.

[0142] Seifert, H., *et al.* (2016). Pigment Cell Melanoma Res *29*, 92-100.

[0143] Siddiqui, I., *et al.* (2019). Immunity *50*, 195-211 e110.

[0144] Simeone, E., *et al.* (2017). Oncoimmunology *6*, e1283462.

[0145] Song, C., *et al.* (2017). Cancer Discov *7*, 1248-1265.

[0146] Tawbi, H. A., *et al.* (2018). N Engl J Med *379*, 722-730.

[0147] Tetu, P., *et al.* (2018). Eur J Cancer *93*, 147-149.

[0148] Wang, J., *et al.* (2017). Pigment Cell Melanoma Res *30*, 428-435.

[0149] Wolchok, J. D., *et al.* (2017). N Engl J Med *377*, 1345-1356.

[0150] Table 1. For S1320 trial, associations between baseline patient characteristics and prior ICT, related to Figure 1. Median (range) or N (%) reported.

Factor	No prior exposure (N = 145)	Prior checkpoint therapy (N = 61)	P-value
Randomized arm			
Continuous Dosing	74 (51)	31 (51)	1
Intermittent Dosing	71 (49)	30 (49)	
Age at randomization (years)	62 (52, 69)	58 (47, 67)	0.16
Age at randomization (years)			
Younger than 45	24 (17)	15 (25)	0.18
45 and older	121 (83)	46 (75)	
Gender			
Female	51 (35)	23 (38)	0.75
Male	94 (65)	38 (62)	
Race			
White	142 (98)	59 (97)	0.6
Asian and white	1 (1)	0 (0)	
Native American	0 (0)	1 (2)	
Unknown race	2 (1)	1 (2)	
Ethnicity			
Hispanic	4 (3)	2 (3)	1
Not hispanic	141 (97)	59 (97)	
PS			
0	82 (57)	35 (58)	0.95
1	60 (42)	24 (40)	
2	2 (1)	1 (2)	
LDH at randomization			
Elevated LDH	53 (37)	24 (39)	0.75
Normal LDH	92 (63)	37 (61)	
Primary			
Cutaneous primary	112 (78)	52 (88)	0.12
Unknown primary	32 (22)	7 (12)	
Stage			
M0	14 (10)	11 (18)	0.41
M1A	25 (17)	11 (18)	
M1B	32 (22)	12 (20)	
M1C	74 (51)	27 (44)	
Response			
CR	13 (9)	9 (15)	0.43
Unconfirmed CR	3 (2)	0 (0)	
PR	76 (54)	38 (64)	
Unconfirmed PR	22 (16)	6 (10)	
Stable	22 (16)	5 (8)	
Increasing disease	2 (1)	0 (0)	
Inadequate assessment	3 (2)	1 (2)	

[0151] Tables 2A & 2B. Multivariable Cox regression models for PFS (A) and OS (B), Related to Figure 1.

[0152] Table 2A

Covariate	HR	80% CI	P-value
Prior checkpoint therapy (ref = No prior exposure)	0.6	(0.47, 0.77)	0.009
Intermittent Dosing (ref = Continuous Dosing)	1.57	(1.27, 1.96)	0.0073
Age at randomization (years)	0.99	(0.98, 1)	0.17
Male (ref = Female)	0.93	(0.73, 1.18)	0.69
PS 1 (ref = PS 0)	1.3	(1.04, 1.62)	0.13
PS 2 (ref = PS 0)	3.2	(1.23, 8.34)	0.12
Normal LDH (ref = Elevated LDH)	0.63	(0.5, 0.79)	0.01
Unknown primary (ref = Cutaneous primary)	0.71	(0.53, 0.95)	0.13
M1A (ref = M0)	1.24	(0.79, 1.95)	0.53
M1B (ref = M0)	1.6	(1.04, 2.46)	0.16
M1C (ref = M0)	1.9	(1.27, 2.82)	0.039

[0153] Table 2B

Covariate	HR	80% CI	P-value
Prior checkpoint therapy (ref = No prior exposure)	0.86	(0.63, 1.17)	0.52
Intermittent Dosing (ref = Continuous Dosing)	1.13	(0.85, 1.49)	0.58
Age at randomization (years)	1	(0.99, 1.01)	0.81
Male (ref = Female)	0.63	(0.47, 0.85)	0.051
PS 1 (ref = PS 0)	2.16	(1.64, 2.85)	<0.001
PS 2 (ref = PS 0)	12.71	(4.48, 36.06)	0.0018
Normal LDH (ref = Elevated LDH)	0.54	(0.41, 0.73)	0.0069
Unknown primary (ref = Cutaneous primary)	0.65	(0.44, 0.95)	0.15
M1A (ref = M0)	1.67	(0.79, 3.5)	0.38
M1B (ref = M0)	3.01	(1.48, 6.13)	0.047
M1C (ref = M0)	3.61	(1.84, 7.09)	0.015

[0154] Table 3. Expansion indices as well as top 5 and 10 clone sizes of CD8+ TC, Ki-67hi CD8+ T and T_{REG} cells in each treatment regimen group and time point, Related to Figure 3. See Figure 2A.

Expansion index			Size of top5 clones			Size of top10 clones			
$CD8^+$ T_C	$Ki\text{-}67^{hi}$ $CD8^+$	T_{REG}	$CD8^+$ T_C	$Ki\text{-}67^{hi}$ $CD8^+$	T_{REG}	$CD8^+$ T_C	$Ki\text{-}67^{hi}$ $CD8^+$	T_{REG}	
0.0630	0.0000	0.0086	0.0465	0.0159	0.0171	0.0734	0.0159	0.0282	
0.1796	0.0204	0.0000	0.1478	0.1063	0.1113	0.1777	0.1096	0.1213	Day 7
0.1852	0.0000	0.0074	0.1022	0.0424	0.0849	0.1283	0.0424	0.0945	
0.0193	0.0000	0.0000	0.1129	0.0000	0.0484	0.1532	0.0000	0.0887	Day 10
0.1392	0.0817	0.0000	0.2160	0.0488	0.0418	0.3031	0.0488	0.0592	
0.1416	0.0817	0.0000	0.1203	0.0253	0.0190	0.1582	0.0253	0.0190	
0.0067	0.0000	0.0067	0.0516	0.0299	0.0387	0.0616	0.0299	0.0464	
0.1175	0.0000	0.0066	0.0235	0.0063	0.0093	0.0334	0.0066	0.0136	Day 14
0.2392	0.0000	0.0334	0.1800	0.0284	0.1411	0.2141	0.0284	0.1492	
0.2210	0.0245	0.0000	0.1018	0.0583	0.0317	0.1372	0.0590	0.0398	

[0155] Throughout this application various publications are referenced. The disclosures of these publications in their entireties are hereby incorporated by reference into this application in order to describe more fully the state of the art to which this invention pertains.

[0156] Those skilled in the art will appreciate that the conceptions and specific embodiments disclosed in the foregoing description may be readily utilized as a basis for modifying or designing other embodiments for carrying out the same purposes of the present invention. Those skilled in the art will also appreciate that such equivalent embodiments do not depart from the spirit and scope of the invention as set forth in the appended claims.

What is claimed is:

1. A method of enhancing efficacy of mitogen-activated protein kinase inhibitor (MAPKi) therapy or immune checkpoint therapy (ICT), the method comprising:

(a) pretreating a subject in need of MAPKi therapy by administering one to two doses of ICT to the subject;

(b) subsequent to the pretreating of (a), administering to the subject a combination of MAPKi and ICT.

2. The method of claim 1, wherein the ICT comprises an anti-PD-1 or anti-PD-L1 agent.

3. The method of claim 2, wherein the ICT further comprises an anti-CTLA-4 agent.

4. The method of claim 1, wherein the subject has a BRAF V600 mutant cancer and the MAPKi is a BRAF inhibitor (BRAFi) or a BRAF plus a MEK inhibitor (MEKi).

5. The method of claim 1, wherein the subject has a NRAS, KRAS, and/or NF1 mutant cancer and the MAPKi is a MEKi.

6. The method of claim 1, wherein the pretreating of (a) consists of administering one to two doses over one to eight weeks.

7. The method of claim 1, wherein the administering of (b) begins two to eight weeks following the initiation of the pretreating of (a).

8. The method of claim 1, wherein the pretreating of (a) further comprises administering one to two additional doses of ICT.

9. The method of claim 1, wherein the pretreating of (a) further comprises administering a modulator of regulatory T cells and/or M2-like TAMs.

10. The method of claim 9, wherein the modulator of regulatory T cells is a CD25-depleting antibody.

11. The method of claim 9, wherein the modulator of M2-like TAMs is a peptide agonist of CD206.

12. The method of claim 8, wherein the pretreating of (a) begins two to eight weeks prior to the administering of (b).

13. A method of suppressing melanoma metastasis in a subject, the method comprising:

(a) pretreating a subject in need of treatment for melanoma metastasis by administering one to one to two doses of ICT to the subject;

(b) subsequent to the pretreating of (a), administering to the subject a combination of MAPKi and ICT.

14. The method of claim 13, wherein the metastasis is a brain metastasis.

15. A method of enhancing the inhibition of M2-like tumor associated macrophages (TAMs) in a subject, the method comprising:

(a) pretreating a subject in need of inhibition of M2-like TAMs by administering one to one to two doses of ICT plus a pharmacologic M2-like TAM inhibitor to the subject;

(b) subsequent to the pretreating of (a), administering to the subject a combination of MAPKi and ICT.

16. The method of claim 15, wherein the inhibiting of M2-like TAMs effects a selective upregulation of pro-inflammatory or M1-like TAMs in the subject.

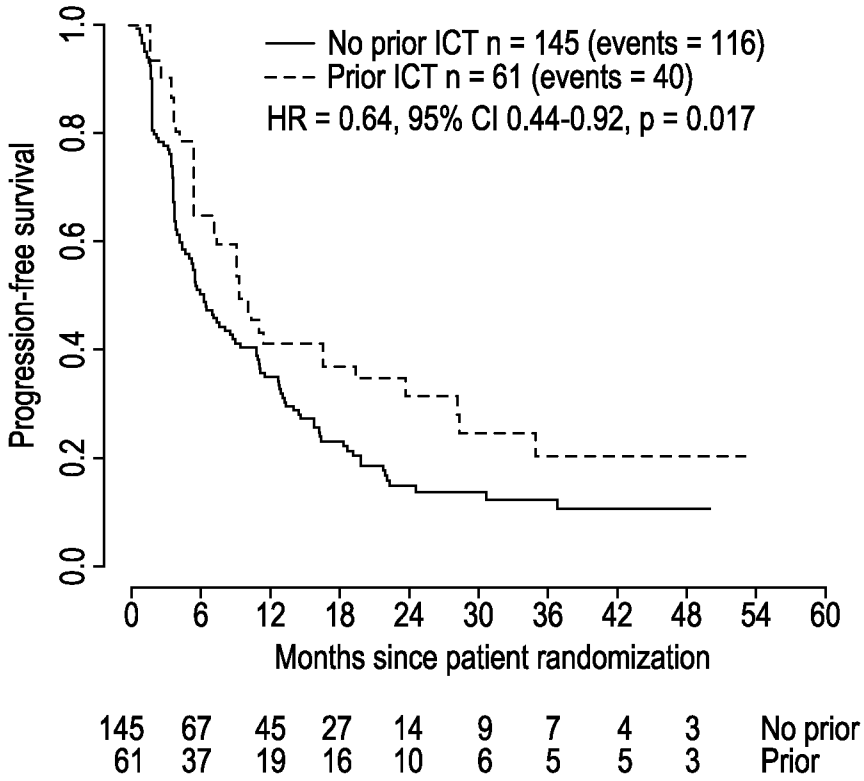
No prior ICT n = 145 (events = 116)
Prior ICT n = 61 (events = 40)
HR = 0.64, 95% CI 0.44-0.92, p = 0.017
Progression-free survival
0.0
0.2
0.4
0.6
0.8
1.0
0 6 12 18 24 30 36 42 48 54 60
Months since patient randomization
145 67 45 27 14 9 7 4 3 No prior
61 37 19 16 10 6 5 5 3 Prior

FIG. 1

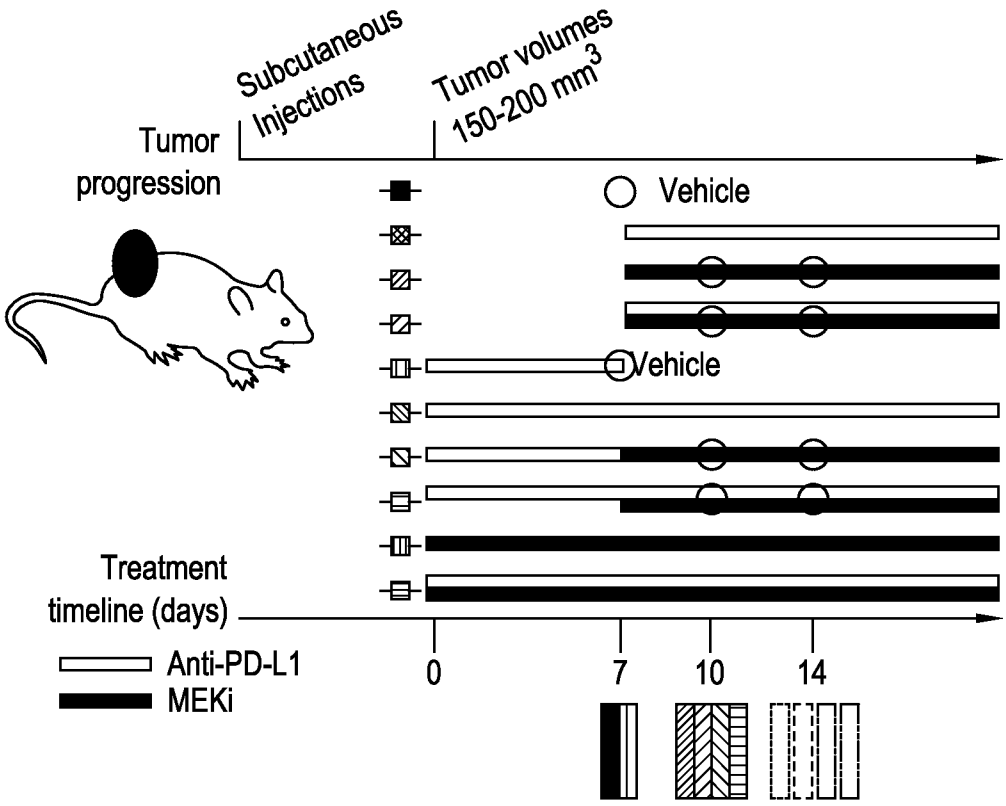
Subcutaneous Injections
Tumor volumes 150-200 mm3
Tumor progression
Vehicle
Vehicle
Treatment timeline (days)
Anti-PD-L1
MEKi
0
7
10
14

FIG. 2A

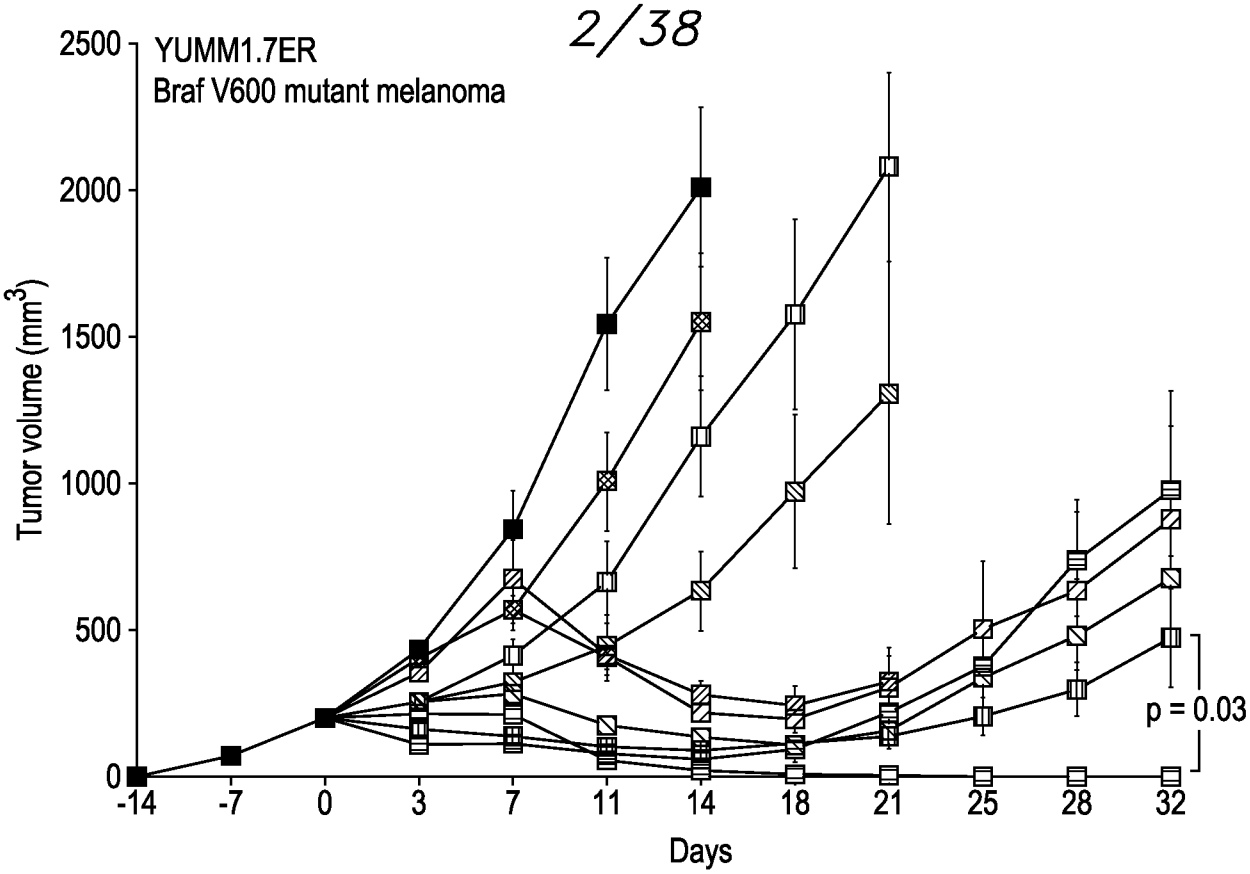
YUMM1.7ER
Braf V600 mutant melanoma
Tumor volume (mm3)
2500
2000
1500
1000
500
0
-14
-7
0
3
7
11
14
18
21
25
28
32
Days
p = 0.03

FIG. 2B

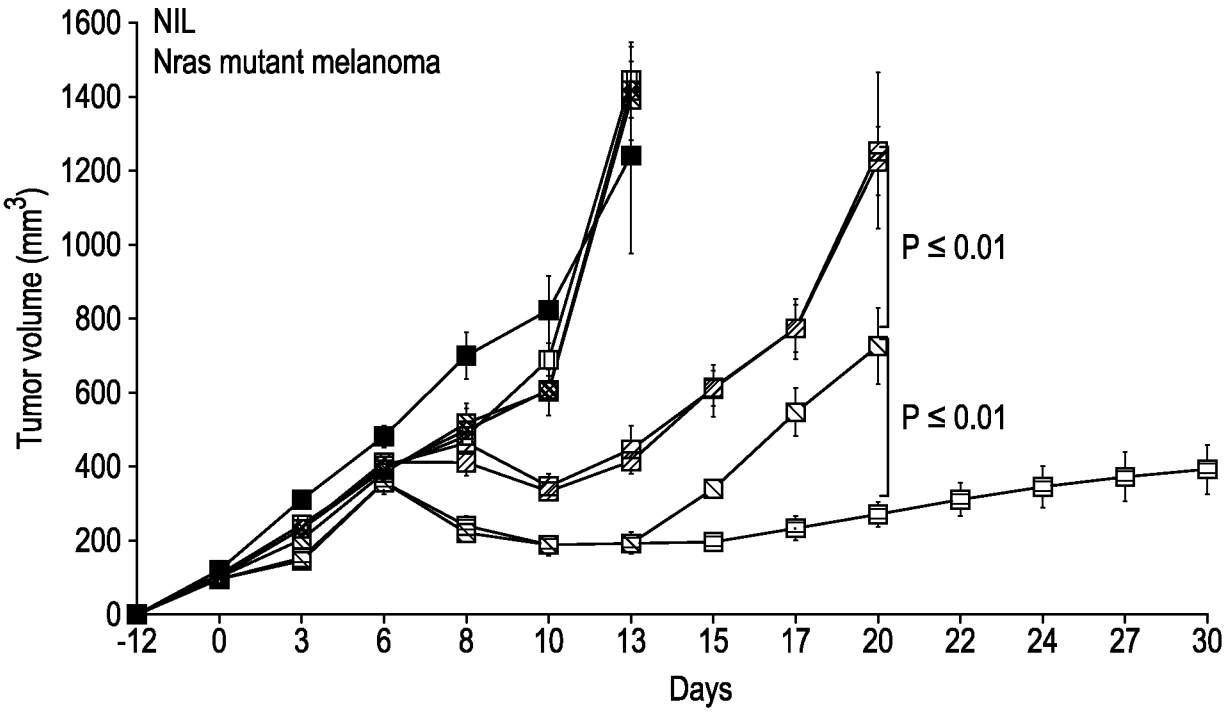
NIL
Nras mutant melanoma
Tumor volume (mm3)
1600
1400
1200
1000
800
600
400
200
0
-12
0
3
6
8
10
13
15
17
20
22
24
27
30
Days
P ≤ 0.01
P ≤ 0.01

FIG. 2C

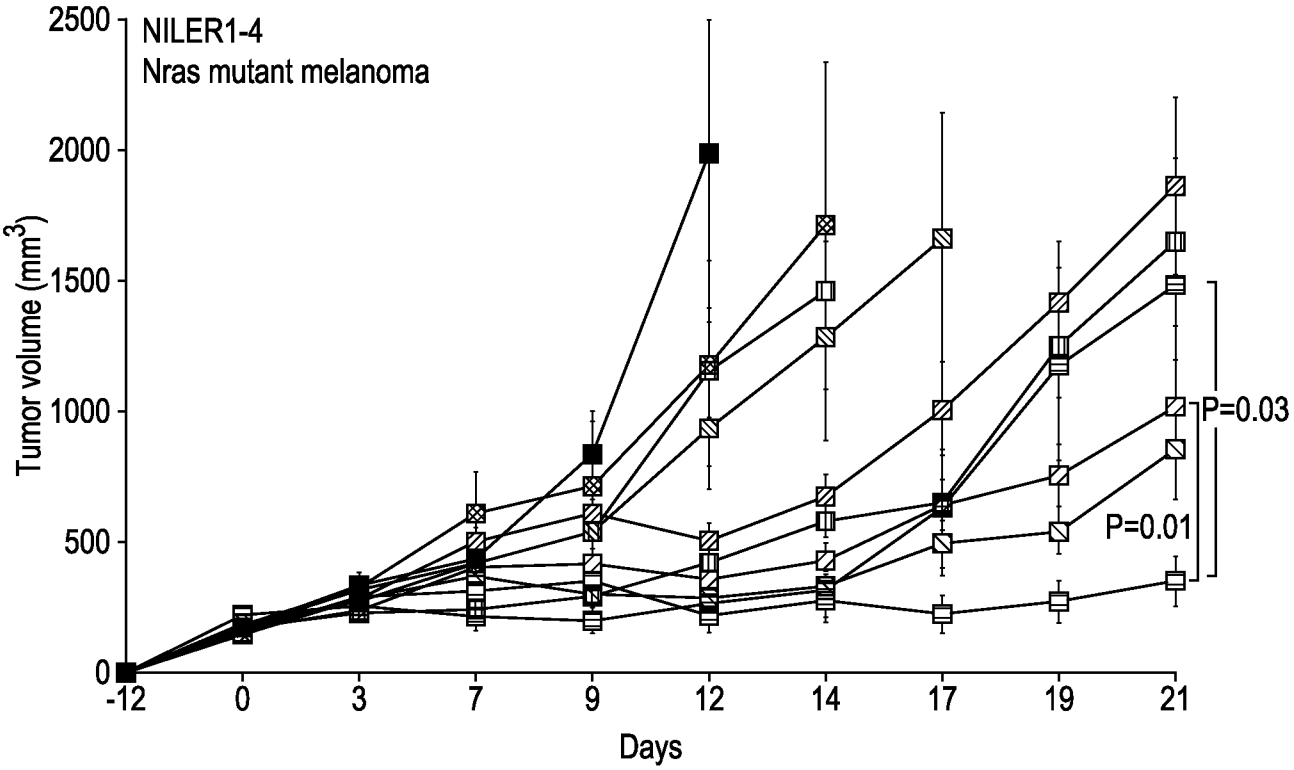
NILER1-4
Nras mutant melanoma
Tumor volume (mm3)
2500
2000
1500
1000
500
0
-12
0
3
7
9
12
14
17
19
21
Days
P=0.03
P=0.01

FIG. 2D

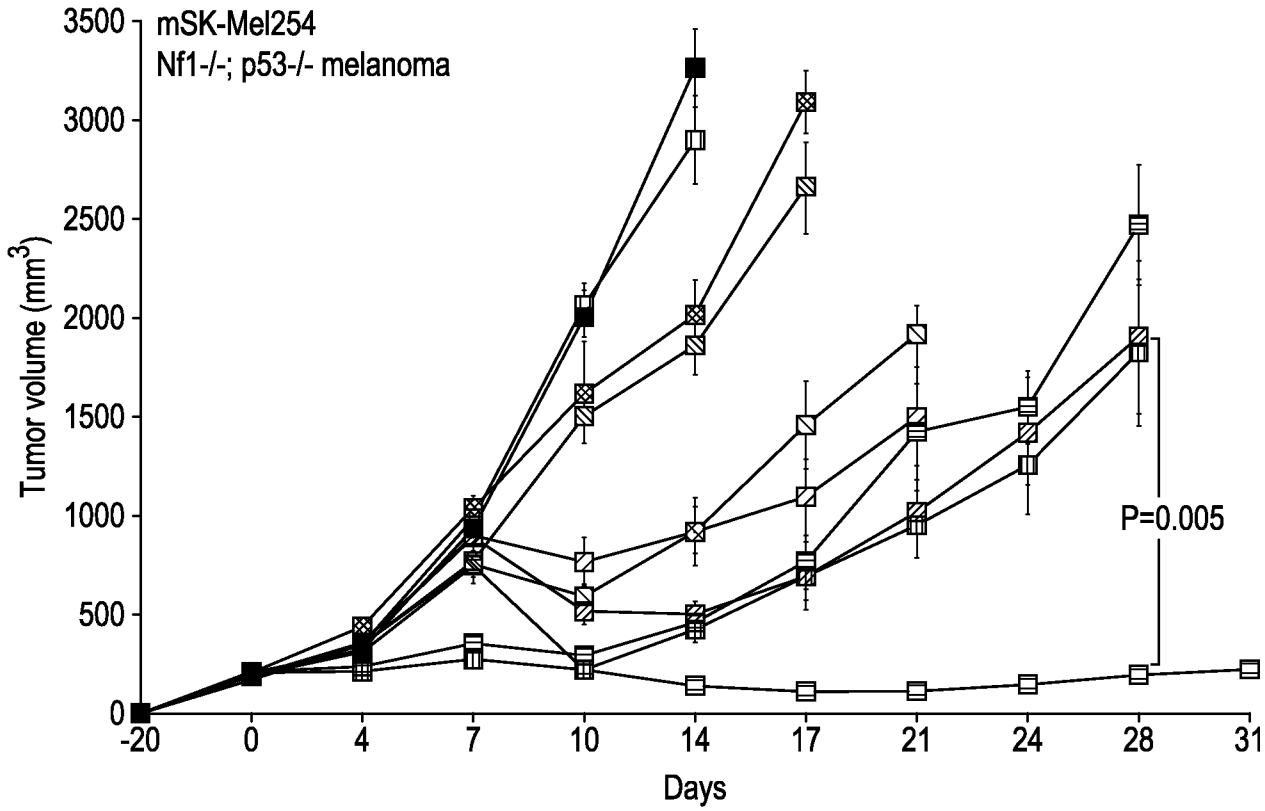
mSK-Mel254
Nf1-/-; p53-/- melanoma
Tumor volume (mm3)
3500
3000
2500
2000
1500
1000
500
0
-20
0
4
7
10
14
17
21
24
28
31
Days
P=0.005

FIG. 2E

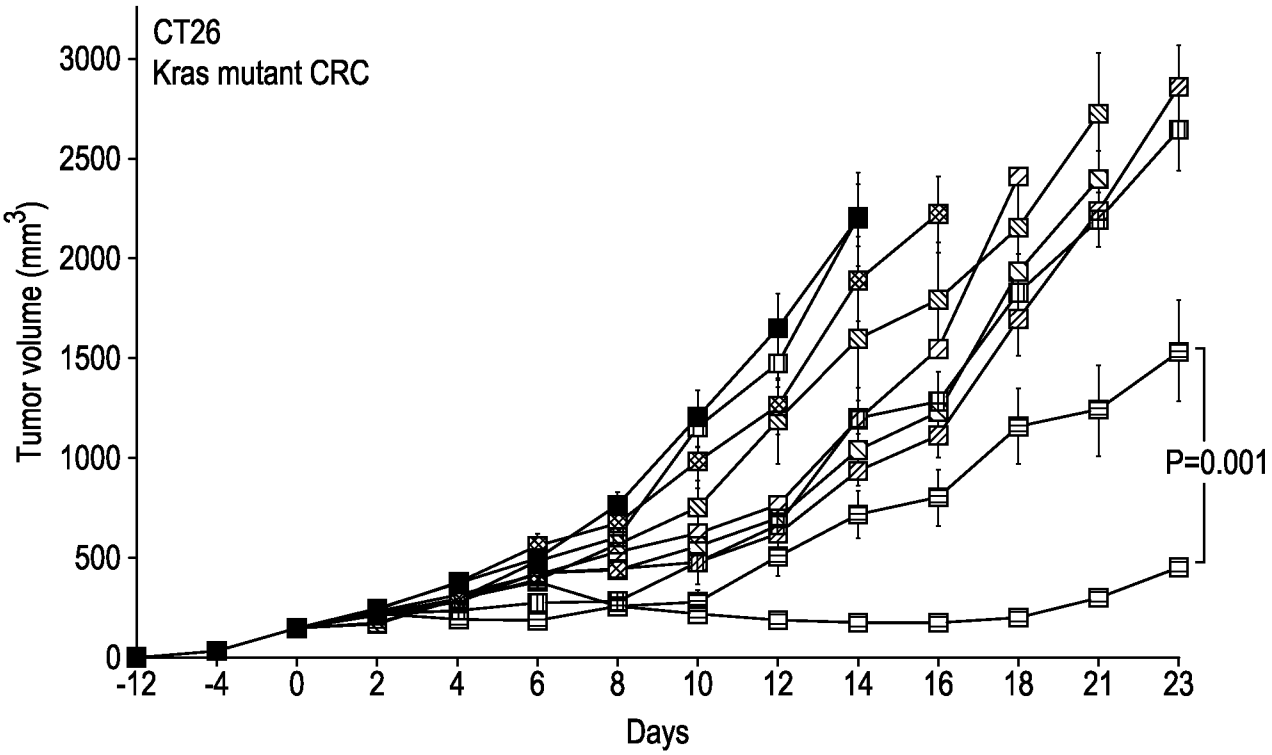
CT26
Kras mutant CRC
Tumor volume (mm3)
3000
2500
2000
1500
1000
500
0
-12
-4
0
2
4
6
8
10
12
14
16
18
21
23
Days
P=0.001

FIG. 2F

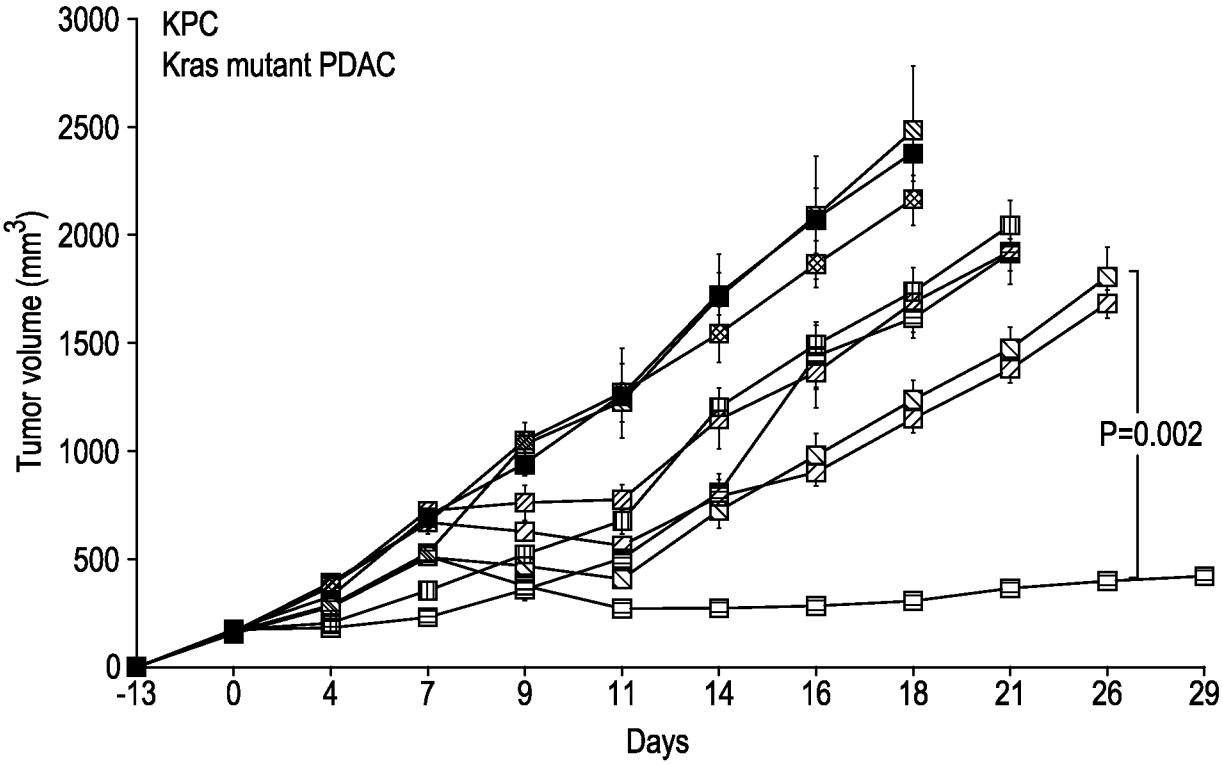
KPC
Kras mutant PDAC
Tumor volume (mm3)
3000
2500
2000
1500
1000
500
0
-13
0
4
7
9
11
14
16
18
21
26
29
Days
P=0.002

FIG. 2G

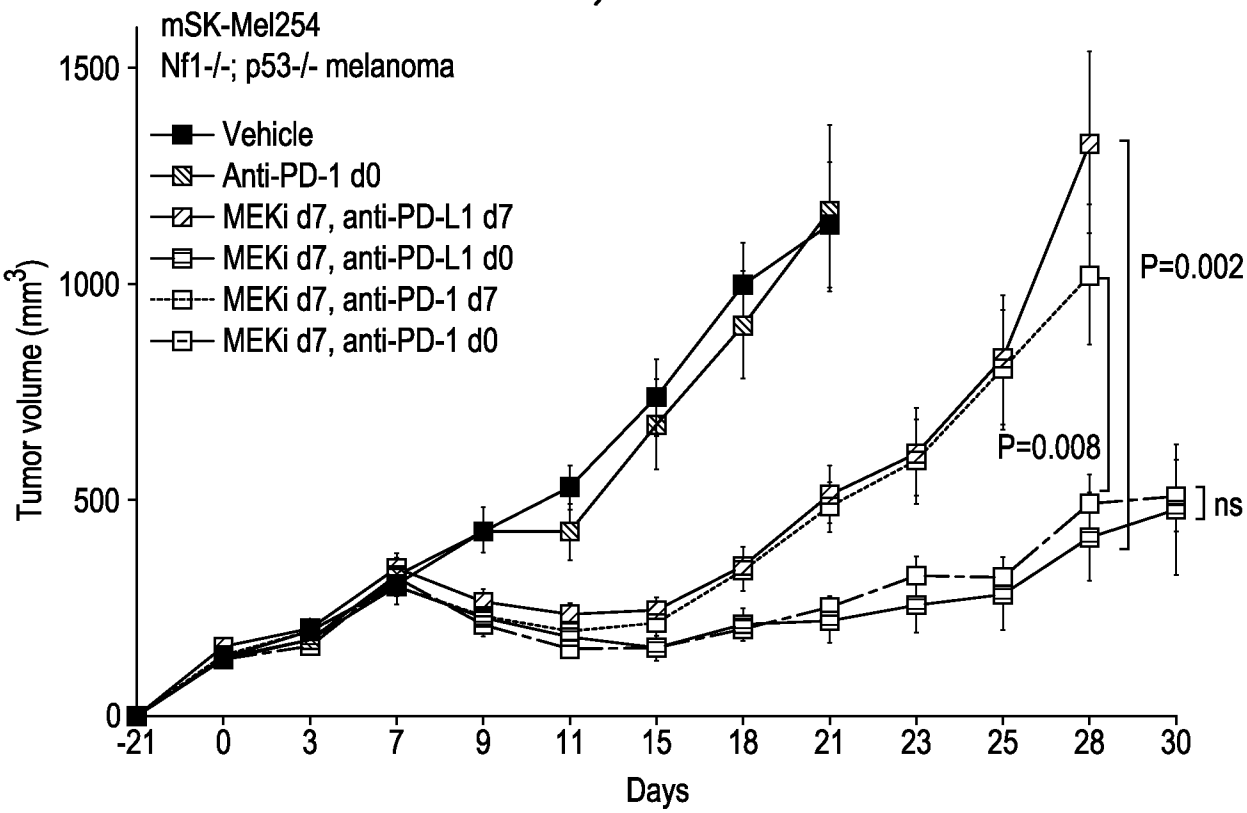
mSK-Mel254
Nf1-/-; p53-/- melanoma
Vehicle
Anti-PD-1 d0
MEKi d7, anti-PD-L1 d7
MEKi d7, anti-PD-L1 d0
MEKi d7, anti-PD-1 d7
MEKi d7, anti-PD-1 d0
Tumor volume (mm3)
1500
1000
500
0
-21
0
3
7
9
11
15
18
21
23
25
28
30
Days
P=0.002
P=0.008
ns

FIG. 2H

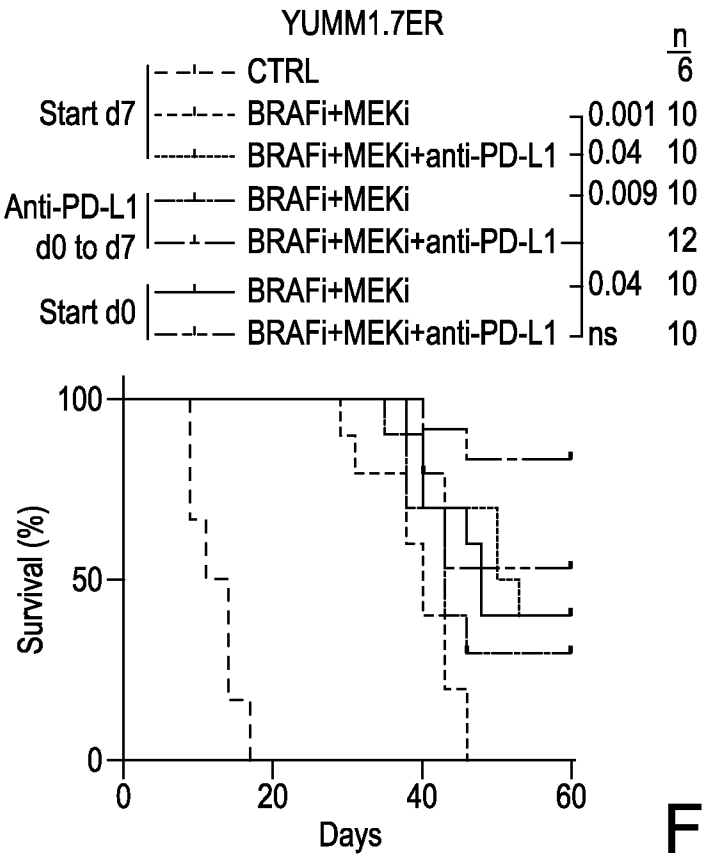
YUMM1.7ER
n
6
Start d7
CTRL
BRAFi+MEKi
BRAFi+MEKi+anti-PD-L1
0.001 10
0.04 10
Anti-PD-L1 d0 to d7
BRAFi+MEKi
BRAFi+MEKi+anti-PD-L1
0.009 10
12
Start d0
BRAFi+MEKi
BRAFi+MEKi+anti-PD-L1
0.04 10
ns 10
Survival (%)
100
50
0
0
20
40
60
Days

FIG. 2I

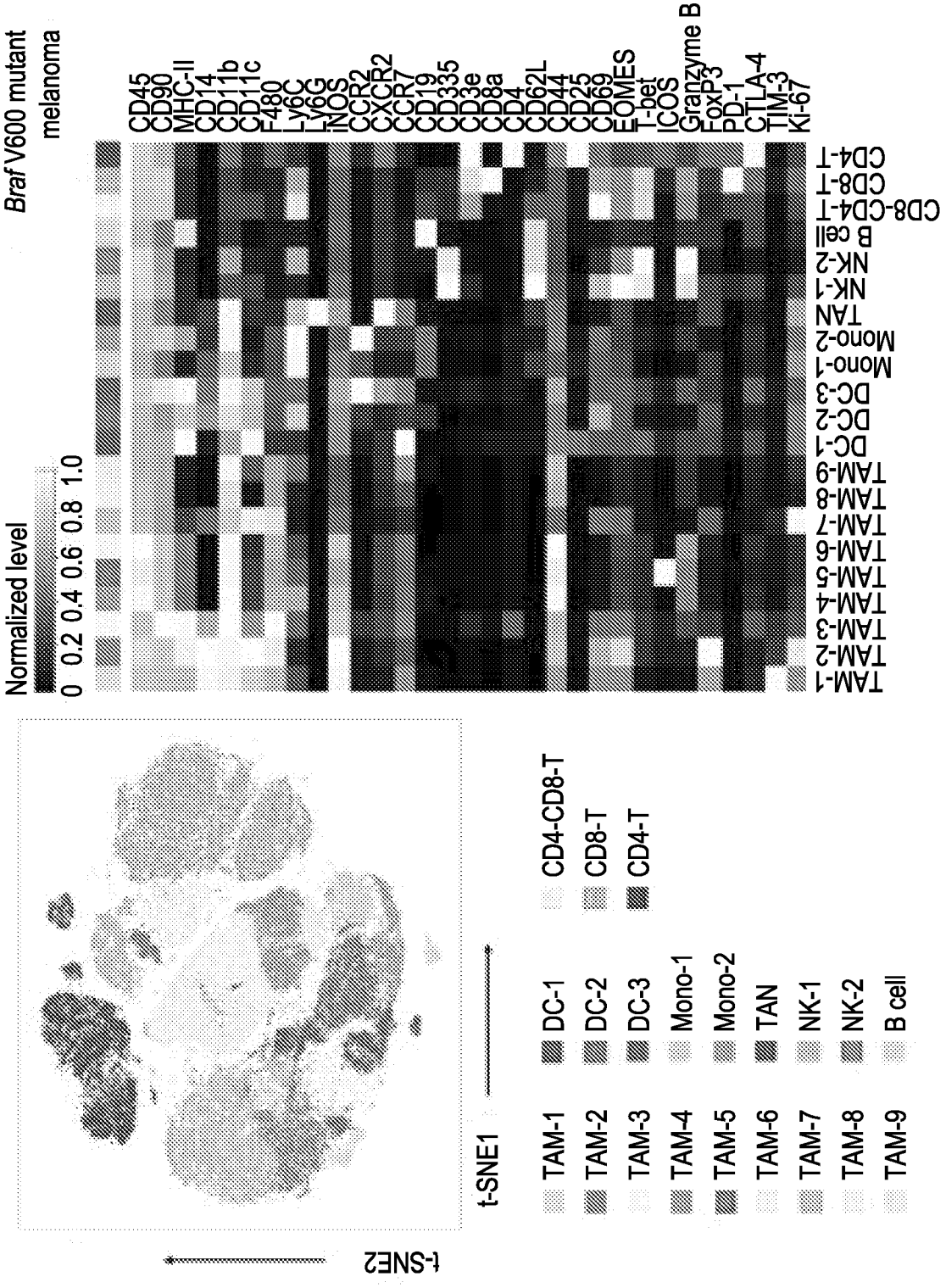
Braf V600 mutant melanoma
Normalized level
0 0.2 0.4 0.6 0.8 1.0
CD45
CD90
MHC-II
CD14
CD11b
CD11c
F480
Ly6C
Ly6G
iNOS
CCR2
CXCR2
CCR7
CD19
CD335
CD3e
CD8a
CD4
CD62L
CD44
CD25
CD69
EOMES
T-bet
ICOS
Granzyme B
FoxP3
PD-1
CTLA-4
TIM-3
Ki-67
TAM-1
TAM-2
TAM-3
TAM-4
TAM-5
TAM-6
TAM-7
TAM-8
TAM-9
DC-1
DC-2
DC-3
Mono-1
Mono-2
TAN
NK-1
NK-2
B cell
CD4-CD8-T
CD8-T
CD4-T
t-SNE1
t-SNE2

FIG. 2J

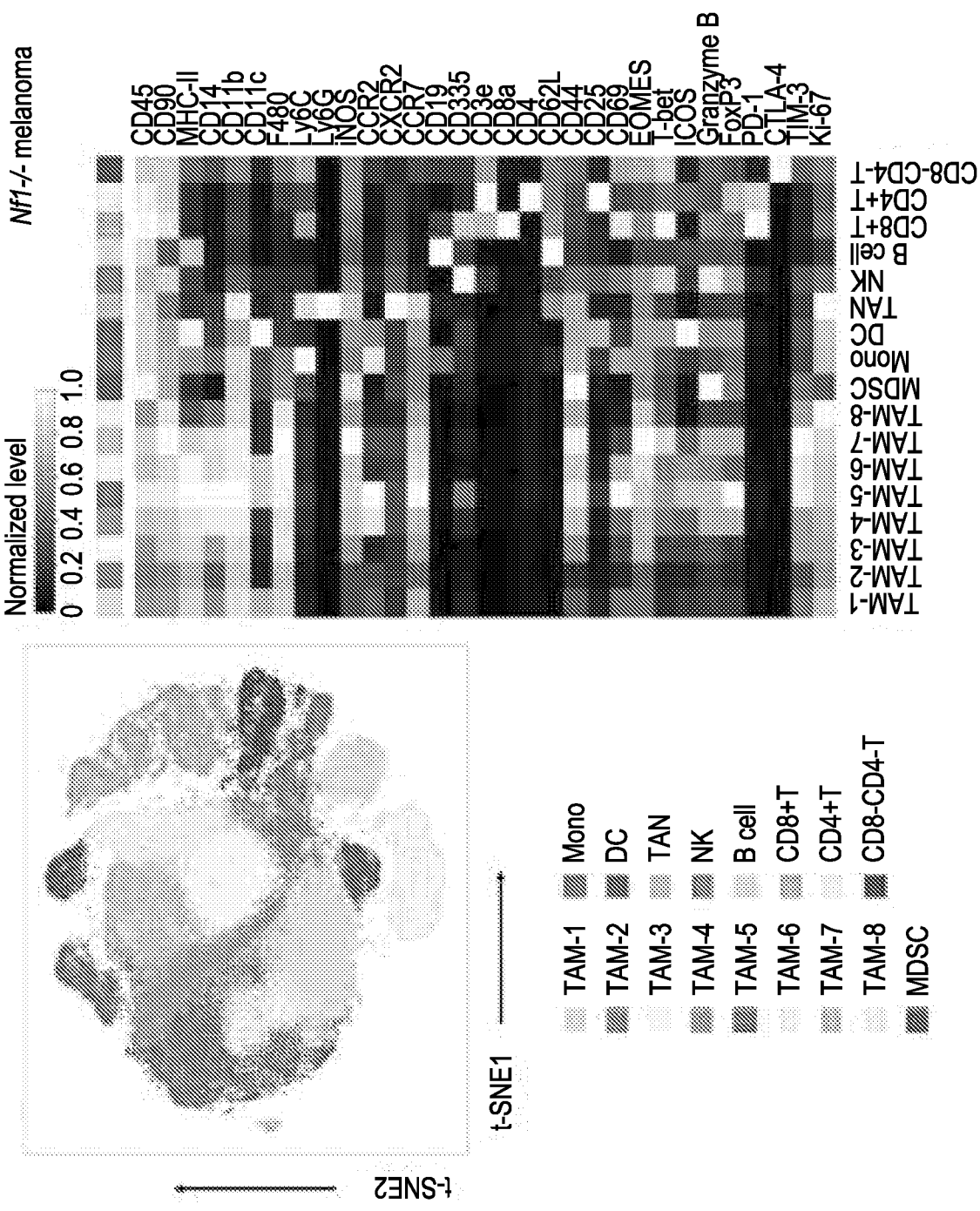

FIG. 2J (continue)

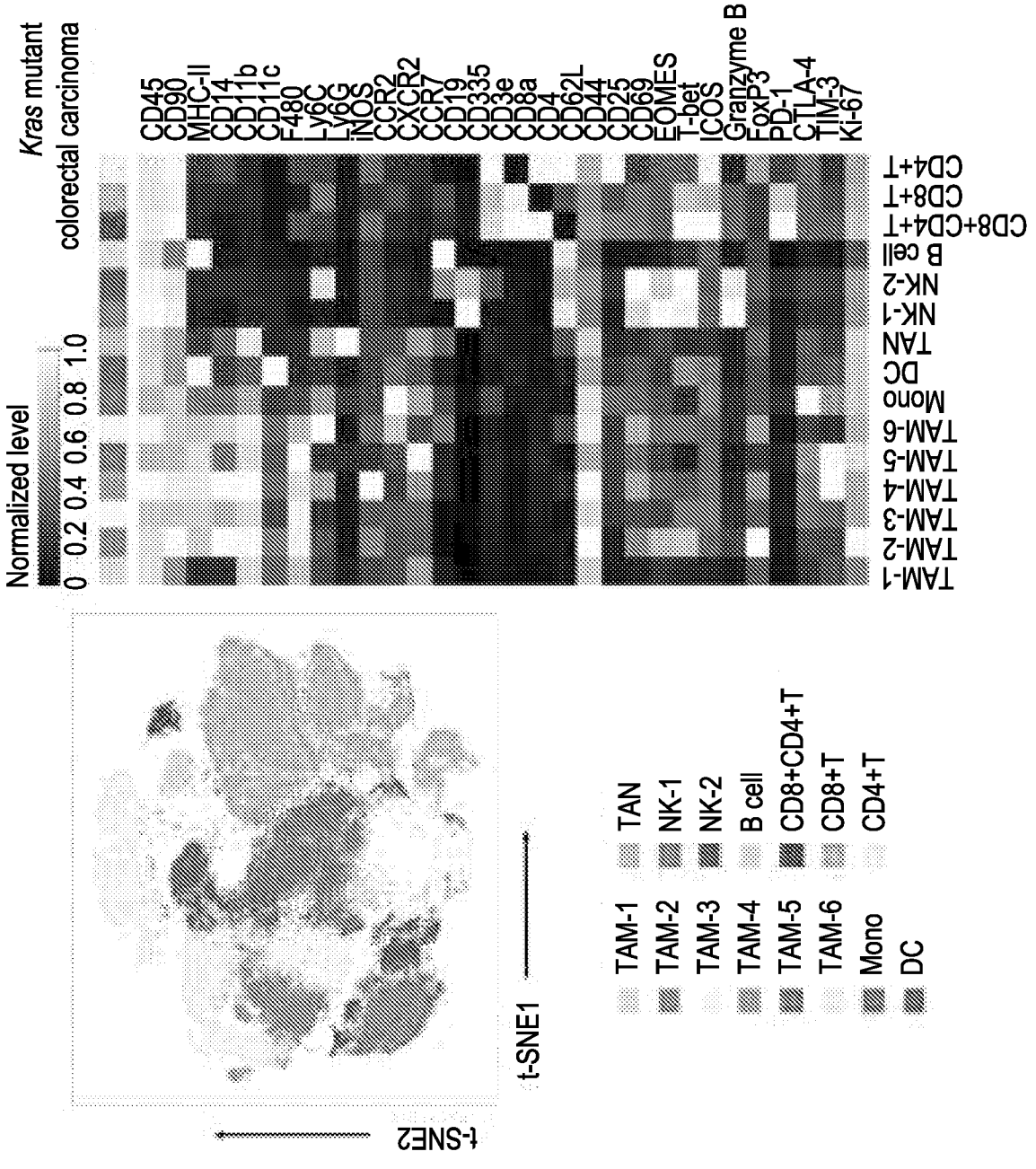

FIG. 2J (continue)

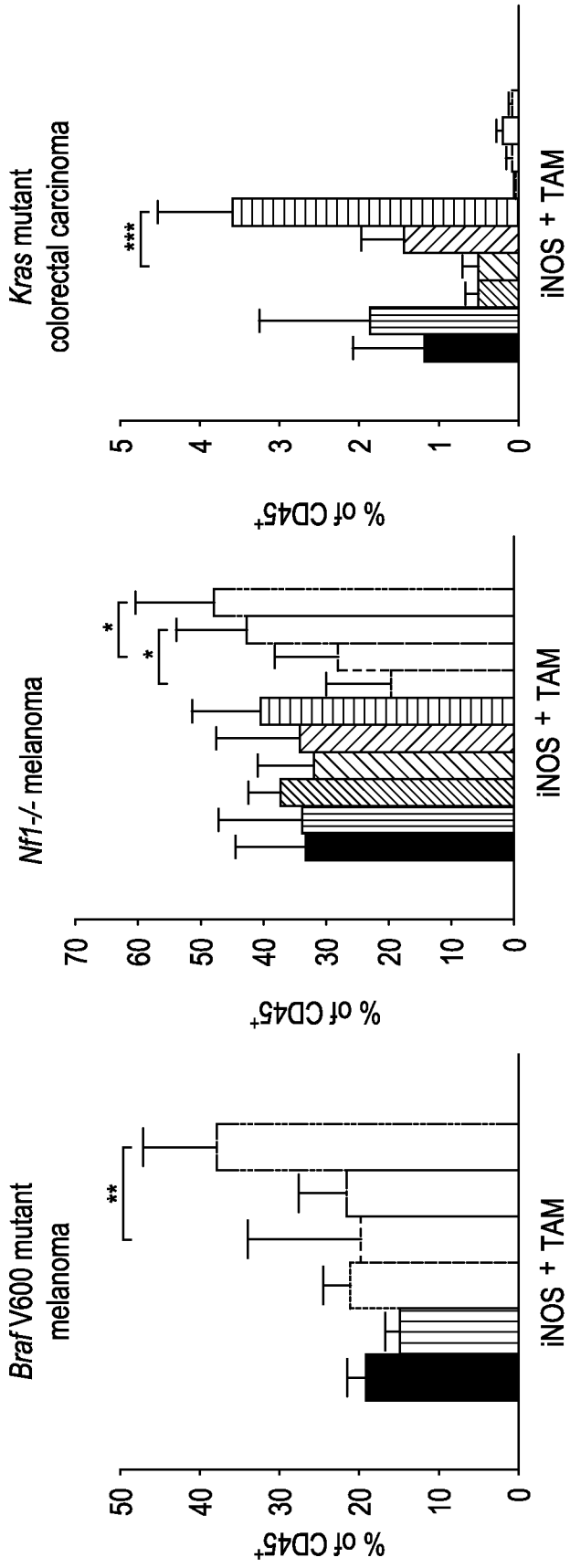
Braf V600 mutant melanoma
Nf1-/- melanoma
Kras mutant colorectal carcinoma
% of CD45+
iNOS + TAM
**
*
*
***

FIG. 2K

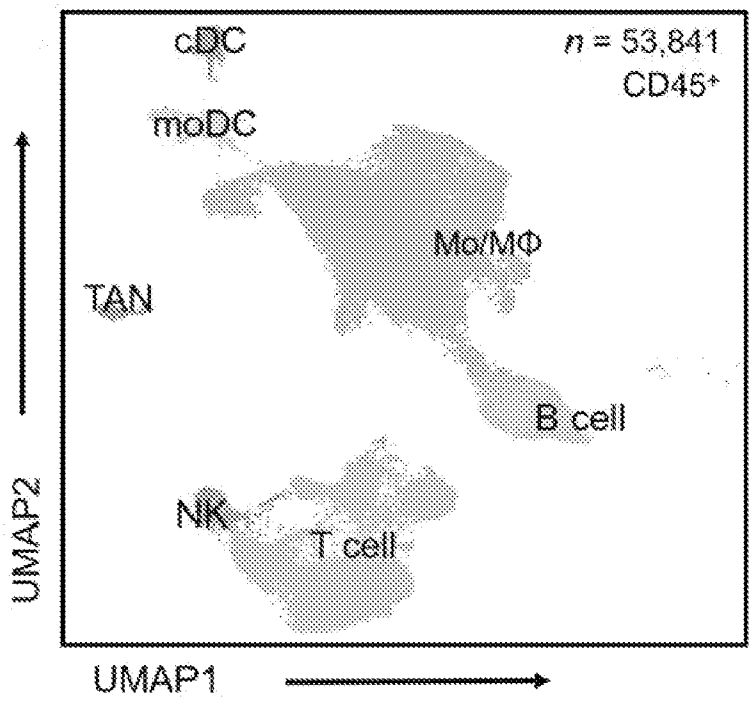
cDC
n = 53,841
CD45+
moDC
Mo/MΦ
TAN
B cell
NK
T cell
UMAP2
UMAP1

FIG. 3A

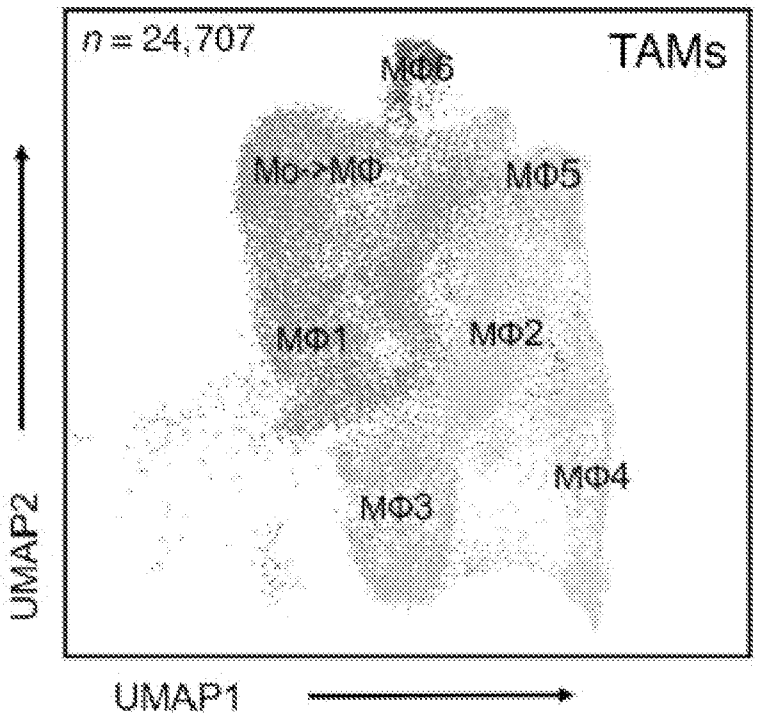
n = 24,707
TAMs
MΦ6
Mo->MΦ
MΦ5
MΦ1
MΦ2
MΦ4
MΦ3
UMAP2
UMAP1

FIG. 3B

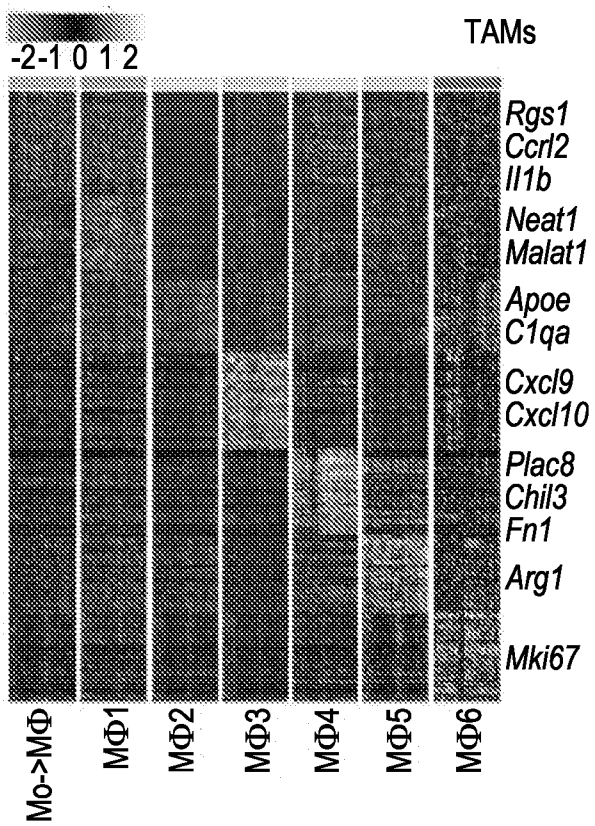

FIG. 3C

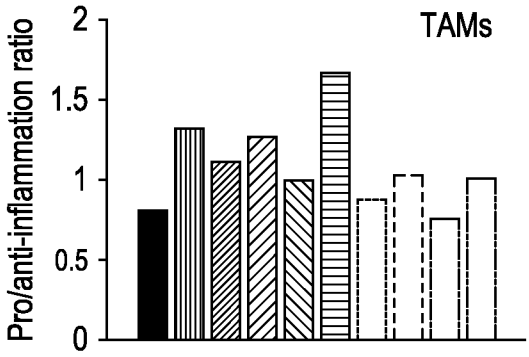

FIG. 3D

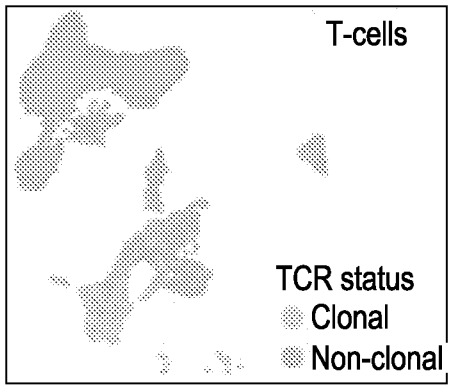

FIG. 3G

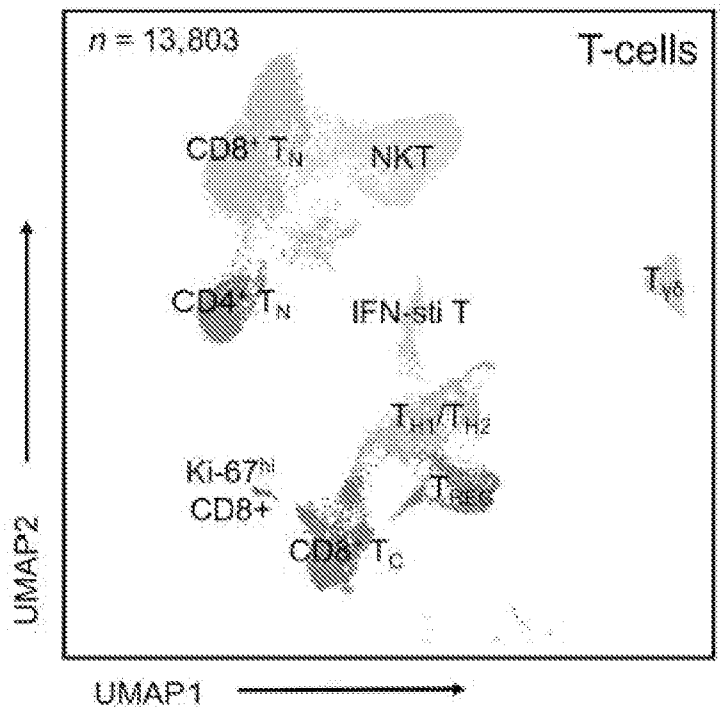

FIG. 3E

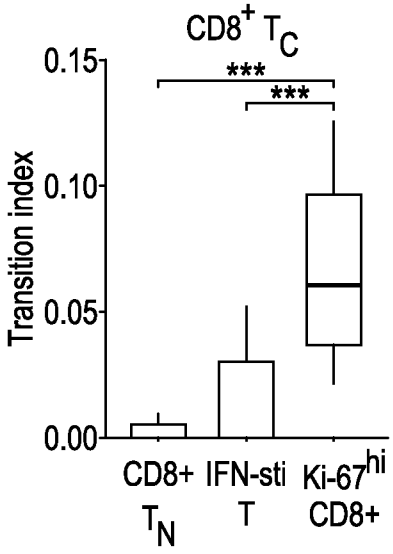

FIG. 3I

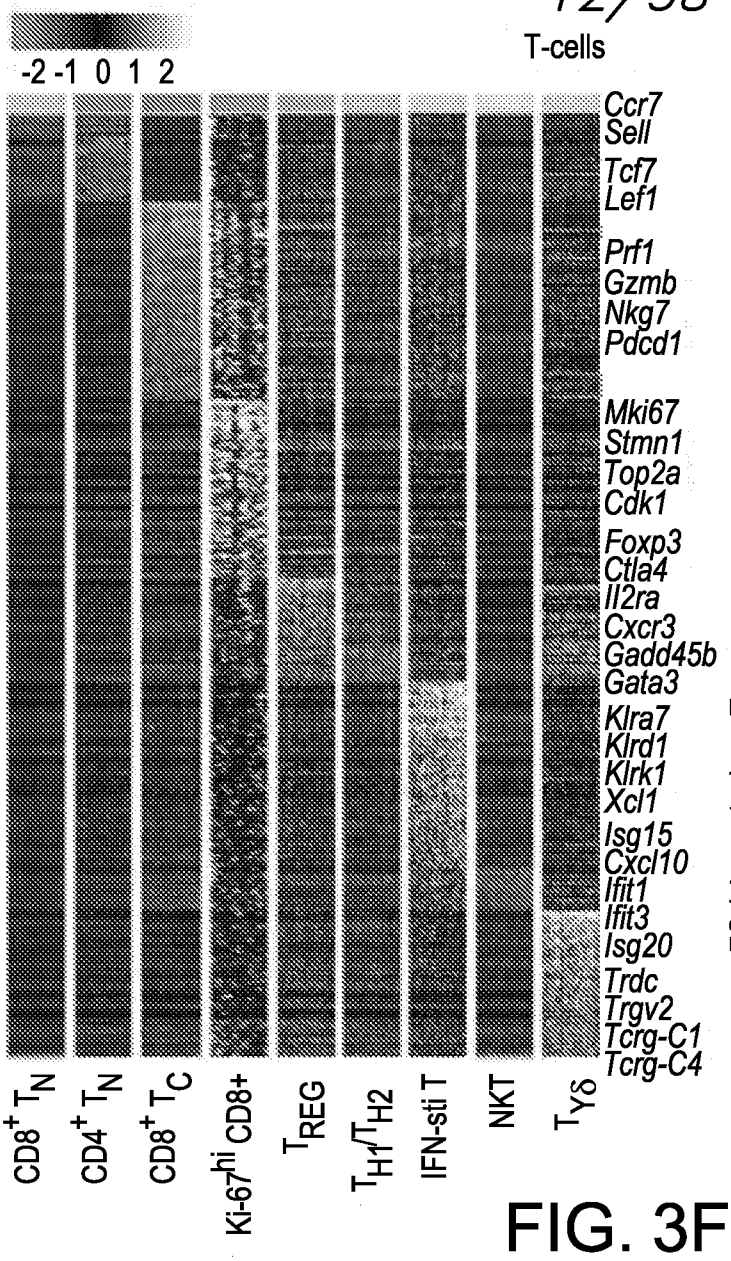

FIG. 3F

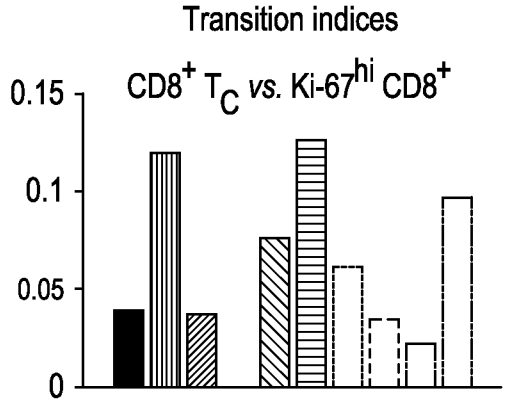

FIG. 3K

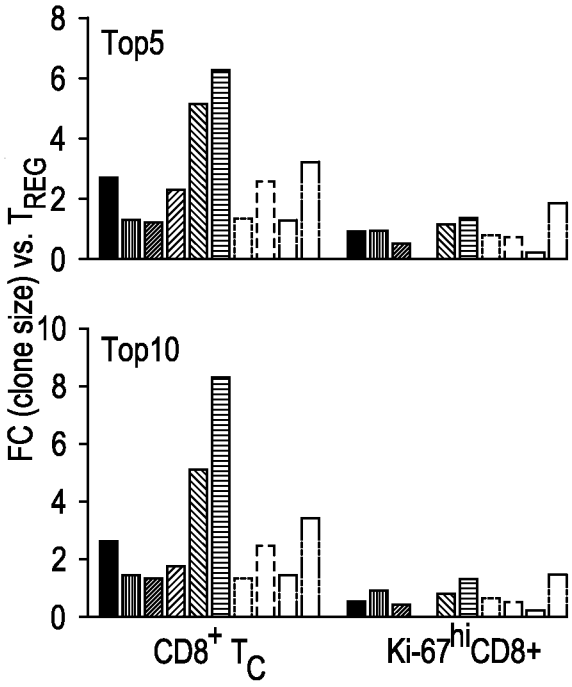

FIG. 3L

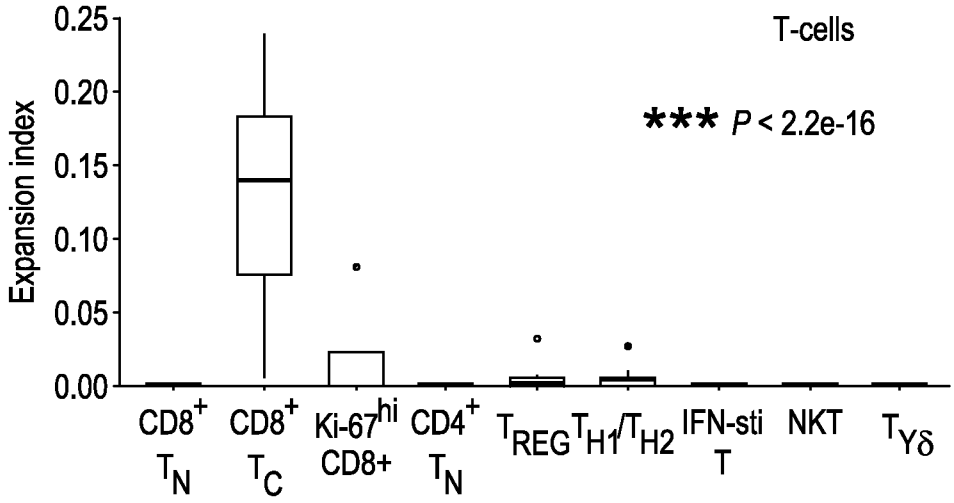

FIG. 3H

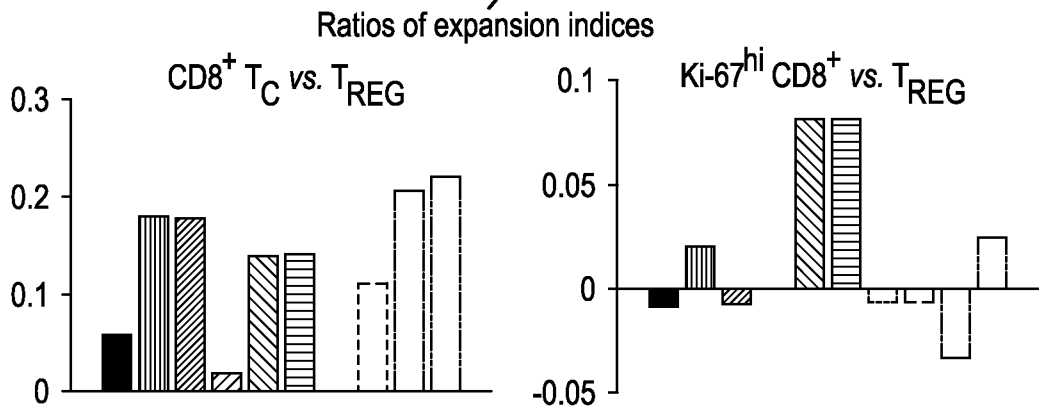

FIG. 3J

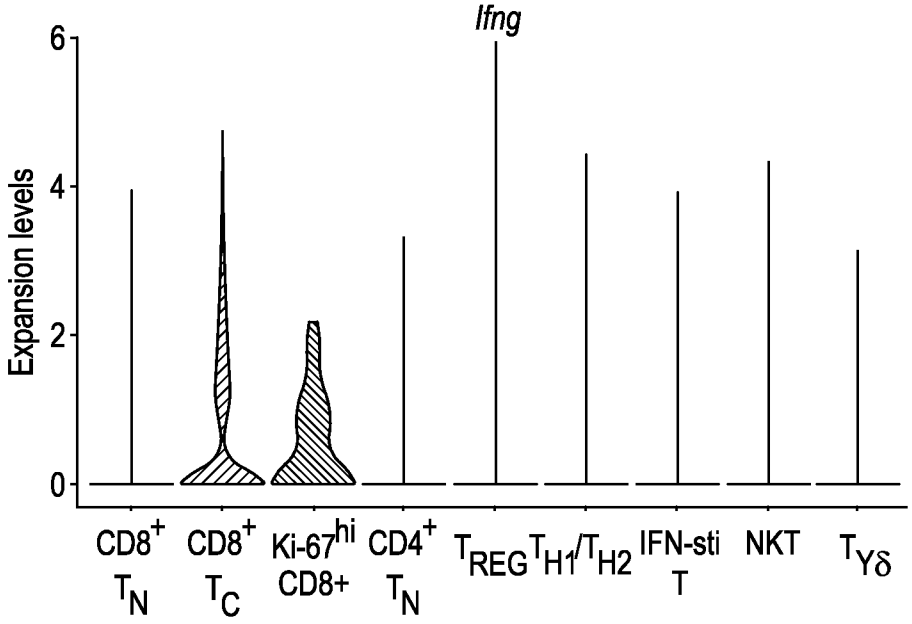

FIG. 3M

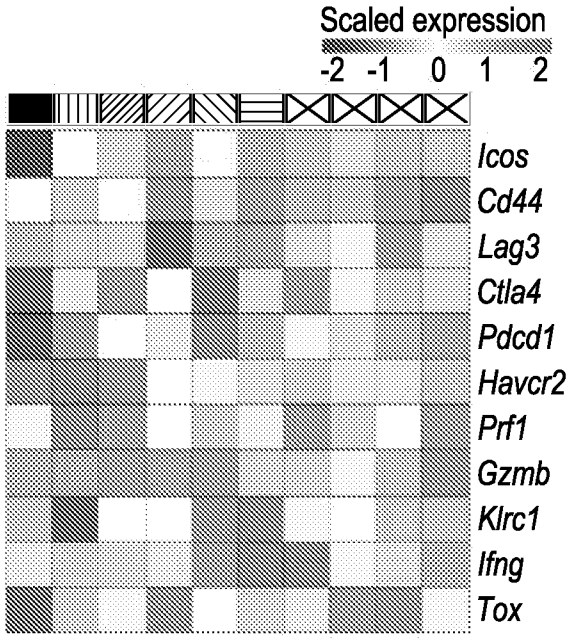

FIG. 3N

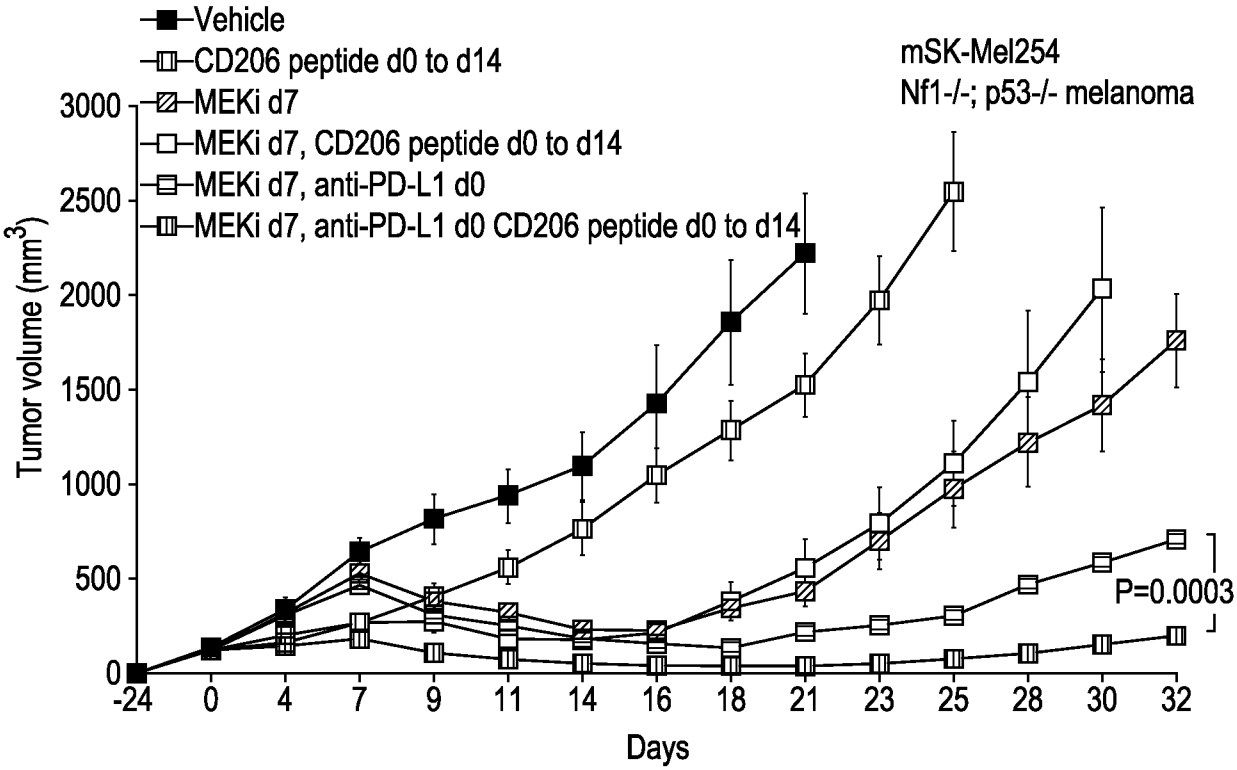
Vehicle
CD206 peptide d0 to d14
MEKi d7
MEKi d7, CD206 peptide d0 to d14
MEKi d7, anti-PD-L1 d0
MEKi d7, anti-PD-L1 d0 CD206 peptide d0 to d14
mSK-Mel254
Nf1-/-; p53-/- melanoma
Tumor volume (mm3)
3000
2500
2000
1500
1000
500
0
-24
0
4
7
9
11
14
16
18
21
23
25
28
30
32
Days
P=0.0003

FIG. 4A

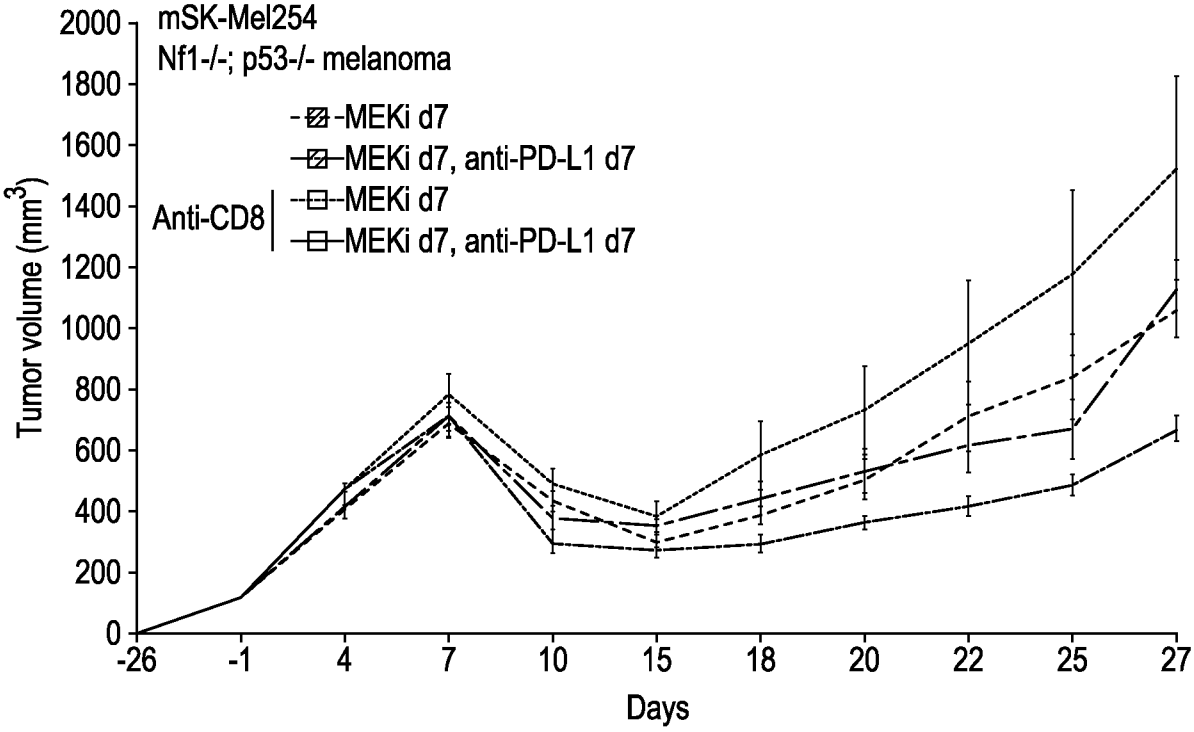
mSK-Mel254
Nf1-/-; p53-/- melanoma
MEKi d7
MEKi d7, anti-PD-L1 d7
Anti-CD8
MEKi d7
MEKi d7, anti-PD-L1 d7
Tumor volume (mm3)
2000
1800
1600
1400
1200
1000
800
600
400
200
0
-26
-1
4
7
10
15
18
20
22
25
27
Days

FIG. 4B

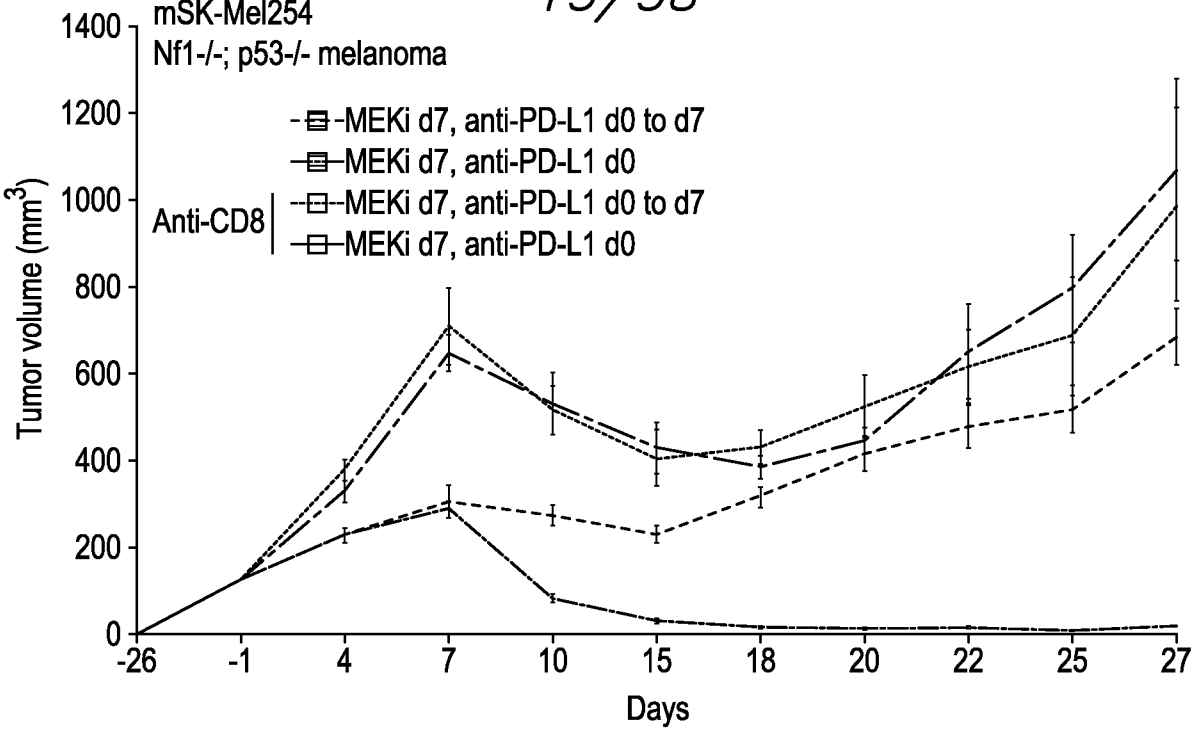

FIG. 4C

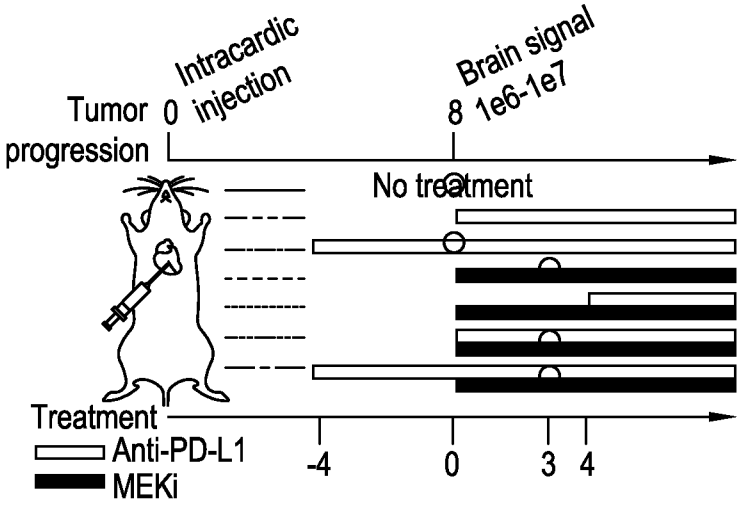

FIG. 5A

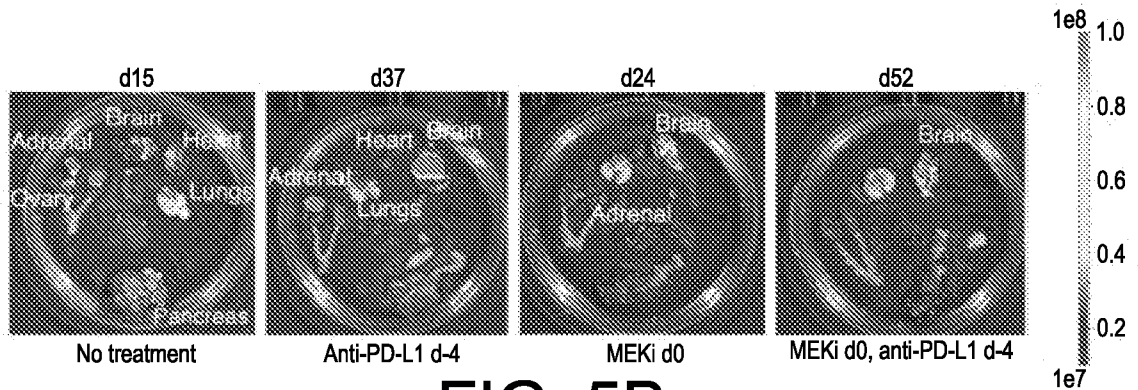

FIG. 5B

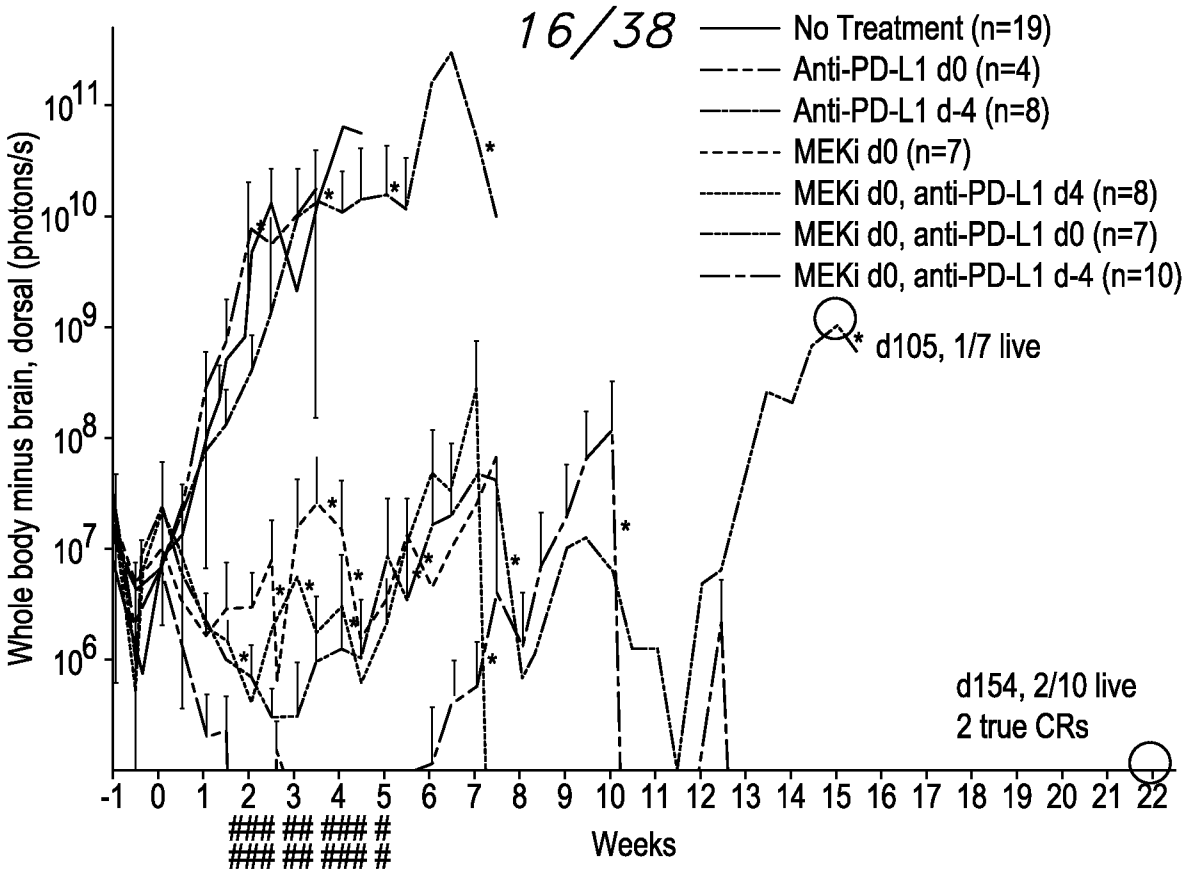
No Treatment (n=19)
Anti-PD-L1 d0 (n=4)
Anti-PD-L1 d-4 (n=8)
MEKi d0 (n=7)
MEKi d0, anti-PD-L1 d4 (n=8)
MEKi d0, anti-PD-L1 d0 (n=7)
MEKi d0, anti-PD-L1 d-4 (n=10)
Whole body minus brain, dorsal (photons/s)
d105, 1/7 live
d154, 2/10 live
2 true CRs
Weeks

FIG. 5C

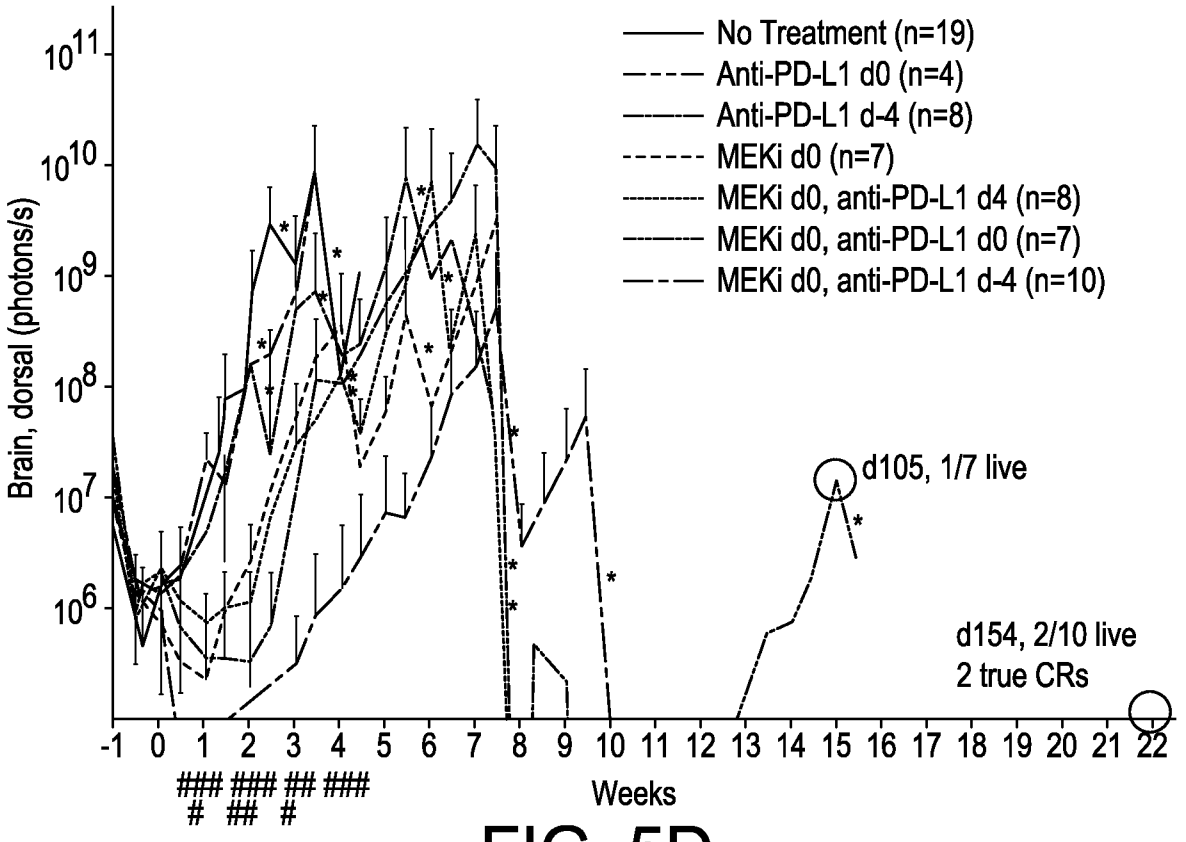
No Treatment (n=19)
Anti-PD-L1 d0 (n=4)
Anti-PD-L1 d-4 (n=8)
MEKi d0 (n=7)
MEKi d0, anti-PD-L1 d4 (n=8)
MEKi d0, anti-PD-L1 d0 (n=7)
MEKi d0, anti-PD-L1 d-4 (n=10)
Brain, dorsal (photons/s)
d105, 1/7 live
d154, 2/10 live
2 true CRs
Weeks

FIG. 5D

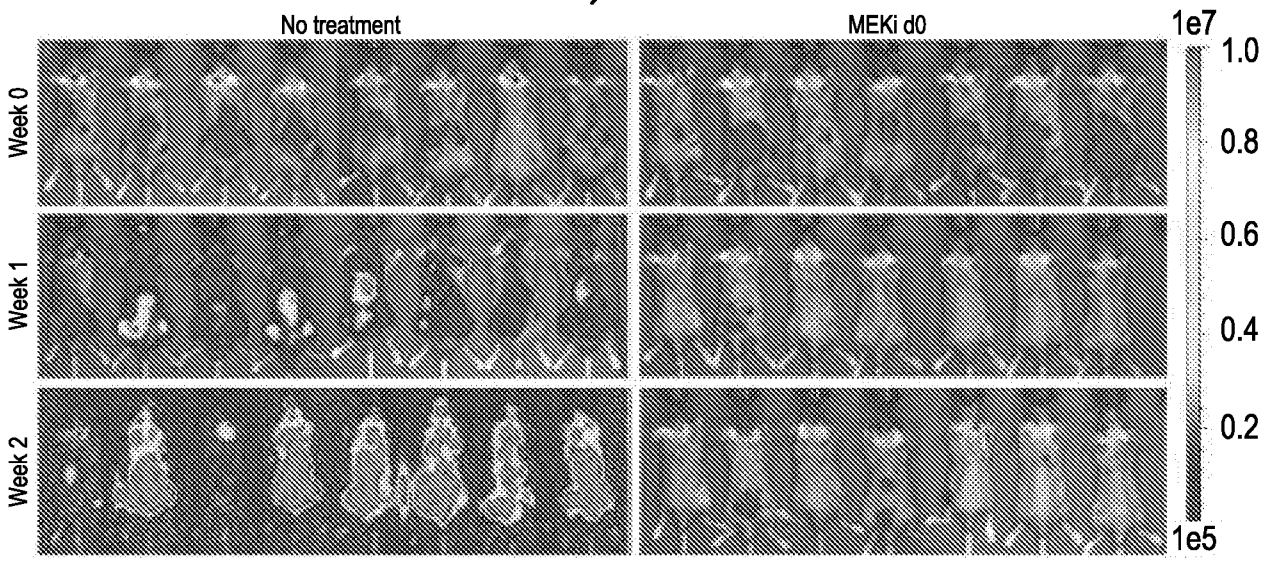
No treatment
MEKi d0
Week 0
Week 1
Week 2
1e7
1.0
0.8
0.6
0.4
0.2
1e5

FIG. 5E

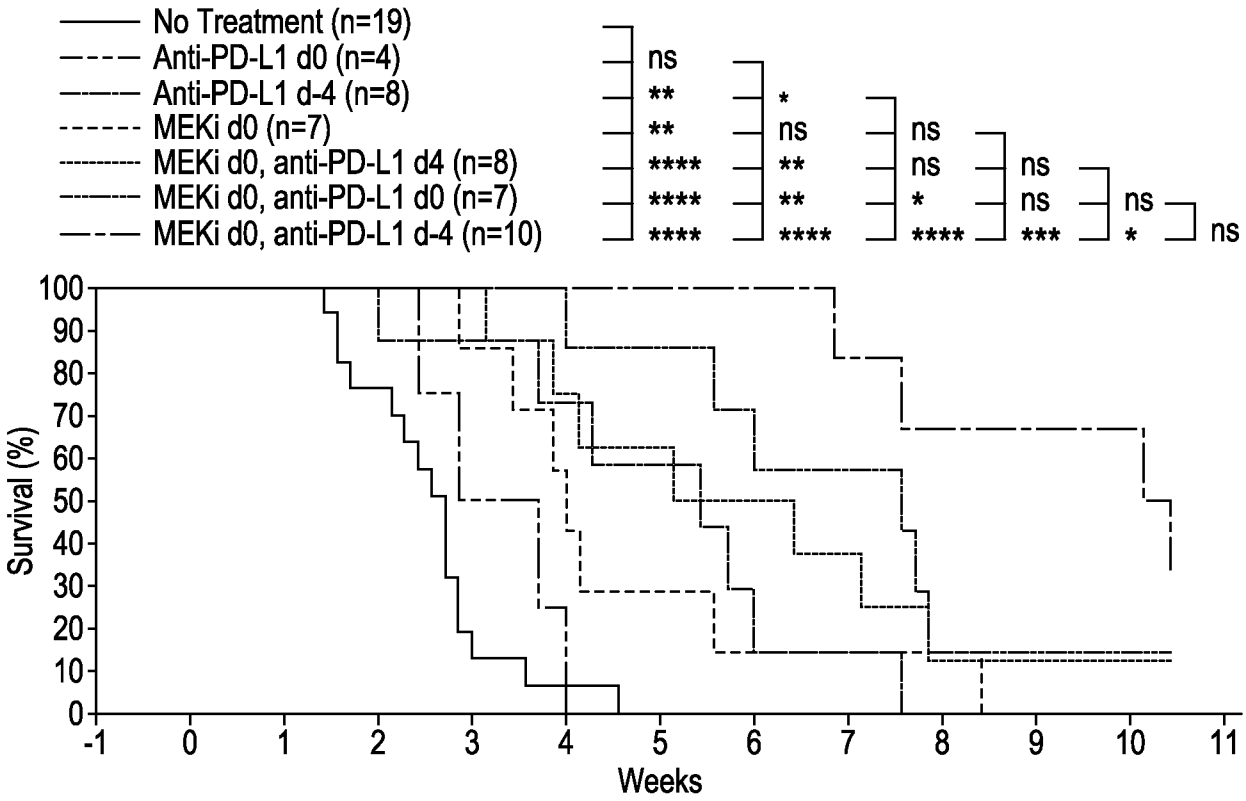
No Treatment (n=19)
Anti-PD-L1 d0 (n=4)
Anti-PD-L1 d-4 (n=8)
MEKi d0 (n=7)
MEKi d0, anti-PD-L1 d4 (n=8)
MEKi d0, anti-PD-L1 d0 (n=7)
MEKi d0, anti-PD-L1 d-4 (n=10)
ns
**
**
****
****
****
*
ns
**
**
****
ns
ns
*
****
ns
ns
***
ns
*
ns
Survival (%)
100
90
80
70
60
50
40
30
20
10
0
-1
0
1
2
3
4
5
6
7
8
9
10
11
Weeks

FIG. 5F

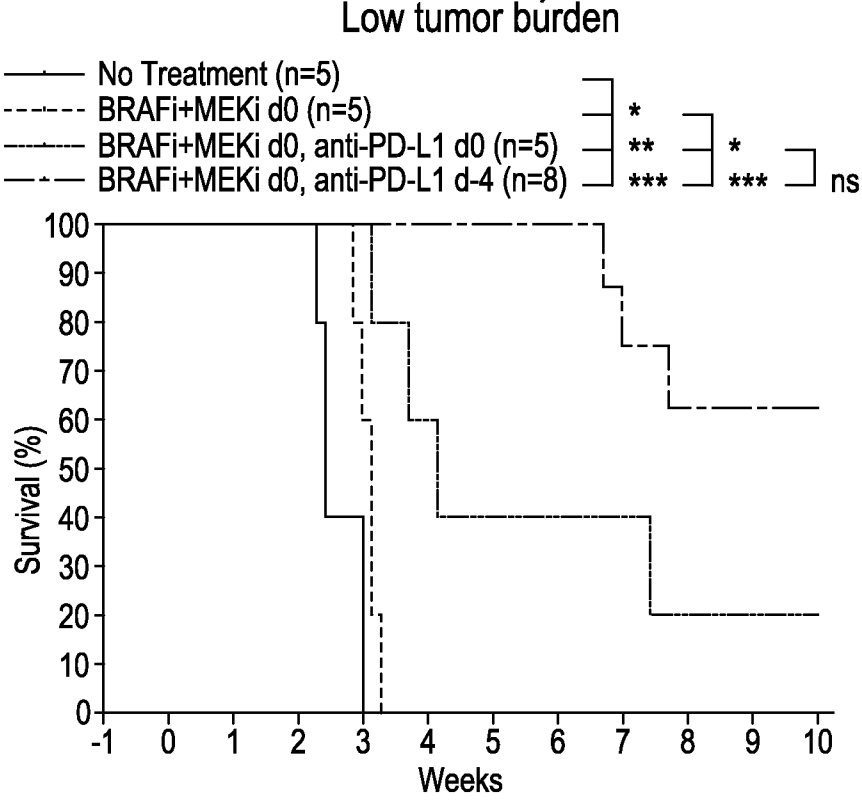
Low tumor burden
No Treatment (n=5)
BRAFi+MEKi d0 (n=5)
BRAFi+MEKi d0, anti-PD-L1 d0 (n=5)
BRAFi+MEKi d0, anti-PD-L1 d-4 (n=8)
*
**
***
*
***
ns
Survival (%)
Weeks

FIG. 5G

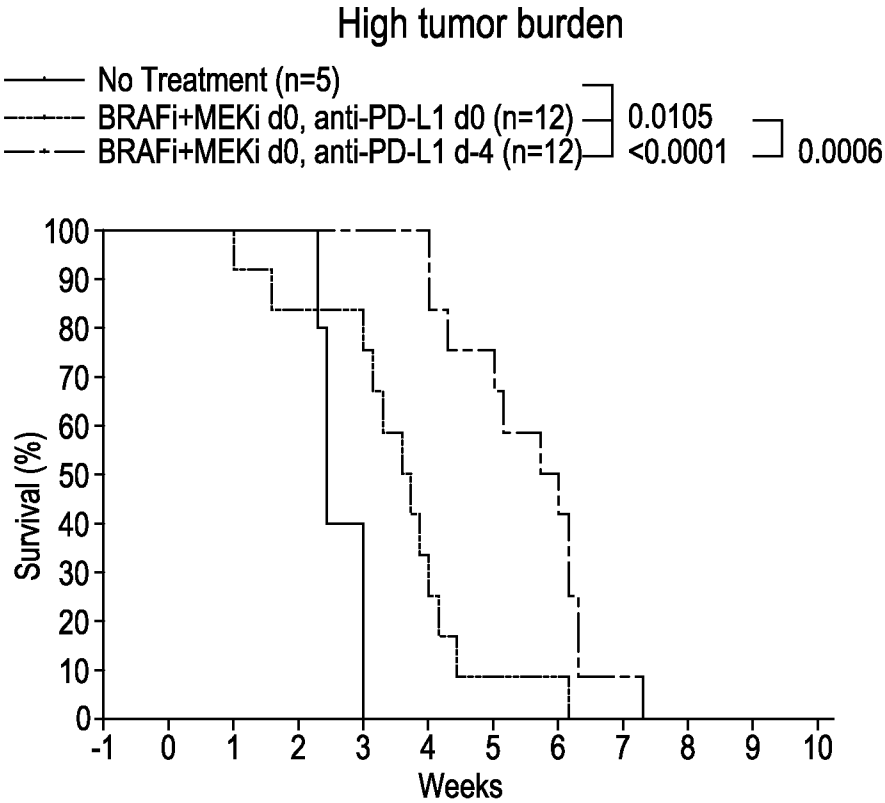
High tumor burden
No Treatment (n=5)
BRAFi+MEKi d0, anti-PD-L1 d0 (n=12)
BRAFi+MEKi d0, anti-PD-L1 d-4 (n=12)
0.0105
<0.0001
0.0006
Survival (%)
Weeks

FIG. 5H

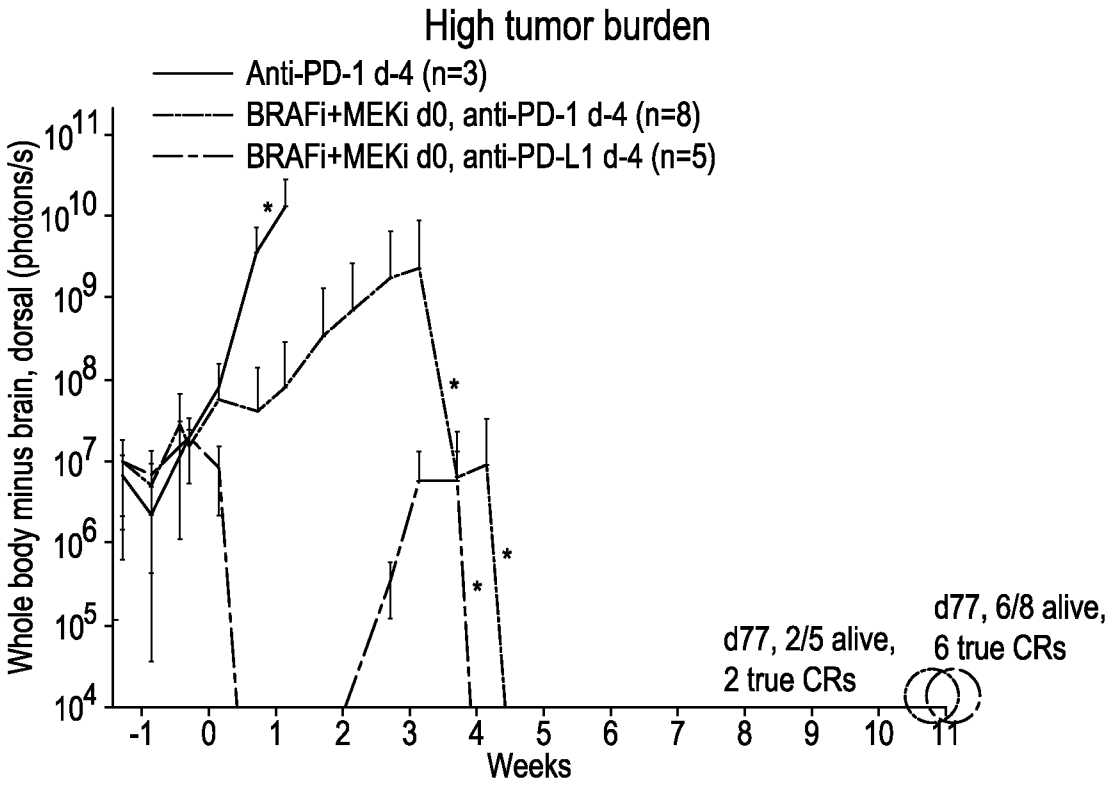
High tumor burden
Anti-PD-1 d-4 (n=3)
BRAFi+MEKi d0, anti-PD-1 d-4 (n=8)
BRAFi+MEKi d0, anti-PD-L1 d-4 (n=5)
Whole body minus brain, dorsal (photons/s)
10^{11}
10^{10}
10^{9}
10^{8}
10^{7}
10^{6}
10^{5}
10^{4}
-1 0 1 2 3 4 5 6 7 8 9 10 11
Weeks
d77, 2/5 alive,
2 true CRs
d77, 6/8 alive,
6 true CRs

FIG. 5I

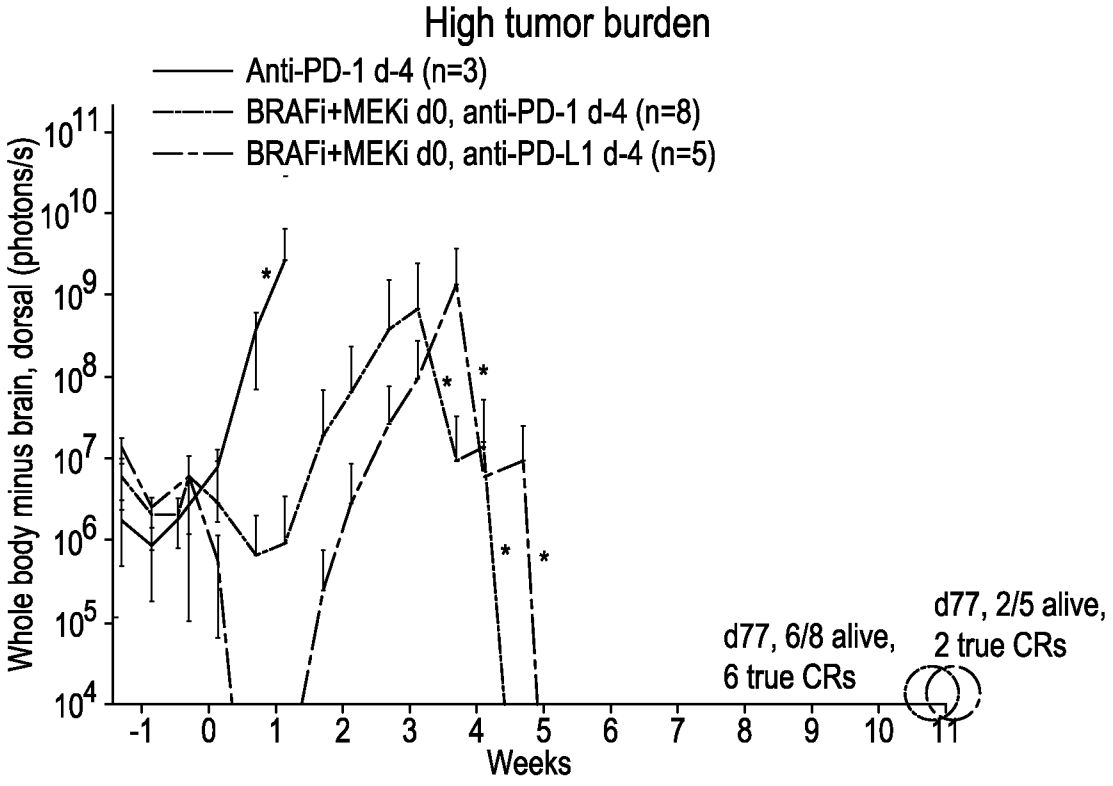
High tumor burden
Anti-PD-1 d-4 (n=3)
BRAFi+MEKi d0, anti-PD-1 d-4 (n=8)
BRAFi+MEKi d0, anti-PD-L1 d-4 (n=5)
Whole body minus brain, dorsal (photons/s)
10^{11}
10^{10}
10^{9}
10^{8}
10^{7}
10^{6}
10^{5}
10^{4}
-1 0 1 2 3 4 5 6 7 8 9 10 11
Weeks
d77, 6/8 alive,
6 true CRs
d77, 2/5 alive,
2 true CRs

FIG. 5J

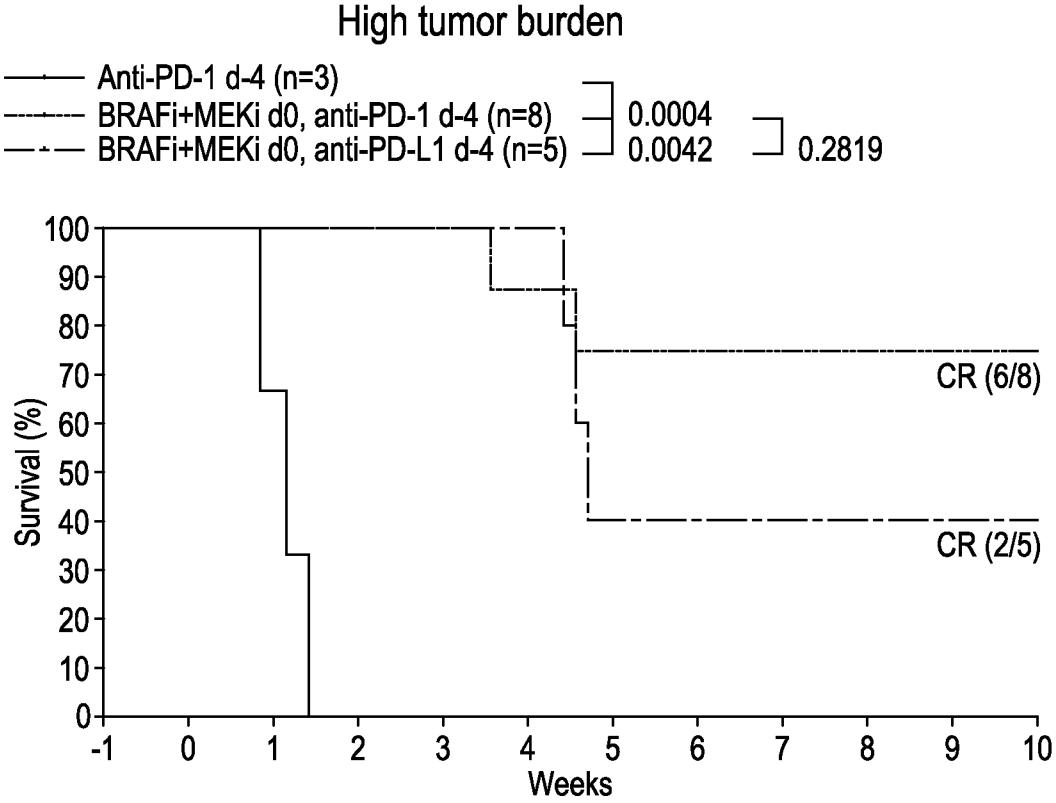
High tumor burden
Anti-PD-1 d-4 (n=3)
BRAFi+MEKi d0, anti-PD-1 d-4 (n=8)
BRAFi+MEKi d0, anti-PD-L1 d-4 (n=5)
0.0004
0.0042
0.2819
Survival (%)
Weeks
CR (6/8)
CR (2/5)

FIG. 5K

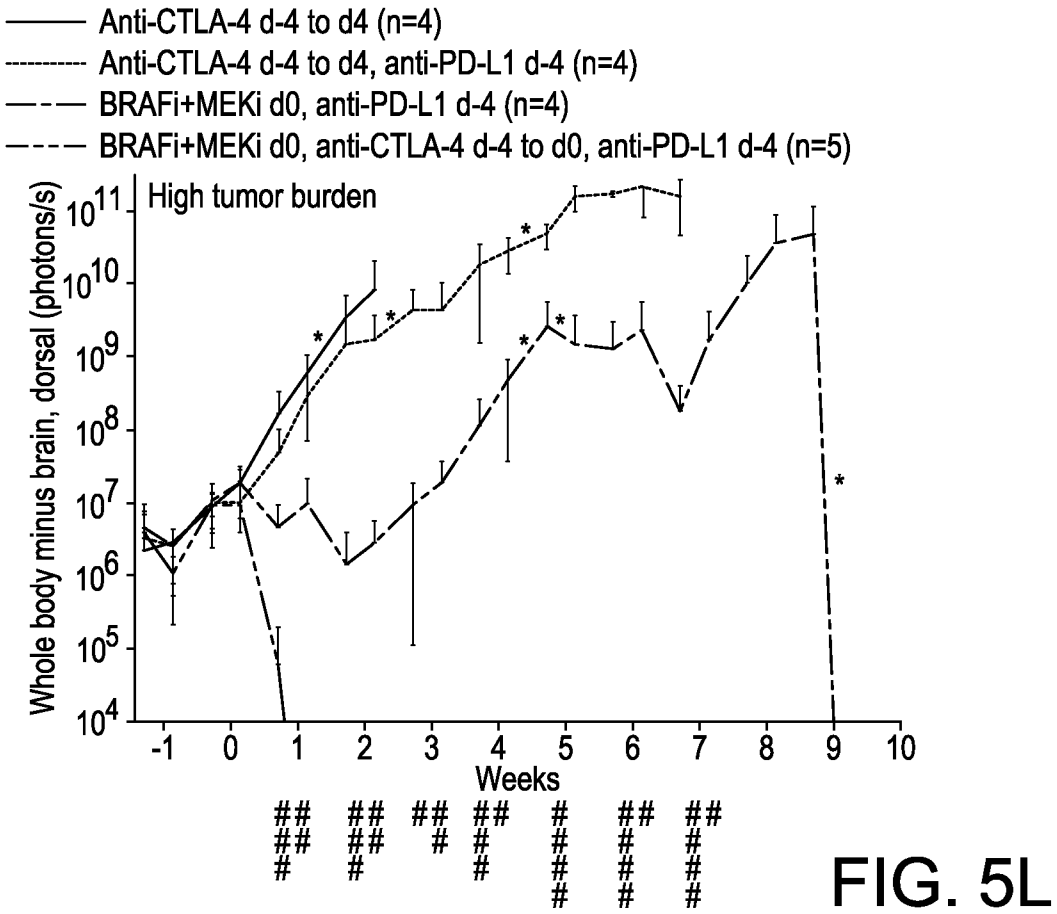
Anti-CTLA-4 d-4 to d4 (n=4)
Anti-CTLA-4 d-4 to d4, anti-PD-L1 d-4 (n=4)
BRAFi+MEKi d0, anti-PD-L1 d-4 (n=4)
BRAFi+MEKi d0, anti-CTLA-4 d-4 to d0, anti-PD-L1 d-4 (n=5)
High tumor burden
Whole body minus brain, dorsal (photons/s)
Weeks

FIG. 5L

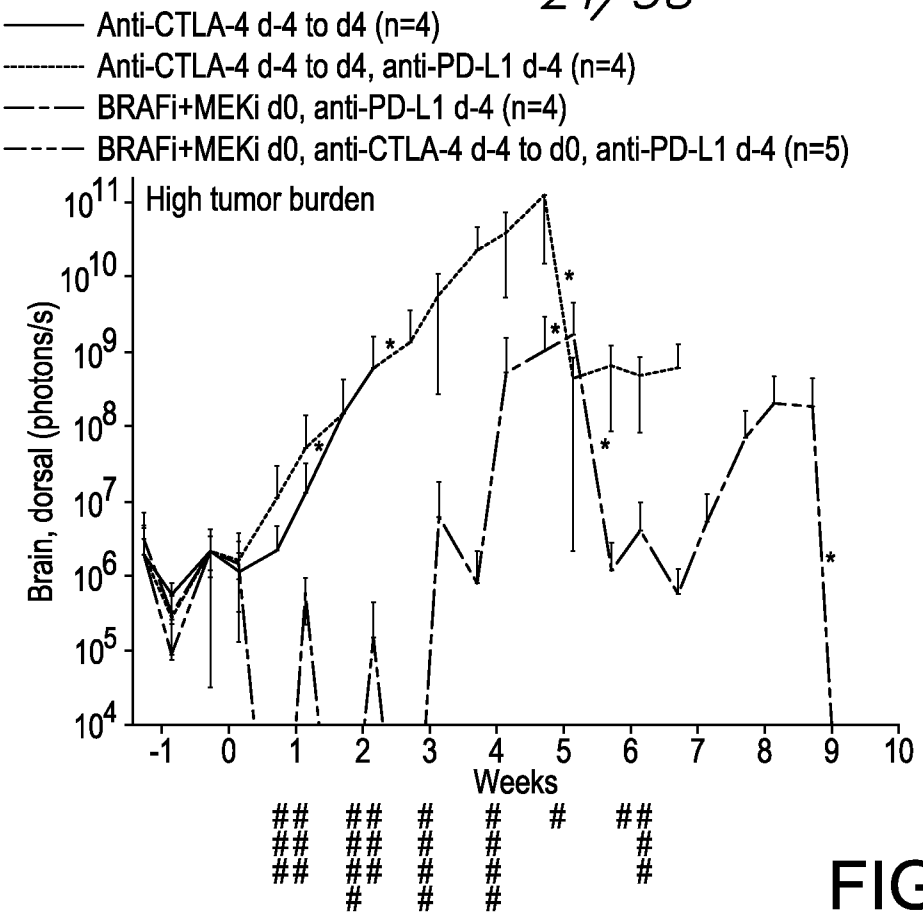
Anti-CTLA-4 d-4 to d4 (n=4)
Anti-CTLA-4 d-4 to d4, anti-PD-L1 d-4 (n=4)
BRAFi+MEKi d0, anti-PD-L1 d-4 (n=4)
BRAFi+MEKi d0, anti-CTLA-4 d-4 to d0, anti-PD-L1 d-4 (n=5)
High tumor burden
Brain, dorsal (photons/s)
Weeks

FIG. 5M

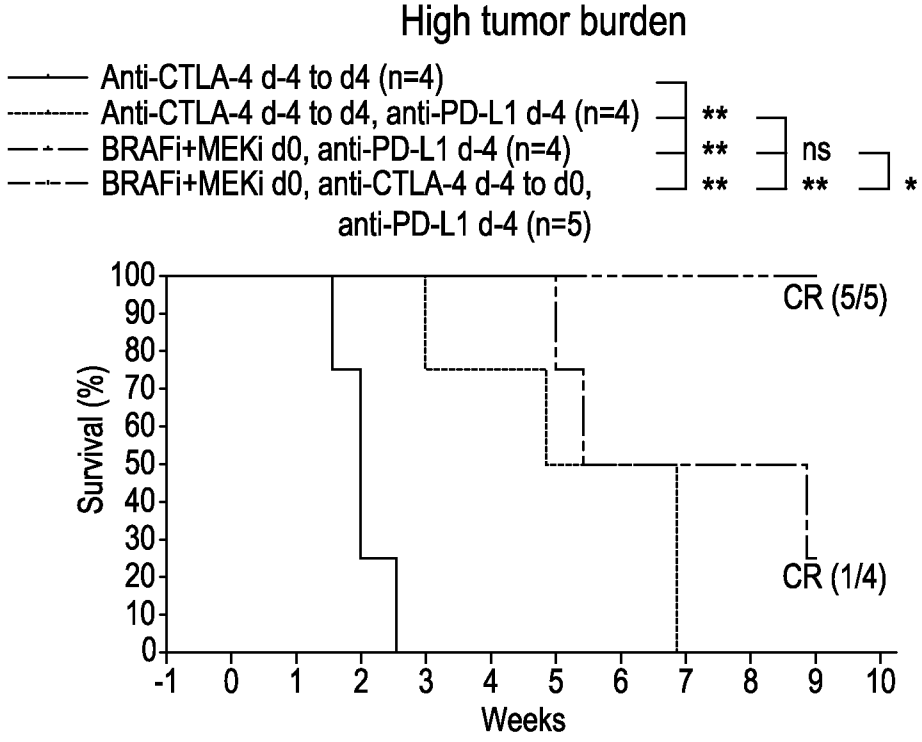
High tumor burden
Anti-CTLA-4 d-4 to d4 (n=4)
Anti-CTLA-4 d-4 to d4, anti-PD-L1 d-4 (n=4)
BRAFi+MEKi d0, anti-PD-L1 d-4 (n=4)
BRAFi+MEKi d0, anti-CTLA-4 d-4 to d0, anti-PD-L1 d-4 (n=5)
**
**
**
ns
**
*
CR (5/5)
CR (1/4)
Survival (%)
Weeks

FIG. 5N

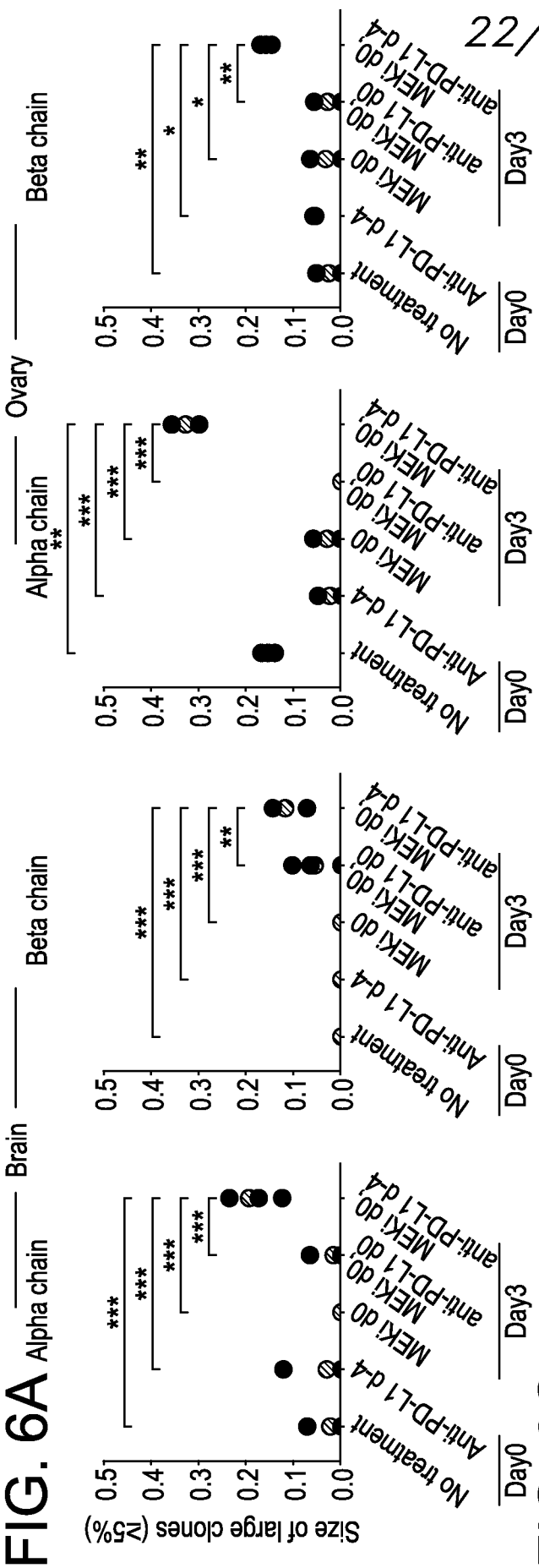
FIG. 6A
Brain
Ovary
Alpha chain
Beta chain
Size of large clones (≥5%)
No treatment
Anti-PD-L1 d-4
MEKi do
MEKi do, Anti-PD-L1 d-4
Day0
Day3

FIG. 6C
Brain
Ovary
Alpha chain
Beta chain
Lesion1
Lesion2
Size of common large clones (≥5%)
No treatment
Anti-PD-L1 d-4
MEKi do
MEKi do, Anti-PD-L1 d-4
Day0
Day3

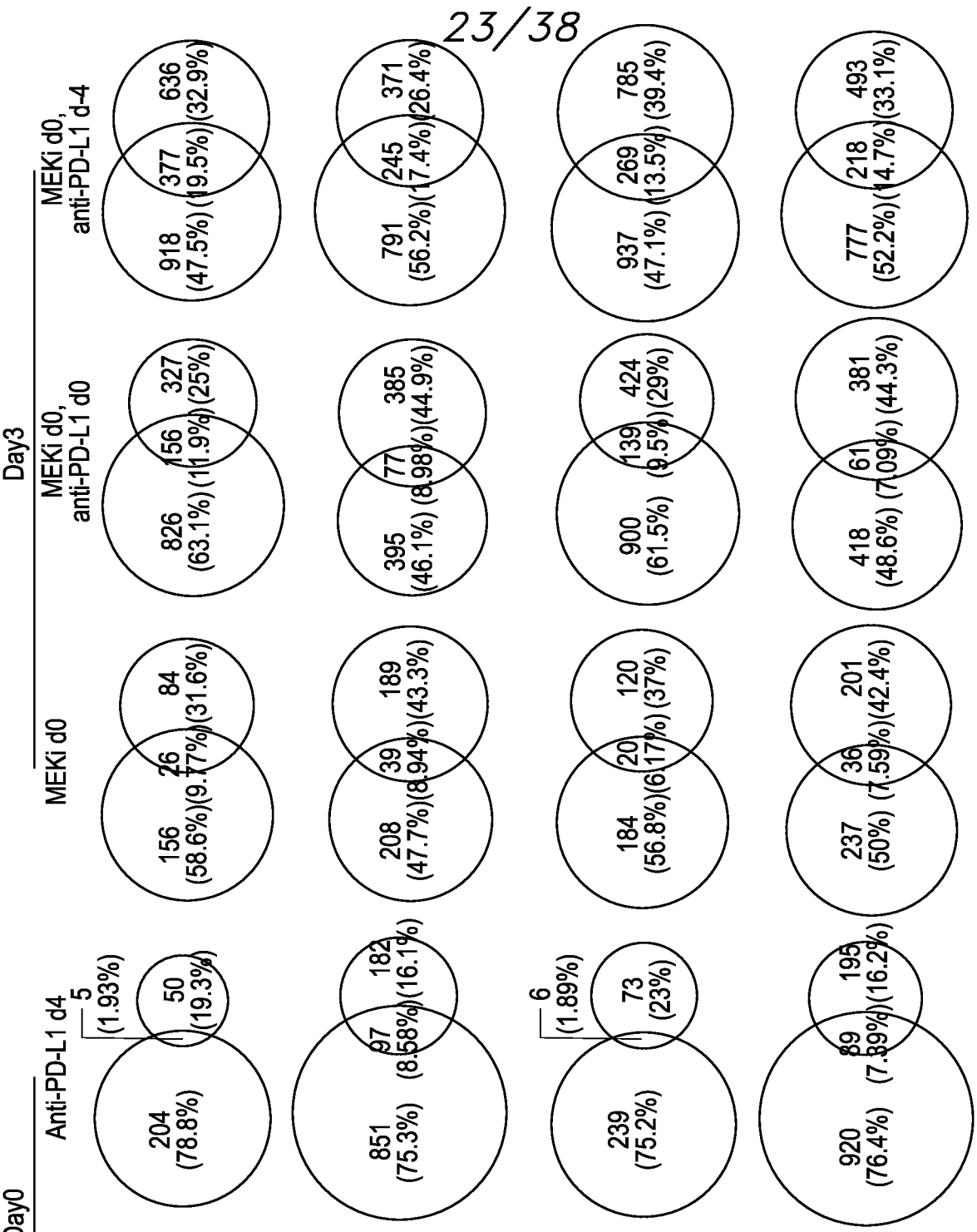
Brain
Day0
Day3
No treatment
Anti-PD-L1 d4
MEKi d0
MEKi d0, anti-PD-L1 d0
MEKi d0, anti-PD-L1 d-4
Alpha
Beta
106 (50.5%)
12 (5.71%)
92 (43.8%)
204 (78.8%)
5 (1.93%)
50 (19.3%)
156 (58.6%)
26 (9.77%)
84 (31.6%)
826 (63.1%)
156 (11.9%)
327 (25%)
918 (47.5%)
377 (19.5%)
636 (32.9%)
132 (50.2%)
12 (4.56%)
119 (45.2%)
851 (75.3%)
97 (8.58%)
182 (16.1%)
208 (47.7%)
39 (8.94%)
189 (43.3%)
395 (46.1%)
77 (8.98%)
385 (44.9%)
791 (56.2%)
245 (17.4%)
371 (26.4%)
239 (75.2%)
6 (1.89%)
73 (23%)
184 (56.8%)
20 (6.17%)
120 (37%)
900 (61.5%)
139 (9.5%)
424 (29%)
937 (47.1%)
269 (13.5%)
785 (39.4%)
920 (76.4%)
89 (7.39%)
195 (16.2%)
237 (50%)
36 (7.59%)
201 (42.4%)
418 (48.6%)
61 (7.09%)
381 (44.3%)
777 (52.2%)
218 (14.7%)
493 (33.1%)

FIG. 6B

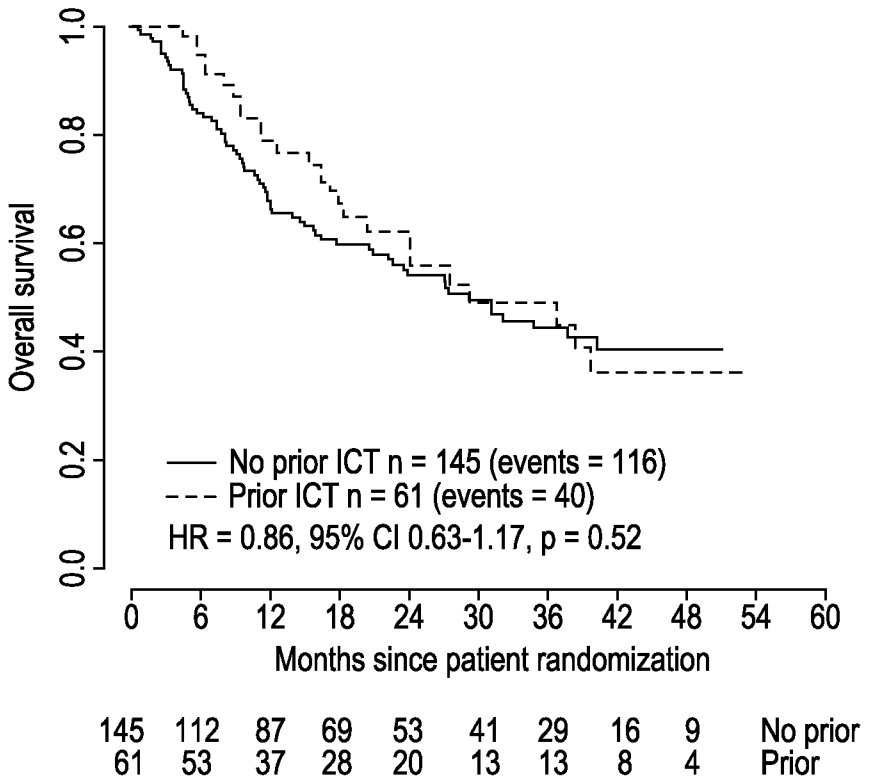
Overall survival
0.0
0.2
0.4
0.6
0.8
1.0
No prior ICT n = 145 (events = 116)
Prior ICT n = 61 (events = 40)
HR = 0.86, 95% CI 0.63-1.17, p = 0.52
0 6 12 18 24 30 36 42 48 54 60
Months since patient randomization
145 112 87 69 53 41 29 16 9 No prior
61 53 37 28 20 13 13 8 4 Prior

FIG. 7

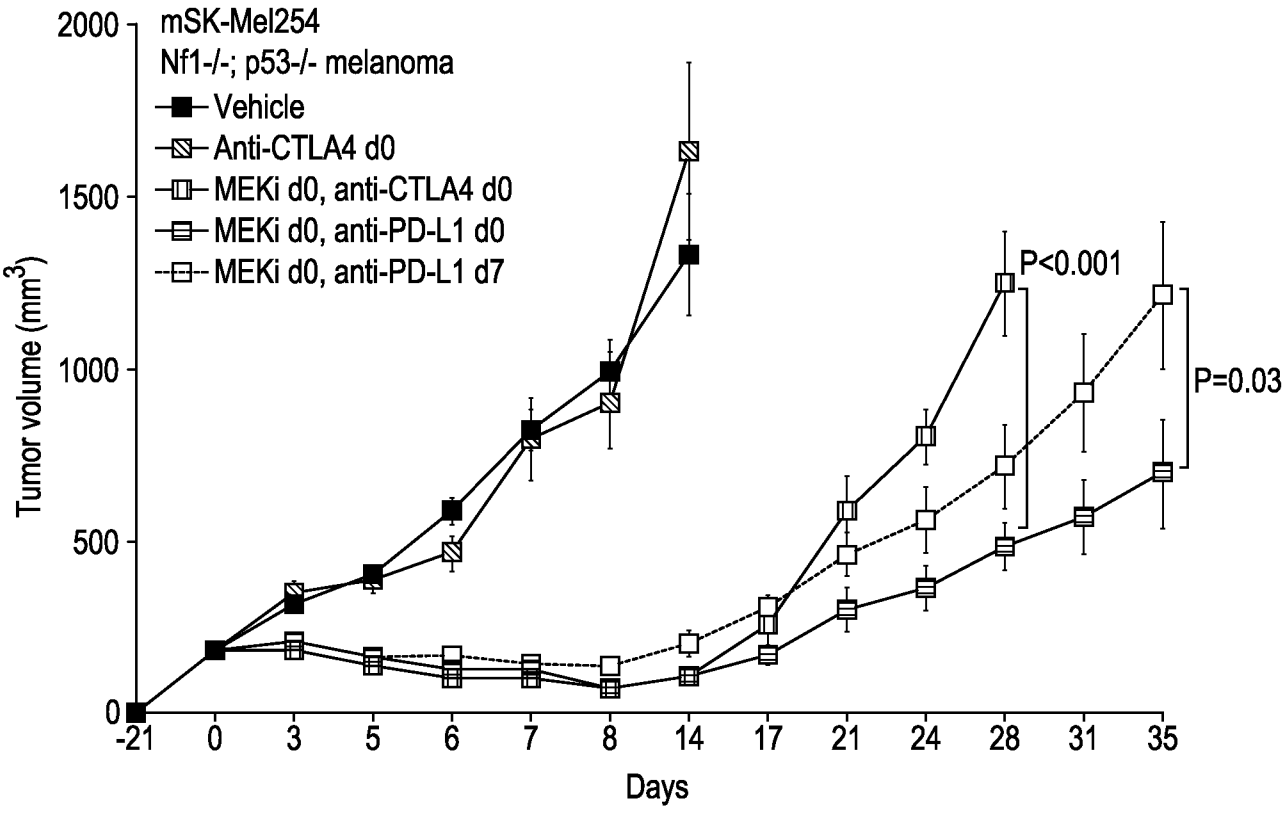
mSK-Mel254
Nf1-/-; p53-/- melanoma
Vehicle
Anti-CTLA4 d0
MEKi d0, anti-CTLA4 d0
MEKi d0, anti-PD-L1 d0
MEKi d0, anti-PD-L1 d7
Tumor volume (mm3)
0
500
1000
1500
2000
P<0.001
P=0.03
-21 0 3 5 6 7 8 14 17 21 24 28 31 35
Days

FIG. 8B

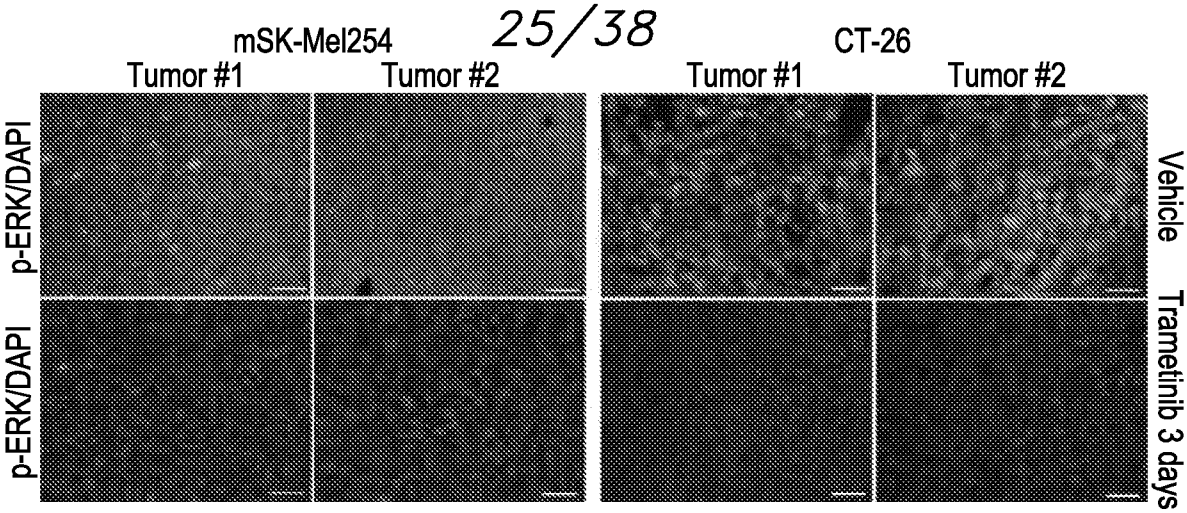

FIG. 8A

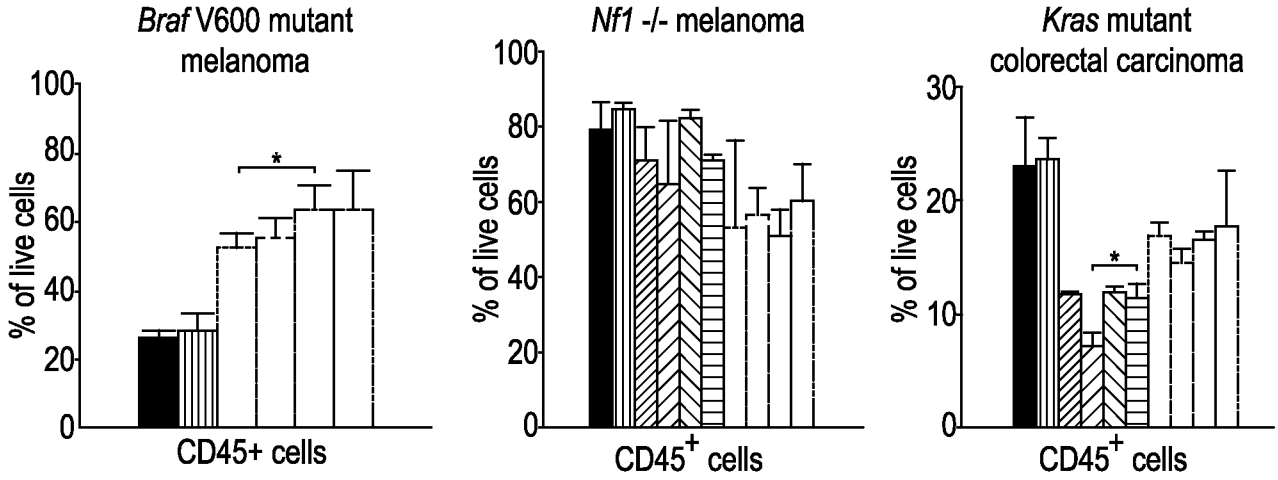

FIG. 8C

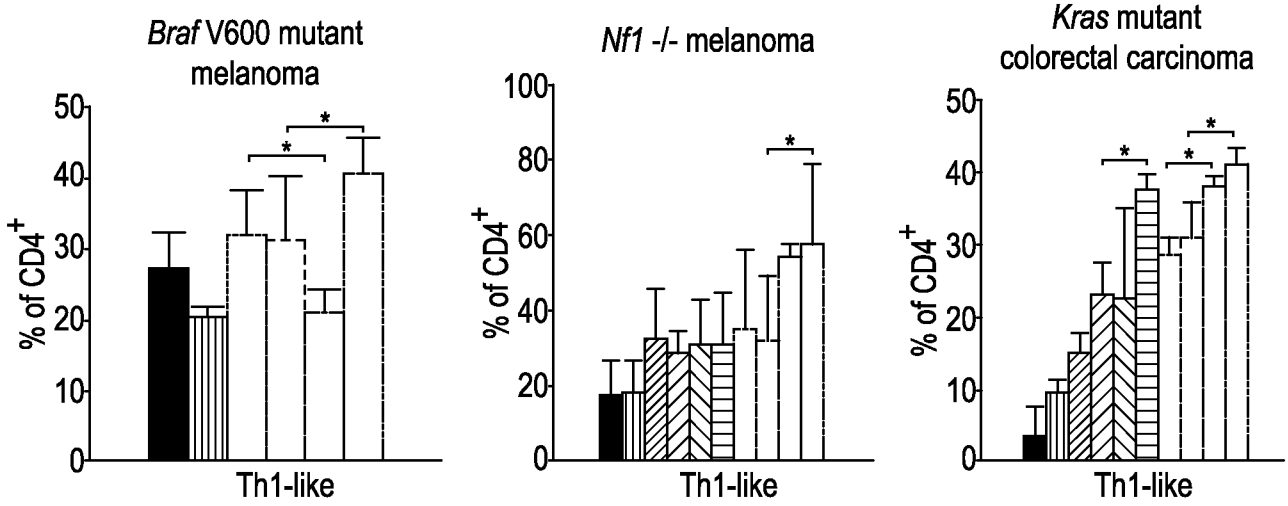

FIG. 8E

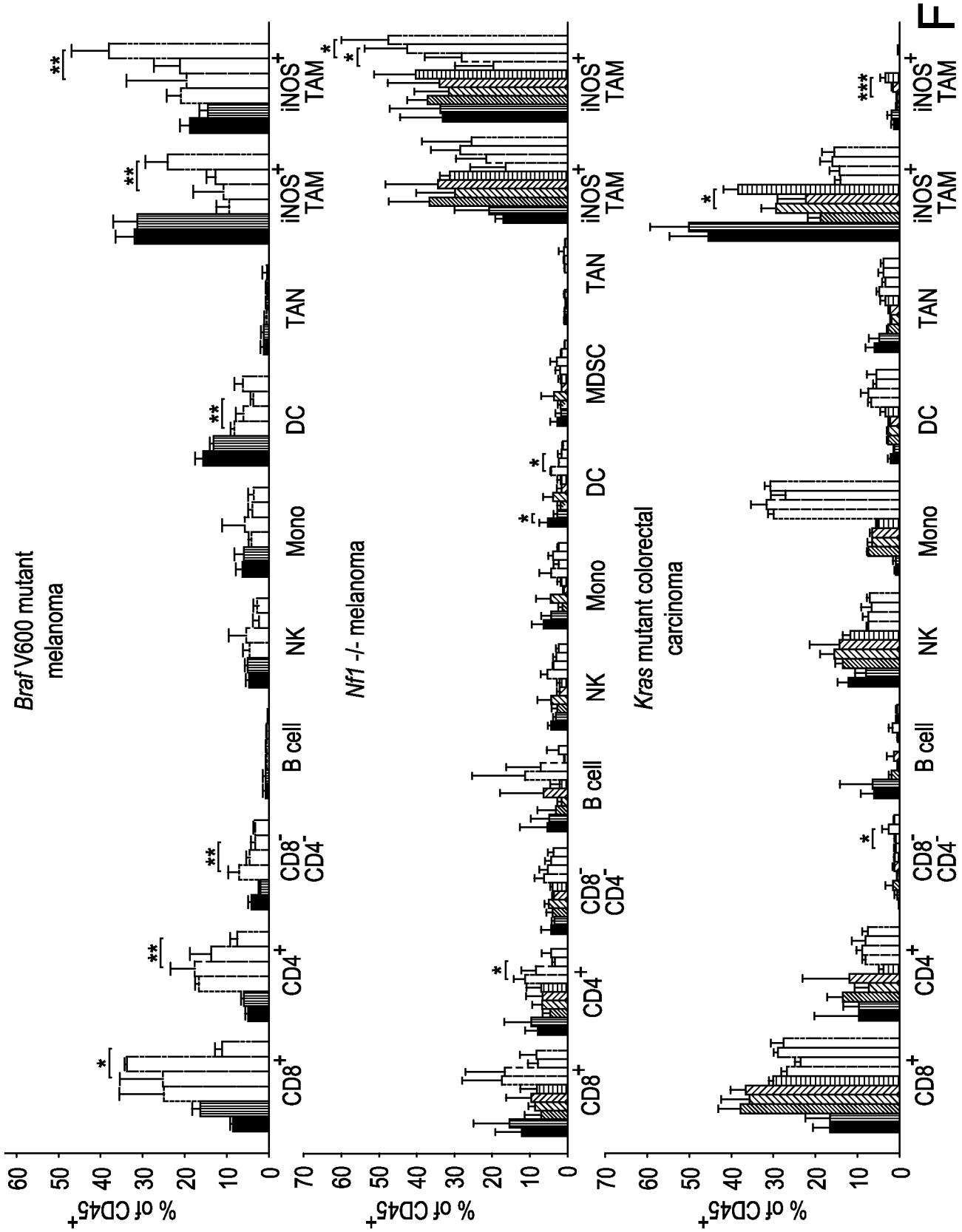
Braf V600 mutant melanoma
Nf1 -/- melanoma
Kras mutant colorectal carcinoma
% of CD45+
CD8+
CD4+
CD8-CD4-
B cell
NK
Mono
DC
MDSC
TAN
iNOS+ TAM

FIG. 8D

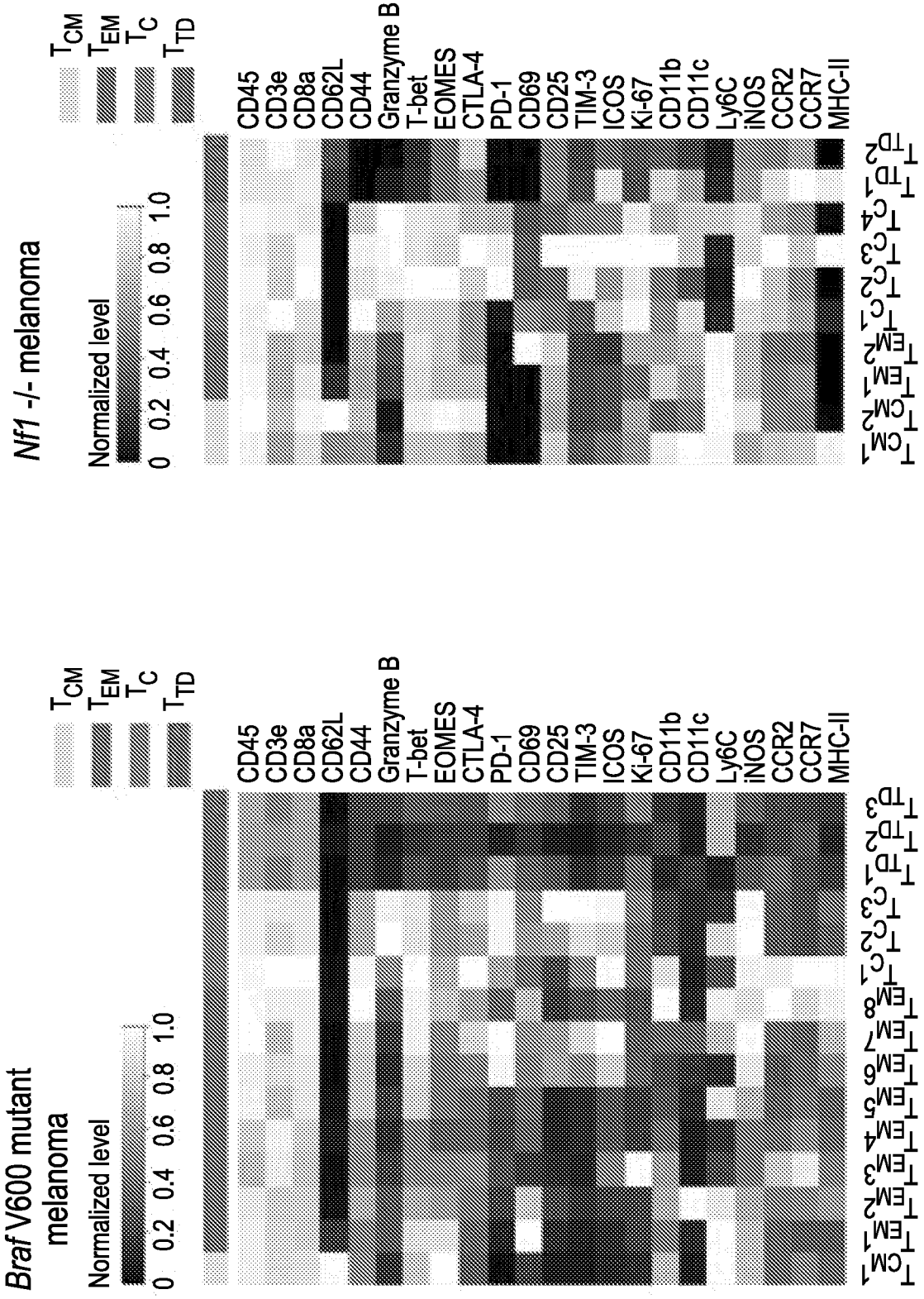
Braf V600 mutant melanoma
Normalized level
0 0.2 0.4 0.6 0.8 1.0
TCM
TEM
TC
TTD
CD45
CD3e
CD8a
CD62L
CD44
Granzyme B
T-bet
EOMES
CTLA-4
PD-1
CD69
CD25
TIM-3
ICOS
Ki-67
CD11b
CD11c
Ly6C
iNOS
CCR2
CCR7
MHC-II
TCM1 TEM1 TEM2 TEM3 TEM4 TEM5 TEM6 TEM7 TEM8 TC1 TC2 TC3 TC4 TTD1 TTD2 TTD3
Nf1 -/- melanoma
Normalized level
0 0.2 0.4 0.6 0.8 1.0
TCM
TEM
TC
TTD
CD45
CD3e
CD8a
CD62L
CD44
Granzyme B
T-bet
EOMES
CTLA-4
PD-1
CD69
CD25
TIM-3
ICOS
Ki-67
CD11b
CD11c
Ly6C
iNOS
CCR2
CCR7
MHC-II
TCM1 TCM2 TEM1 TEM2 TC1 TC2 TC3 TC4 TTD1 TTD2

FIG. 8F

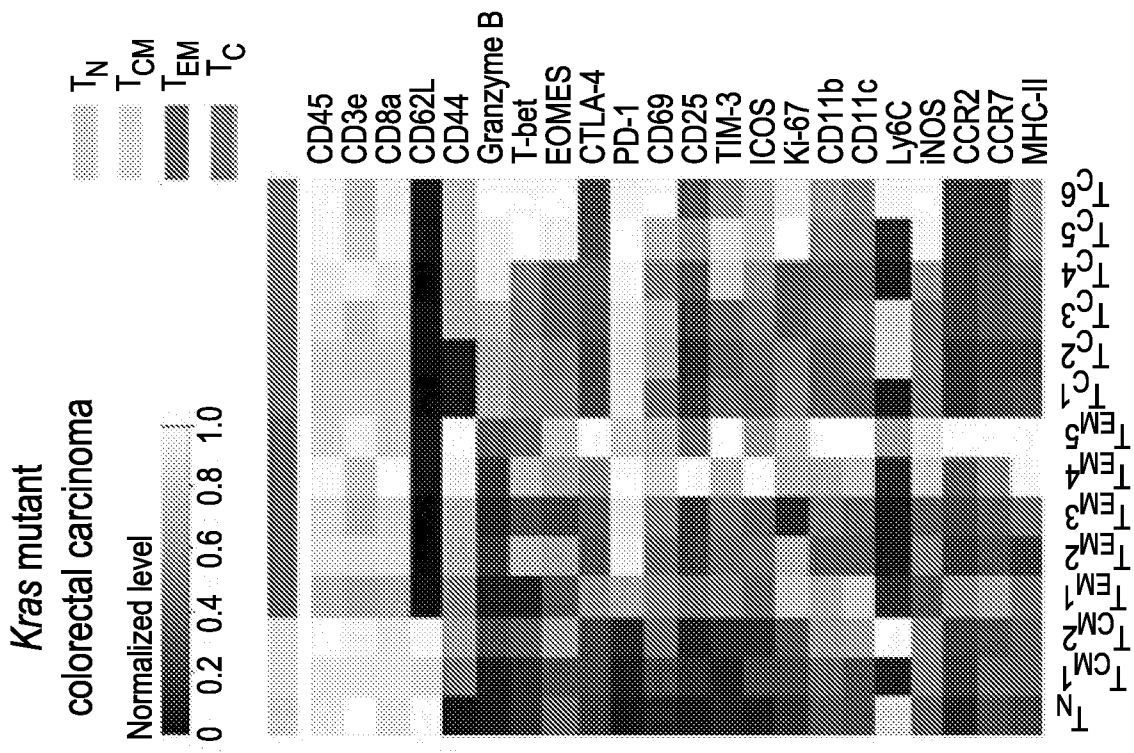

FIG. 8F (continue)

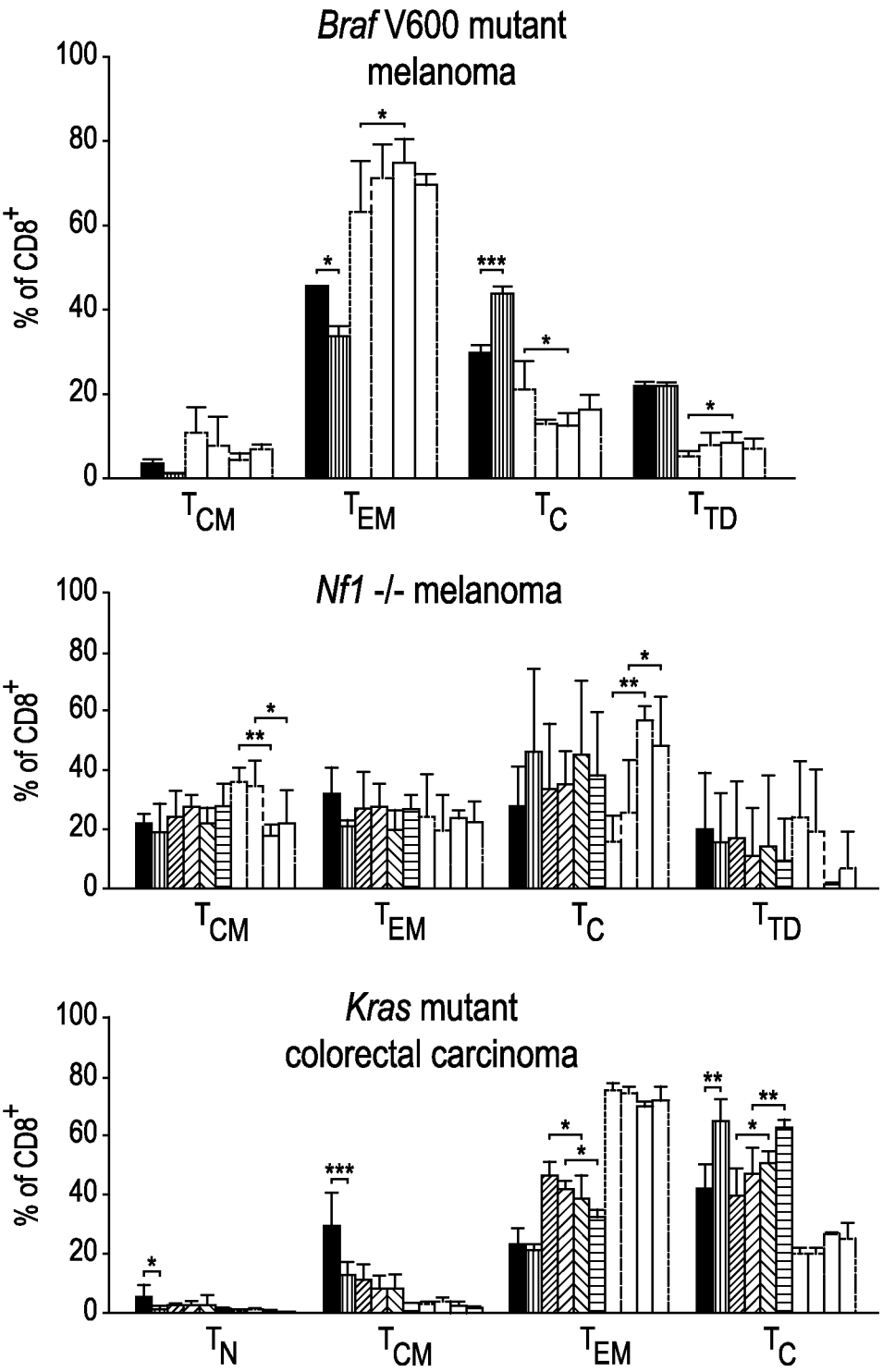
Braf V600 mutant melanoma
% of CD8+
100
80
60
40
20
0
TCM
TEM
TC
TTD
Nf1 -/- melanoma
% of CD8+
TCM
TEM
TC
TTD
Kras mutant colorectal carcinoma
% of CD8+
TN
TCM
TEM
TC

FIG. 8G

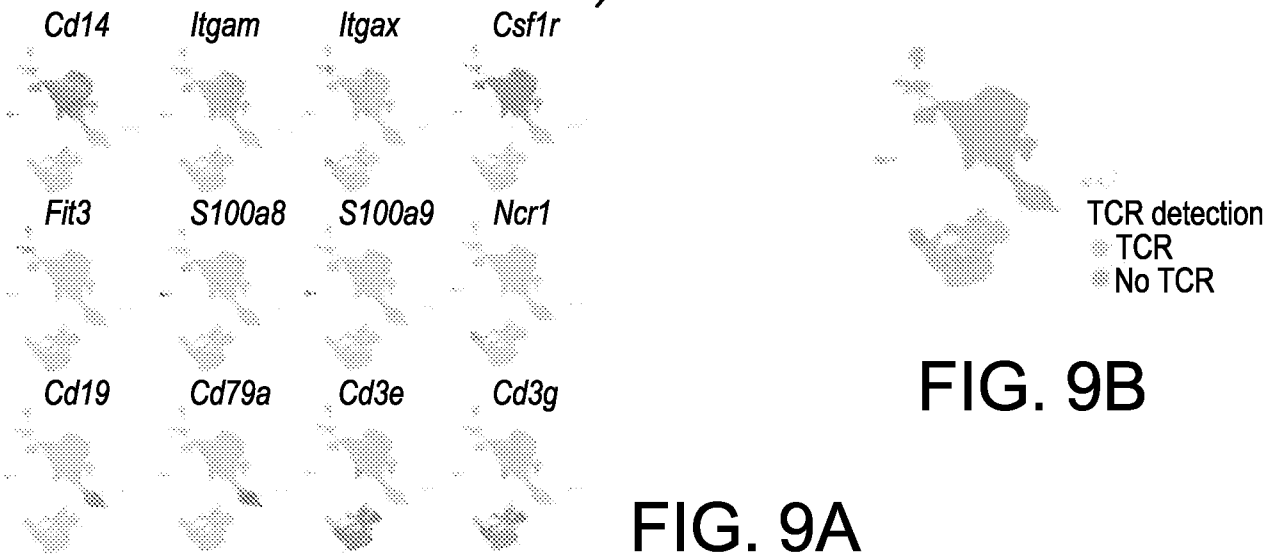

FIG. 9B

FIG. 9A

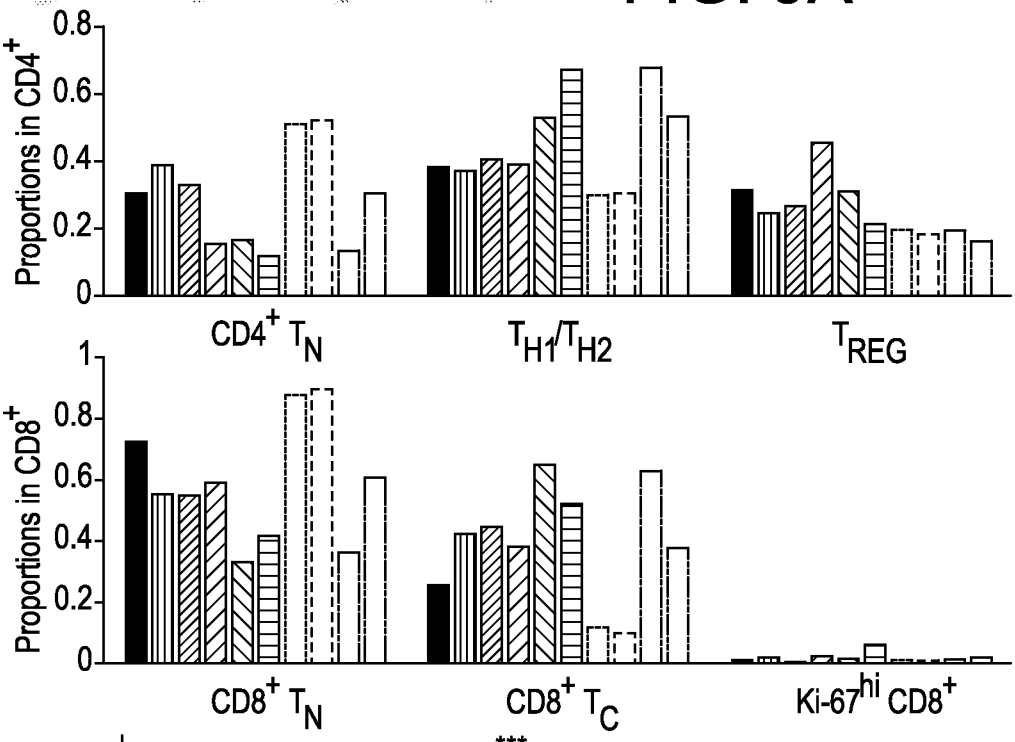

FIG. 9E

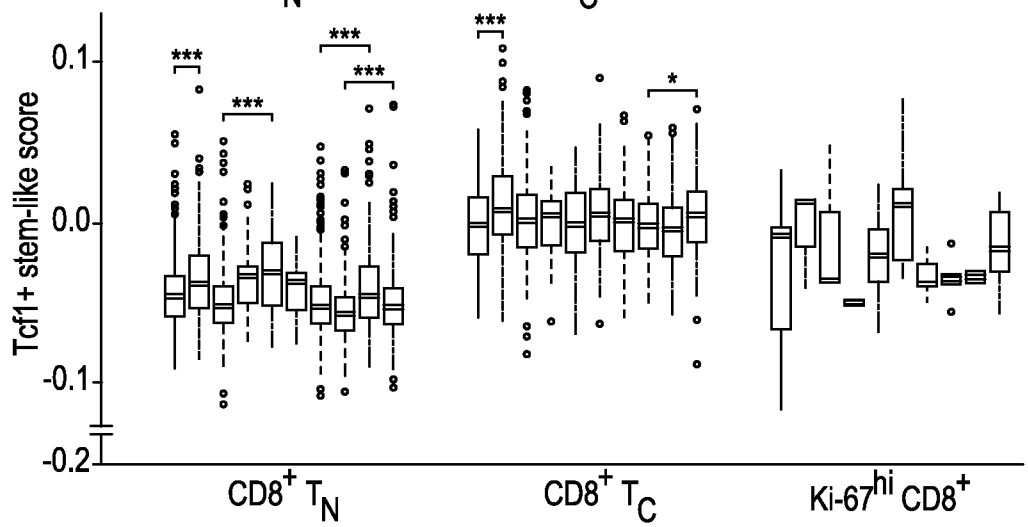

FIG. 9F

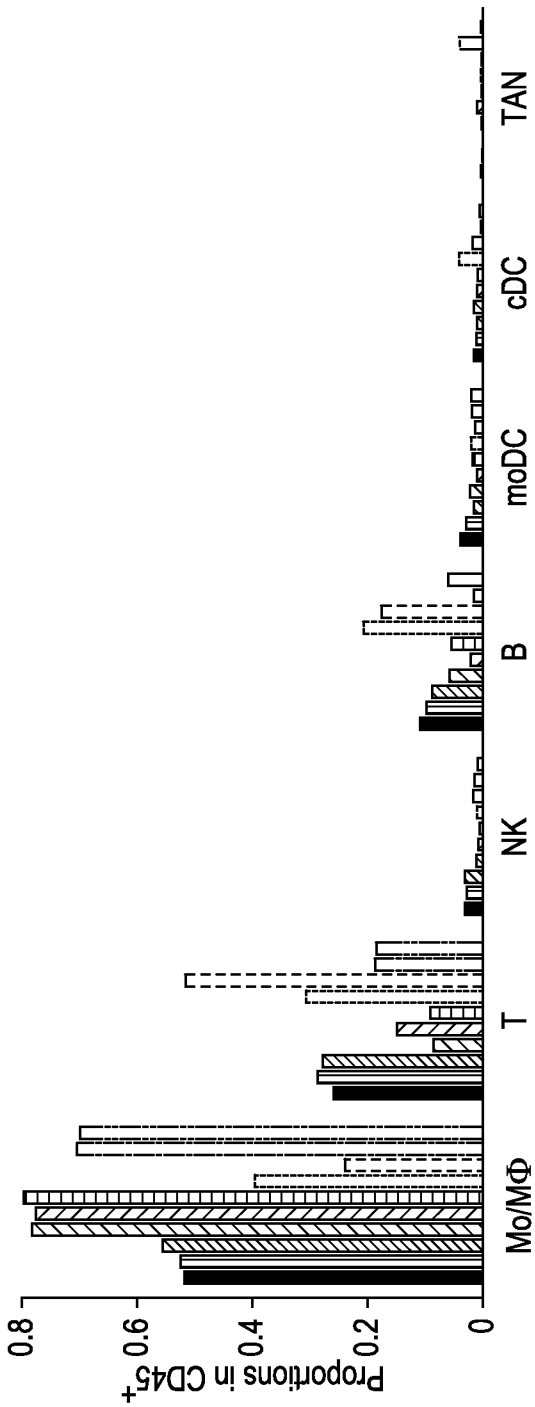
Proportions in CD45+
0
0.2
0.4
0.6
0.8
Mo/MΦ
T
NK
B
moDC
cDC
TAN

FIG. 9C

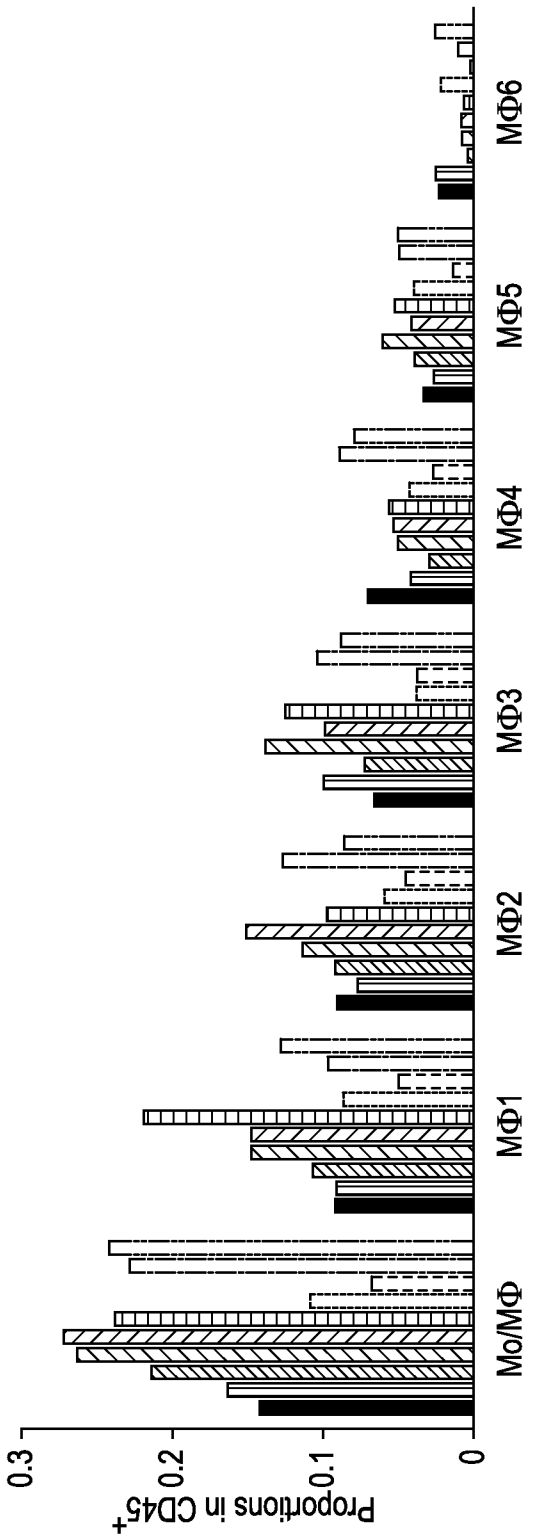
Proportions in CD45+
0
0.1
0.2
0.3
Mo/MΦ
MΦ1
MΦ2
MΦ3
MΦ4
MΦ5
MΦ6

FIG. 9D

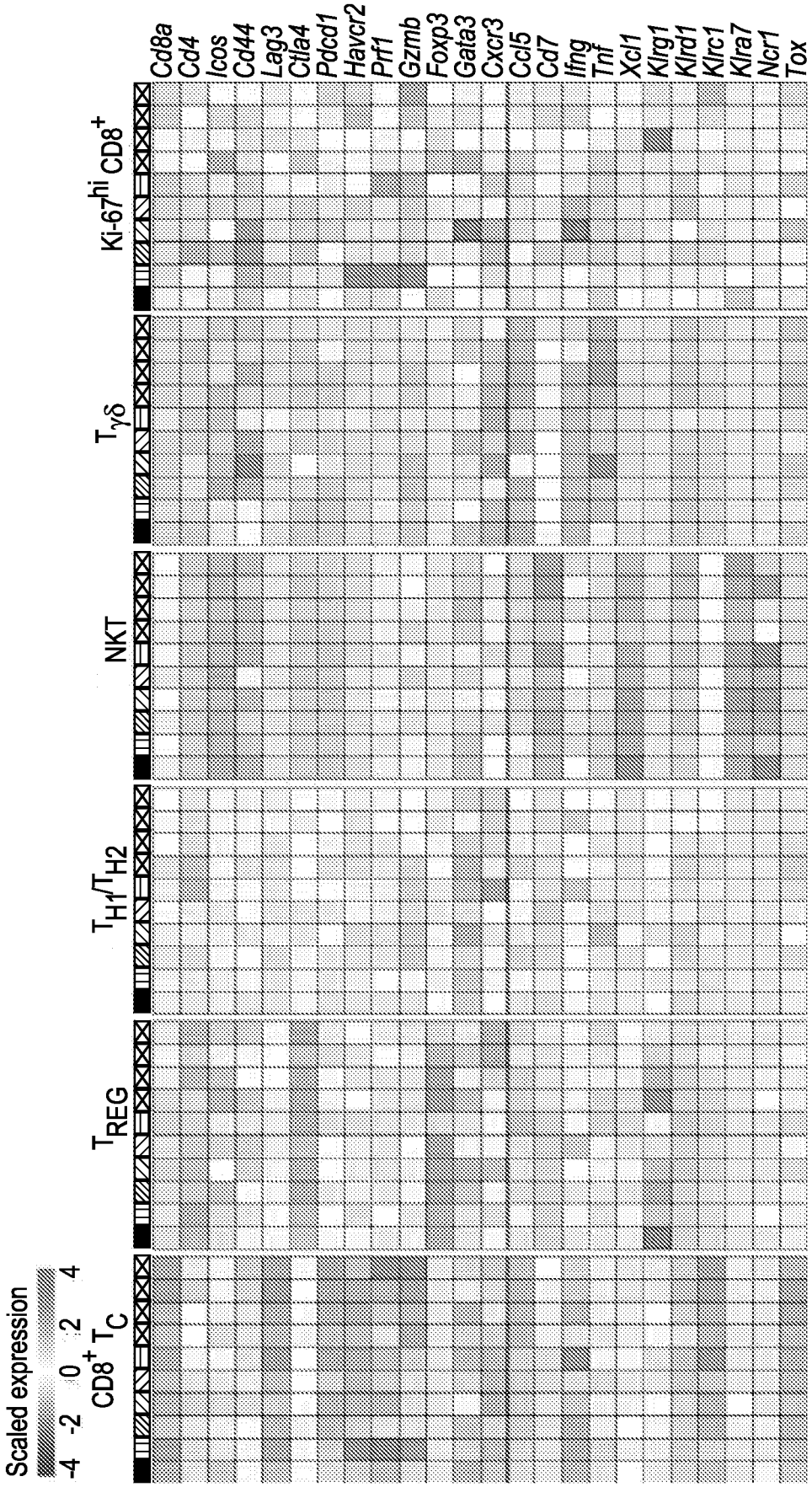
Scaled expression
-4 -2 0 2 4
CD8+ TC
TREG
TH1/TH2
NKT
Tγδ
Ki-67hi CD8+
Cd8a
Cd4
Icos
Cd44
Lag3
Ctla4
Pdcd1
Havcr2
Prf1
Gzmb
Foxp3
Gata3
Cxcr3
Ccl5
Cd7
Ifng
Tnf
Xcl1
Klrg1
Klrd1
Klrc1
Klra7
Ncr1
Tox

FIG. 9G

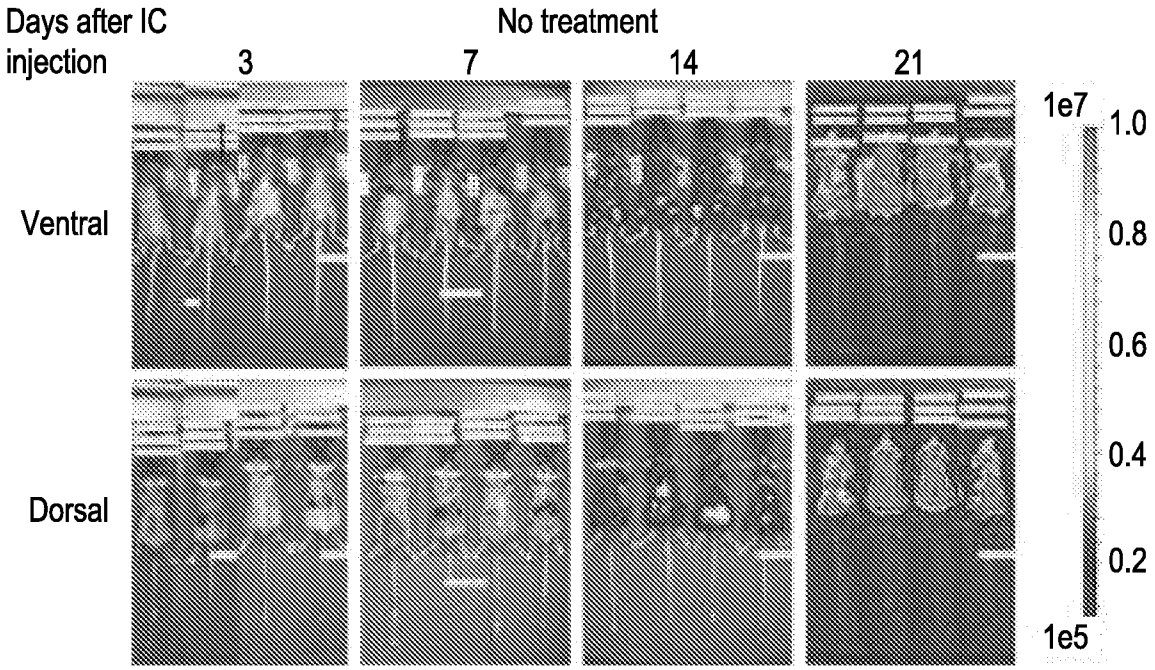

FIG. 10A

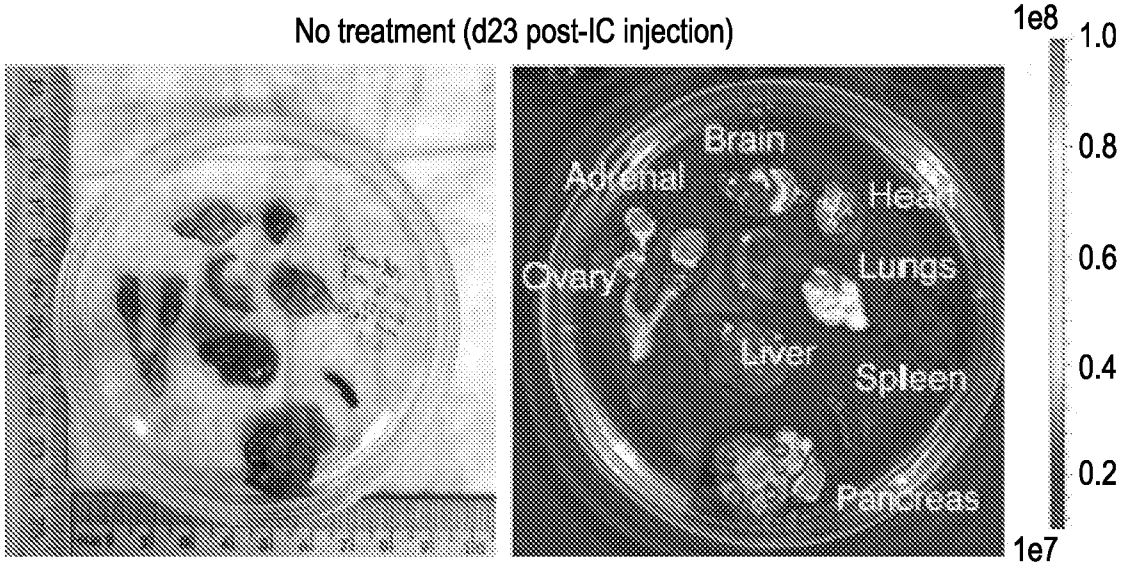

FIG. 10B

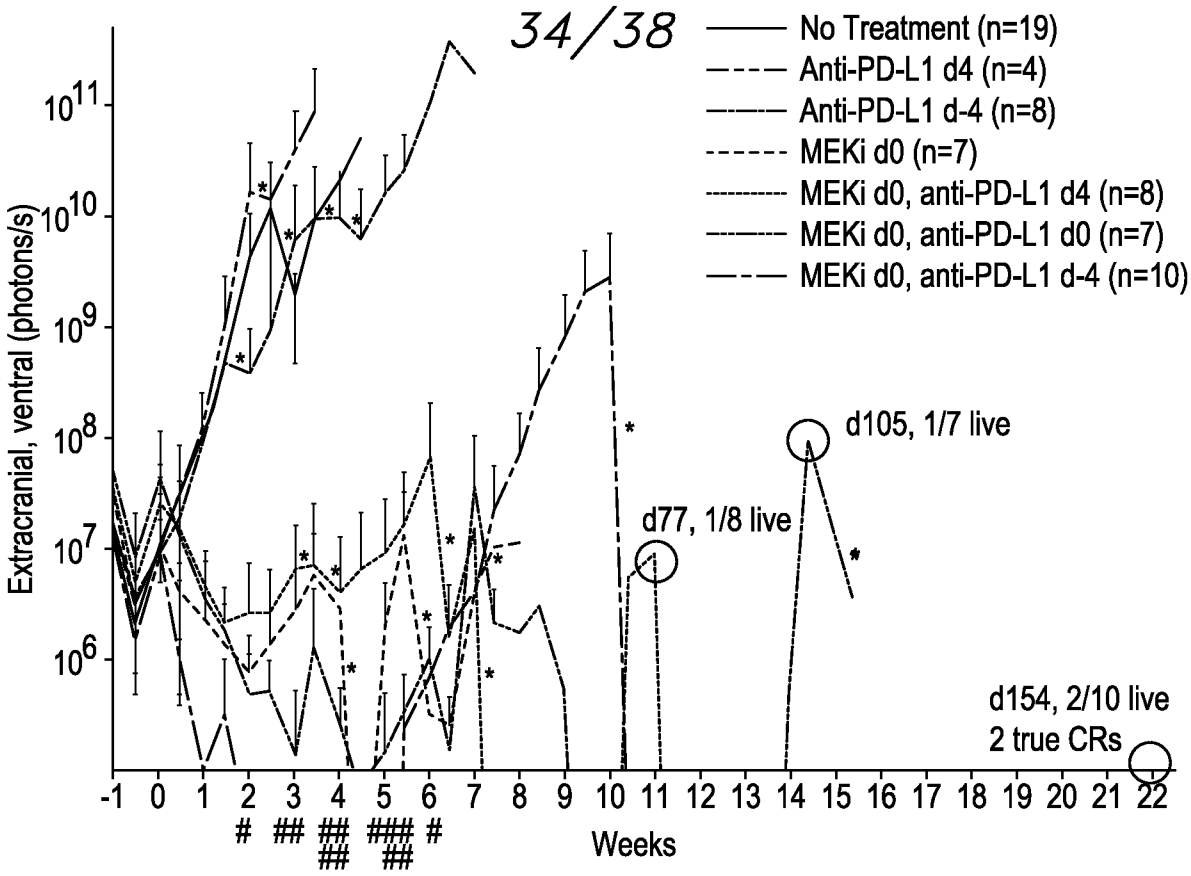

FIG. 10C

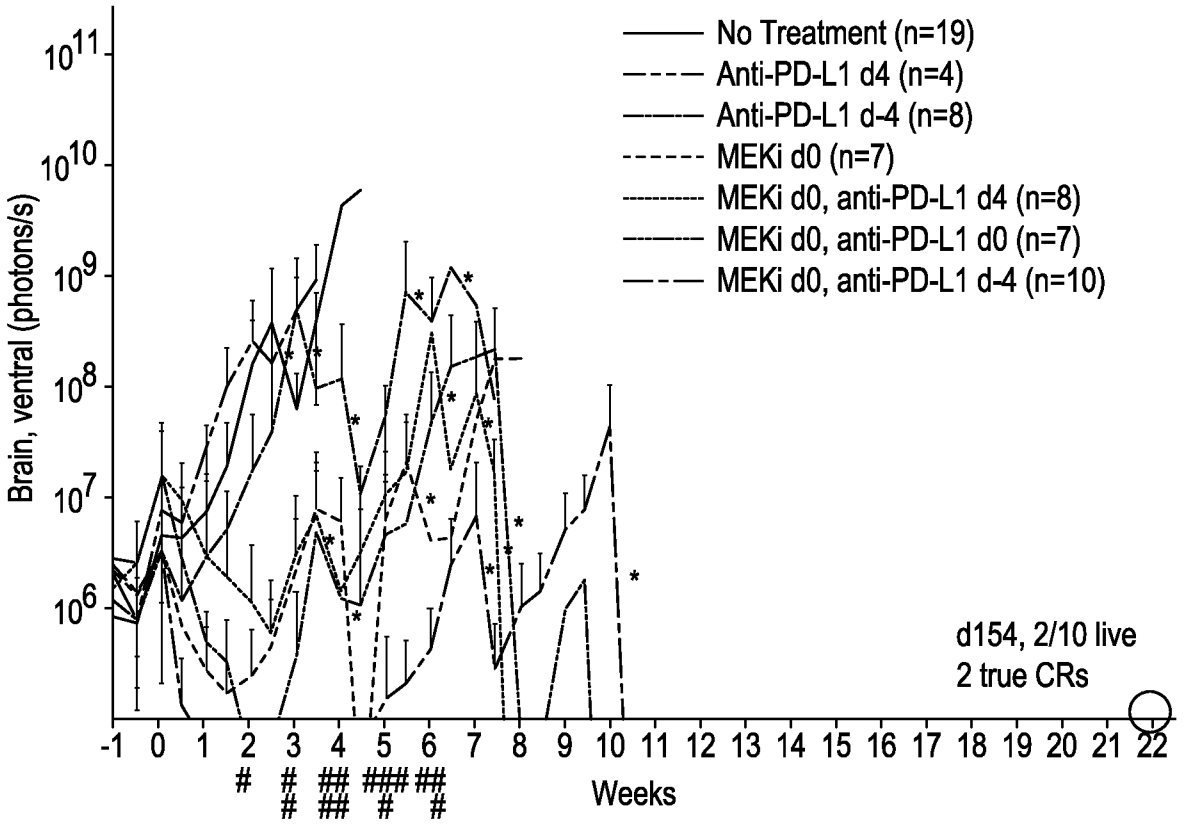

FIG. 10D

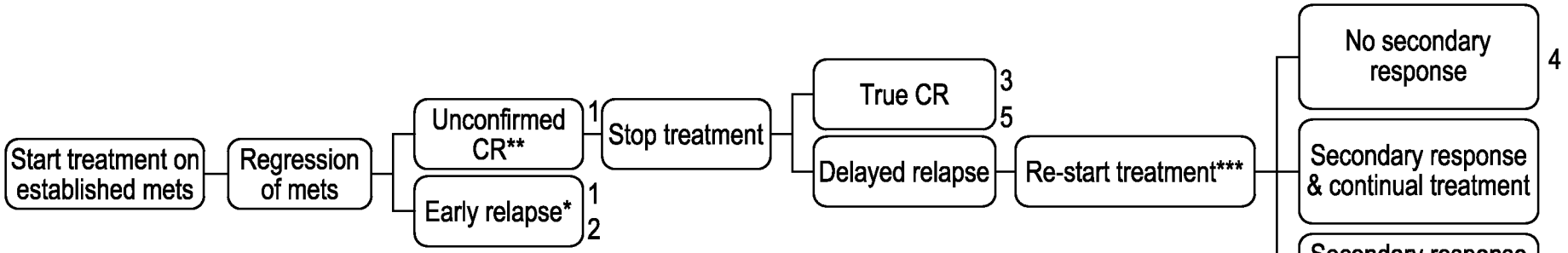

*BLI signal increases from nadir on days 85-100 after starting treatment (early acquired resistance)

**Unconfirmed complete response; no BLI signal beyond background on days 75-100 after starting treatment

***Re-start treatment when BLI signal reaches 1e7 (total ventral or dorsal signal)

****Late acquired resistance

FIG. 10E

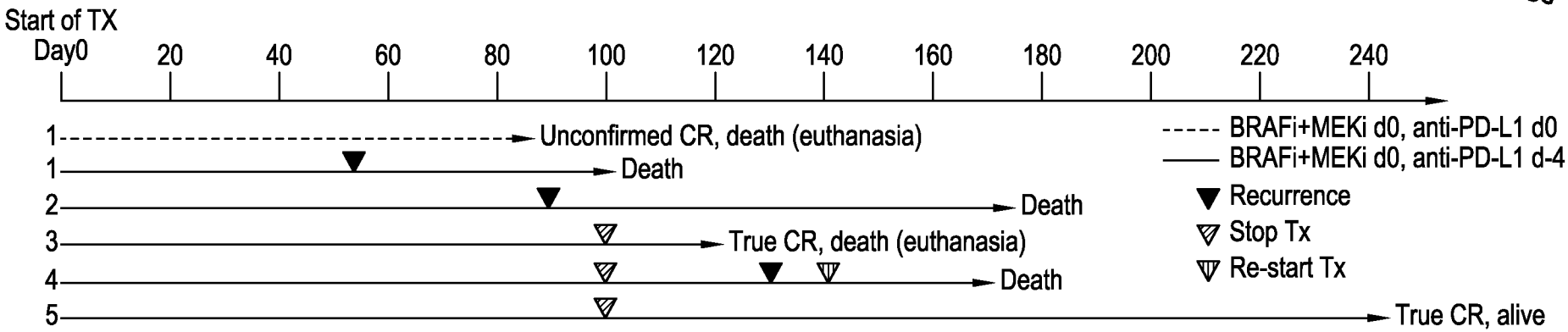

FIG. 10F

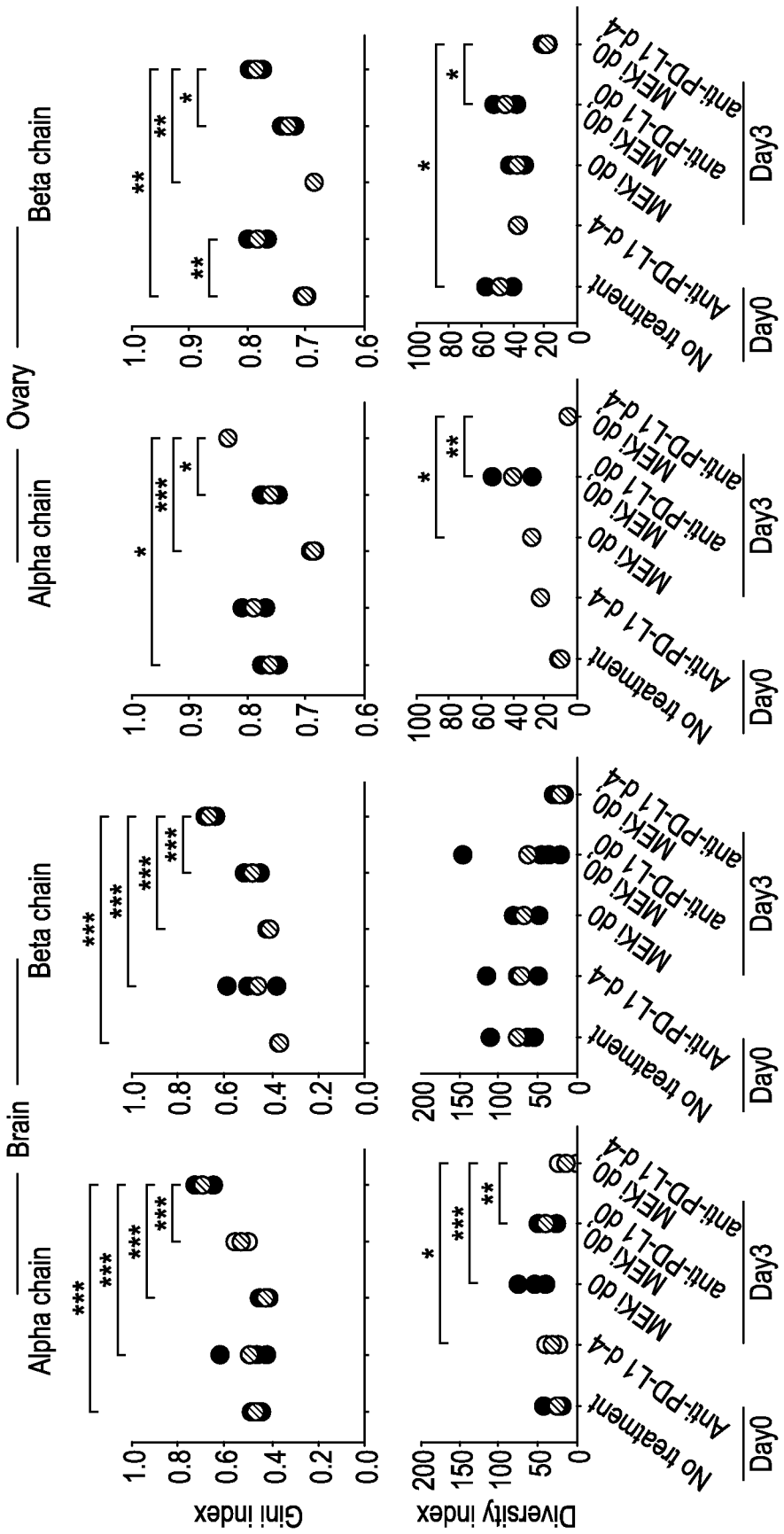
Brain
Ovary
Alpha chain
Beta chain
Gini index
Diversity index
No treatment
Anti-PD-L1 d-4
MEKi d0
MEKi d0, anti-PD-L1 d0
anti-PD-L1 d-4
Day0
Day3

FIG. 10G

FIG. 10I

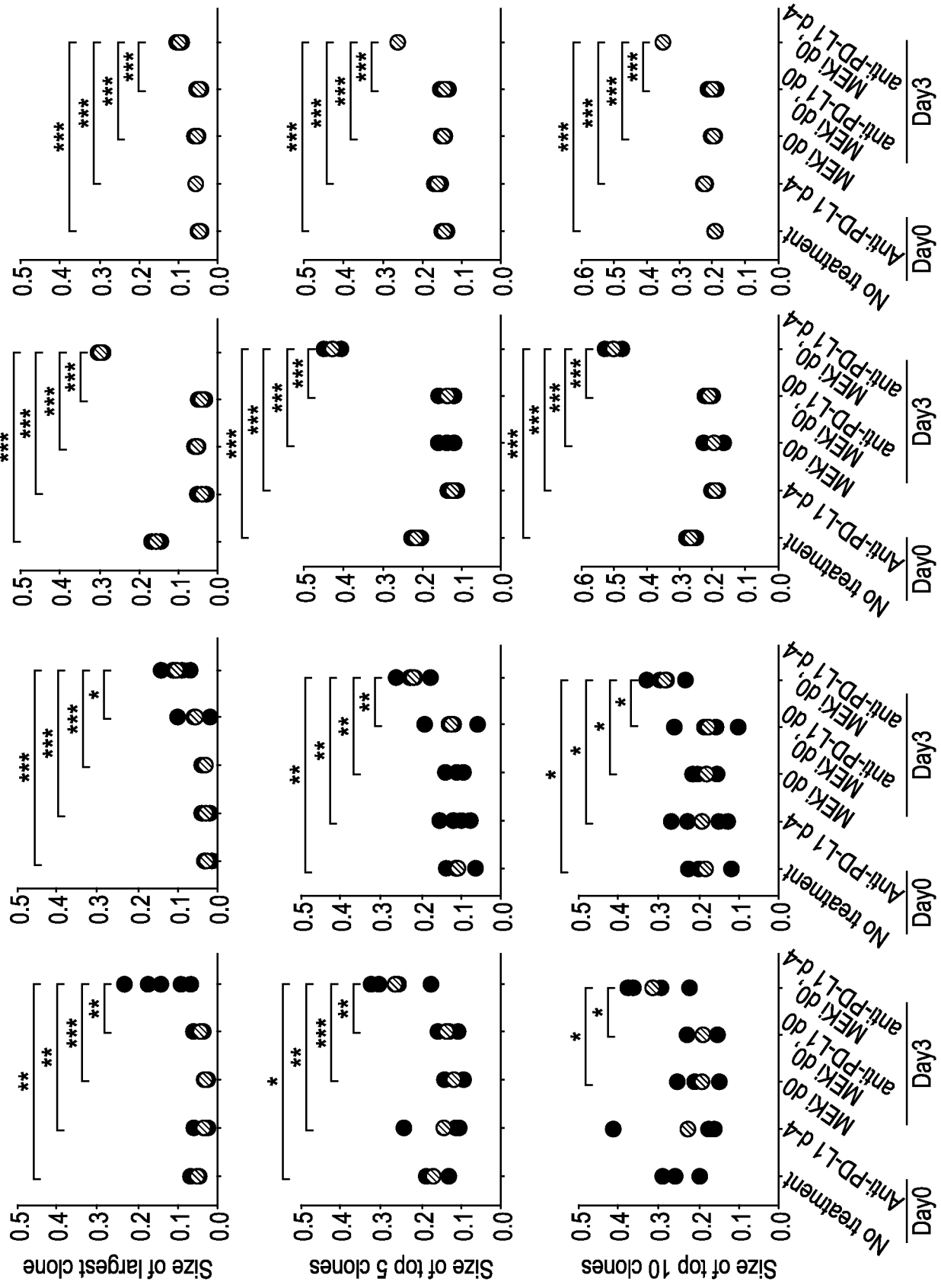
Brain
Ovary
Alpha chain
Beta chain
Size of largest clone
Size of top 5 clones
Size of top 10 clones
No treatment
Anti-PD-L1 d-4
MEKi d0
MEKi d0, anti-PD-L1 d0
Day0
Day3

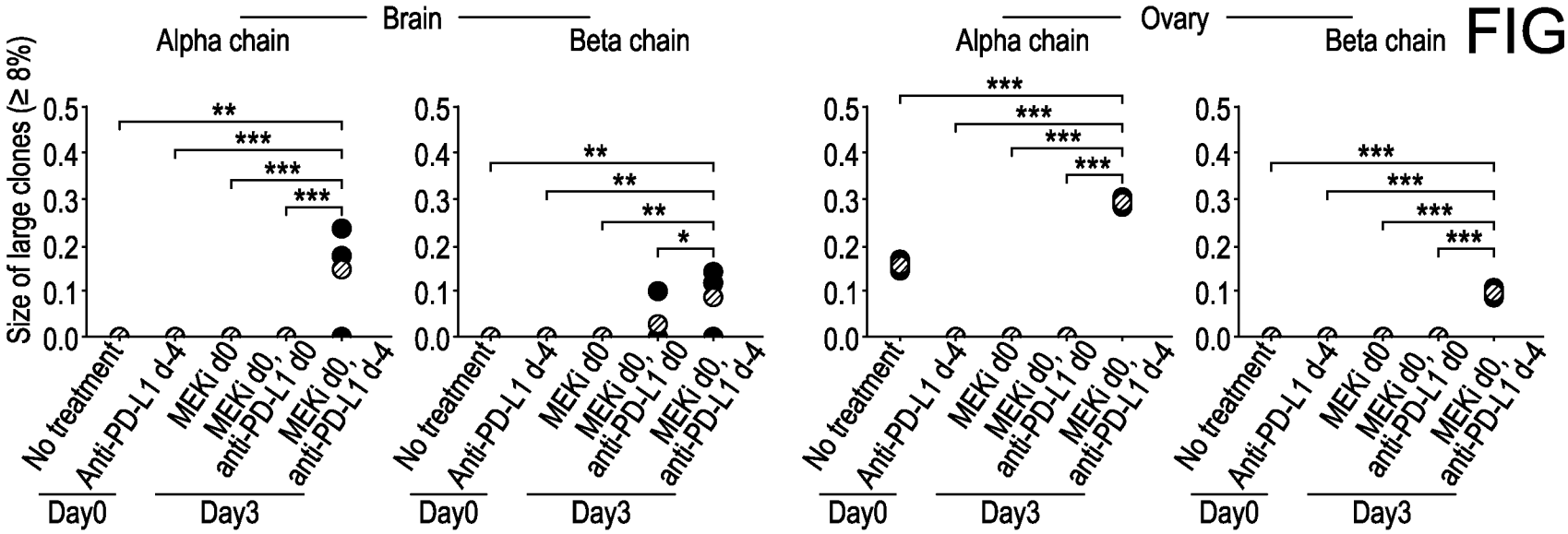

FIG. 10H

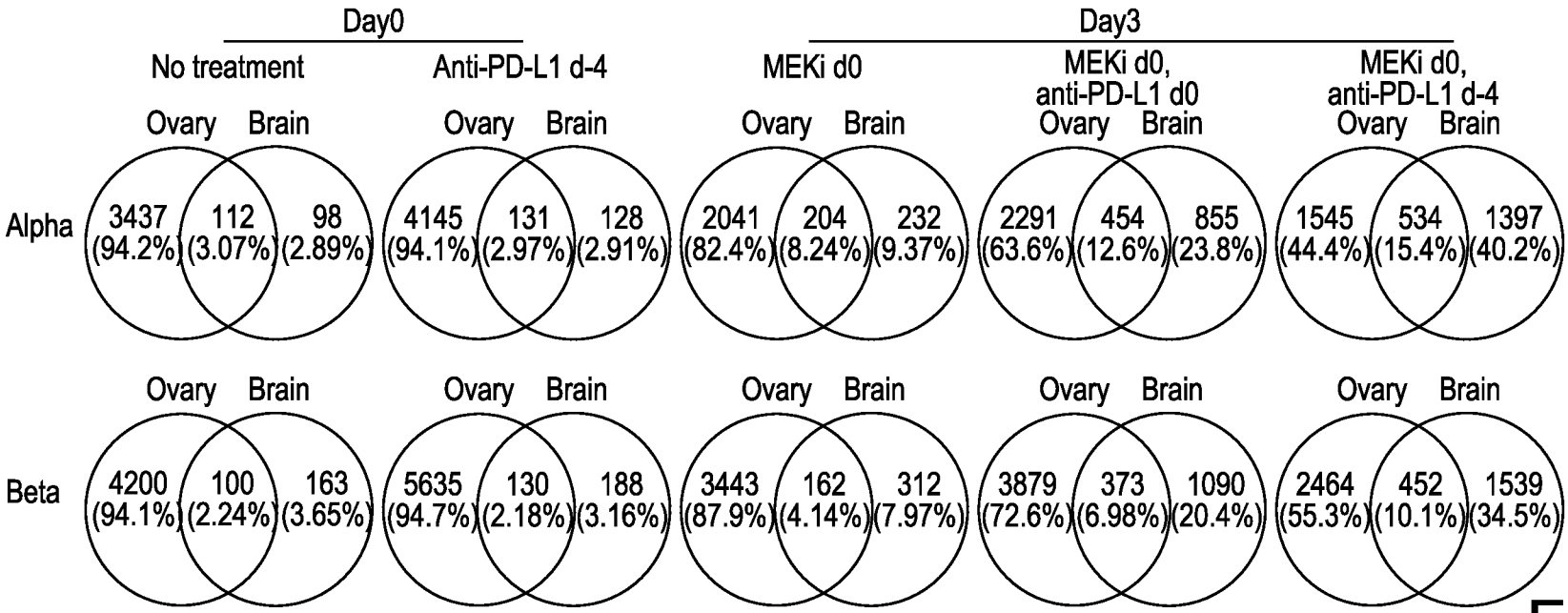

FIG. 10J

INTERNATIONAL SEARCH REPORT

International application No.
PCT/US 22/74383

A. CLASSIFICATION OF SUBJECT MATTER
IPC - INV. A61P 35/00, C07K 16/28 (2022.01)
ADD. G16B 25/10 (2022.01)
CPC - INV. C07K 16/2818, A61K 2039/505
ADD. A61K 39/39558, C12Q 2600/106
According to International Patent Classification (IPC) or to both national classification and IPC

B. FIELDS SEARCHED

Minimum documentation searched (classification system followed by classification symbols)
See Search History document

Documentation searched other than minimum documentation to the extent that such documents are included in the fields searched
See Search History document

Electronic data base consulted during the international search (name of data base and, where practicable, search terms used)
See Search History document

C. DOCUMENTS CONSIDERED TO BE RELEVANT

Category*	Citation of document, with indication, where appropriate, of the relevant passages	Relevant to claim No.
X ---- Y	US 2019/0076399 A1 (THE REGENTS OF THE UNIVERSITY OF CALIFORNIA) 14 March 2019 (14.03.2019) Abstract; Claim 13; Claim 15; Claim 16; para [0024]; para [0026]; para [0028]; para [0038]; para [0079-0080]; para [0114]; para [0117]	1-4, 6-8, 12 ---------- 9-10
Y	US 2020/0339624 A1 (XENCOR, INC.) 29 October 2020 (29.10.2020) Abstract; para [0005]; para [0010]	9-10

☐ Further documents are listed in the continuation of Box C. ☐ See patent family annex.

* Special categories of cited documents:
"A" document defining the general state of the art which is not considered to be of particular relevance
"D" document cited by the applicant in the international application
"E" earlier application or patent but published on or after the international filing date
"L" document which may throw doubts on priority claim(s) or which is cited to establish the publication date of another citation or other special reason (as specified)
"O" document referring to an oral disclosure, use, exhibition or other means
"P" document published prior to the international filing date but later than the priority date claimed
"T" later document published after the international filing date or priority date and not in conflict with the application but cited to understand the principle or theory underlying the invention
"X" document of particular relevance; the claimed invention cannot be considered novel or cannot be considered to involve an inventive step when the document is taken alone
"Y" document of particular relevance; the claimed invention cannot be considered to involve an inventive step when the document is combined with one or more other such documents, such combination being obvious to a person skilled in the art
"&" document member of the same patent family

Date of the actual completion of the international search	Date of mailing of the international search report
2 October 2022	NOV 25 2022
Name and mailing address of the ISA/US Mail Stop PCT, Attn: ISA/US, Commissioner for Patents P.O. Box 1450, Alexandria, Virginia 22313-1450 Facsimile No. 571-273-8300	Authorized officer Kari Rodriquez Telephone No. PCT Helpdesk: 571-272-4300

INTERNATIONAL SEARCH REPORT

International application No.
PCT/US 22/74383

Box No. II Observations where certain claims were found unsearchable (Continuation of item 2 of first sheet)

This international search report has not been established in respect of certain claims under Article 17(2)(a) for the following reasons:

1. ☐ Claims Nos.:
because they relate to subject matter not required to be searched by this Authority, namely:

2. ☐ Claims Nos.:
because they relate to parts of the international application that do not comply with the prescribed requirements to such an extent that no meaningful international search can be carried out, specifically:

3. ☐ Claims Nos.:
because they are dependent claims and are not drafted in accordance with the second and third sentences of Rule 6.4(a).

Box No. III Observations where unity of invention is lacking (Continuation of item 3 of first sheet)

This International Searching Authority found multiple inventions in this international application, as follows:
----Please see continuation in first extra sheet ----------

1. ☐ As all required additional search fees were timely paid by the applicant, this international search report covers all searchable claims.

2. ☐ As all searchable claims could be searched without effort justifying additional fees, this Authority did not invite payment of additional fees.

3. ☐ As only some of the required additional search fees were timely paid by the applicant, this international search report covers only those claims for which fees were paid, specifically claims Nos.:

4. ☒ No required additional search fees were timely paid by the applicant. Consequently, this international search report is restricted to the invention first mentioned in the claims; it is covered by claims Nos.:
1-4, 6-10, 12, limited to treatment of BRAF V600 mutant cancer with pretreatment including a CD25-depleting antibody

Remark on Protest

☐ The additional search fees were accompanied by the applicant's protest and, where applicable, the payment of a protest fee.

☐ The additional search fees were accompanied by the applicant's protest but the applicable protest fee was not paid within the time limit specified in the invitation.

☐ No protest accompanied the payment of additional search fees.

INTERNATIONAL SEARCH REPORT

International application No.

PCT/US 22/74383

Continuation of Box No. III. Observations where unity of invention is lacking.

This application contains the following inventions or groups of inventions which are not so linked as to form a single general inventive concept under PCT Rule 13.1. In order for all inventions to be searched, the appropriate additional search fees must be paid.

Group I+, Claims 1-12, directed to a method of enhancing efficacy of mitogen-activated protein kinase inhibitor (MAPKi) therapy or immune checkpoint therapy (ICT). The method will be searched to the extent that the method encompasses wherein the subject has a BRAF V600 mutant cancer and wherein the pretreating of (a) further comprises administering a modulator of regulatory T cells comprising a CD25-depleting antibody (note, this is the first claimed combination of mutation and immune cell modulator for the inventive method embodiment). The first named invention was determined based on the first claimed combination of mutation (claim 4) and immune cell modulator (claims 9-10) for the inventive method antibody embodiment. This first named invention has been selected based on the guidance set forth in section 10.54 of the PCT International Search and Preliminary Examination Guidelines. It is believed that claims 1-4, 6-10, 12 encompass this first named invention, and thus these claims will be searched without fee to the extent that the method comprises wherein the subject has a BRAF V600 mutant cancer and wherein the pretreating of (a) further comprises administering a modulator of regulatory T cells comprising a CD25-depleting antibody. Additional method(s) comprising additional mutation(s) and/or modulator(s) of M2-like TAMs will be searched upon the payment of additional fees. Applicants must specify the claims that encompass any additionally elected method(s) comprising additional mutation(s) and/or modulator(s) of M2-like TAMs. Applicants must further indicate, if applicable, the claims which encompass the first named invention, if different than what was indicated above for this group. Failure to clearly identify how any paid additional invention fees are to be applied to the "+" group(s) will result in only the first claimed invention to be searched. An exemplary election would be a method wherein the subject has a NRAS mutant cancer and wherein the pretreating of (a) further comprises administering a modulator of regulatory T cells comprising a CD25-depleting antibody (claims 1-3, 5-10, 12).

Group II, Claims 13-14, directed to a method of suppressing melanoma metastasis in a subject.

Group III, Claims 15-16, directed to a method of enhancing the inhibition of M2-like tumor associated macrophages (TAMs) in a subject using pretreatment with a pharmacologic M2-like TAM inhibitor.

The inventions listed as Groups I+, II and III do not relate to a single special technical feature under PCT Rule 13.1 because, under PCT Rule 13.2, they lack the same or corresponding special technical features for the following reasons:

Special technical features

Group I+ has the special technical feature of a method of enhancing efficacy of mitogen-activated protein kinase inhibitor (MAPKi) therapy or immune checkpoint therapy (ICT) requiring a pretreatment comprising a combination of ICT and a CD25-depleting antibody or peptide agonist of CD206, that is not required by Groups II-III.
Group II has the special technical feature of suppressing melanoma metastasis in a subject that requires a subject with brain metastasis, that is not required by Groups I+ and III.
Group III has the special technical feature of a method of enhancing the inhibition of M2-like tumor associated macrophages (TAMs) in a subject by pretreating with a combination of ICT and a pharmacologic M2-like TAM inhibitor, that is not required by Groups I+ and II.

Common technical features

Groups I+, II and III share the technical features of including:
a method comprising
(a) pretreating a subject in need of cancer therapy by administering one to two doses of ICT to the subject;
(b) subsequent to the pretreating of (a). administering to the subject a combination of MAPKi and ICT.

However, these shared technical features are previously disclosed by prior art, as discussed below.

Group I+ inventions additionally share the technical features of including:
a method of enhancing efficacy of mitogen-activated protein kinase inhibitor (MAPKi) therapy or immune checkpoint therapy (ICT), the method comprising:
(a) pretreating a subject in need of MAPKi therapy by administering one to two doses of ICT to the subject;
(b) subsequent to the pretreating of (a). administering to the subject a combination of MAPKi and ICT.

However, these shared technical features are previously disclosed by US 2019/0076399 A1 to the Regents of the University of California, (hereinafter 'Univ California').

----please see continuation on next sheet ----------

Continuation of Box No. III. Observations where unity of invention is lacking.

-------continued from previous sheet ----------

Univ California teaches a method of enhancing efficacy of mitogen-activated protein kinase inhibitor (MAPKi) therapy or immune checkpoint therapy (ICT) (para [0117] - 'Thus, while our findings in this study necessitate confirmation in independent tissue cohorts, the identification of transcriptomic features associated with anti-PD-1 resistance suggests that mitigation of IPRES-related biological processes may enhance response rates to anti-PD-1 (and anti-PD-1 plus MAPKi) therapy.') comprising
(a) pretreating a subject in need of cancer therapy by administering one to two doses of ICT to the subject (Abstract - 'Methods of predicting or detecting sensitivity to therapeutic effects of anti-PD-1 therapy in a patient suffering from melanoma ... The method of the invention can further comprise treating the patient with anti-PD-1 therapy, optionally in conjunction with combinatorial therapy.'; para [0026] - '(1B) Overall survival of anti-PD-1-treated melanoma patients whose pretreatment tumors responded (n=20) or did not respond (n=17).'; para [0028] - 'Heatmap showing GSVA scores of IPRES signatures across four independent RNASeq data sets derived from metastatic melanoma. Cohort 1, pretreatment (anti-PD-1) tumors; cohort 2, pretreatment (anti-CTLA-4) tumors; cohort 3, pretreatment (MAPKi) tumors; cohort 4, TCGA cutaneous melanoma (metastatic only).'; para [0087] - 'All patients received either pembrolizumab or nivolumab as the anti-PD-1 therapy for their metastatic melanoma.');
(b) subsequent to the pretreating of (a). administering to the subject a combination of MAPKi and ICT (Claim 13 - 'The method of claim 1, wherein the anti-PD-1 therapy is administered in conjunction with combinatorial therapy.'; Claim 15 - 'A method of treating a patient suffering from melanoma, the method comprising assaying a tumor sample obtained from the patient for a marker of sensitivity to anti-PD-1 therapy, and either administering anti-PD-1 therapy if the patient is positive for a marker of sensitivity to anti-PD-1 therapy, or administering alternative therapy if the patient is not positive for a marker of sensitivity to anti-PD-1 therapy, wherein the marker of sensitivity to anti-PD-1 therapy is selected from the measures according to claim 1(a).'; Claim 16 - 'The method of claim 15, wherein the alternative therapy is selected from: (a) MAPK targeted therapy (mutant BRAF inhibitors: Vemurafenib/PLX4032, Dabrafenib, Encorafenib/LGX818, MEK inhibitors: Trametinib/GSK1120212, Selumetinib/AZD6244, MEK162/Binimetinib, Cobimetinib/GDC0973, PD0325901, ERK inhibitors: SCH772984, VTX-11e, Pan RAF inhibitors: Sorafenib, CCT196969, CCT241161, PLX7904 and PLX8394); ... (d) any combination of the above with or without anti-PD-1 antibody (nivolumab/BMS-936558/MDX-1106, pembrolizumab/MK-3475, Pidilizumab) or anti-PD-L1 antibody (BMS-986559, MPDL3280A, and MEDI4736).').

As the technical features were known in the art at the time of the invention, they cannot be considered special technical features that would otherwise unify the groups.

Therefore, Group I+, II and III inventions lack unity under PCT Rule 13 because they do not share the same or corresponding special technical feature.